1989

A numerical study of the fluid mechanics within a bubbling fluidized bed /

Bulent Kocatulum
Lehigh University

A NUMERICAL STUDY OF THE FLUID MECHANICS WITHIN A BUBBLING FLUIDIZED BED

by

BULENT KOCATULUM

A Thesis

Presented to the Graduate Committee

of Lehigh University

in Candidacy for the Degree of

Master of Science

in

Mechanical Engineering

Lehigh University

1988

CERTIFICATE OF APPROVAL

This thesis is accepted and approved in partial fulfillment of the requirements for the degree of Master of Science.

December 13, 1988

(date)

Edward Klevy

Professor in Charge

F. Erdogan

Chairman of Department

ACKNOWLEDGEMENTS

I am grateful to Professor Edward K. Levy, my advisor and the Director of Energy Research Center, for his encouragement and guidance throughout the course of this study. I must express my appreciation to Mr. Fikret Bayat for his valuable suggestions.

I extend my special thanks to my whole family for their patience and love.

TABLE OF CONTENTS

LIST OF TABLES

LIST OF FIGURES

ABSTRACT

A numerical analysis of the motion of the emulsion and gas phases driven by a single bubble rising in a fluidized bed has been performed by employing a combination of finite element and finite difference methods to solve the governing equations. The Davidson bubble model was taken as the basis and additional equations were derived to account for the presence of the free surface. The shape of the bubble was obtained from video recordings of laboratory fluidized beds.

Solutions were obtained for both a fast bubble and a slow bubble at six different values of the interstitial gas velocity. The shape of the free surface, the velocity fields of solids and gas, the pressure gradients, gas flow rate through the bubble, and solids flow rate into and out of the wake of the bubble were calculated as the bubble advanced towards the free surface. The results indicate that gas flow rate through the bubble reaches its peak before the bubble is at the very top of the bed. The model predicts a particle flow rate through the wake which is relatively insensitive to the distance of the bubble from the free surface.

1. INTRODUCTION

The fluidization phenomenon occurs when a gas or liquid is forced to flow upward through a bed of solid particles. If the fluid flow rate is low, the bed is said to be in a packed state and the solid particles remain stationary. Increasing the flow rate causes the particles to move apart and the bed is seen to expand slightly. With a further increase in fluid flow rate, an equilibrium point is reached where the drag force applied on a solid particle by the upward flowing fluid just counterbalances the weight of the particle. At this point, all the particles are suspended in the fluid. This is the state of minimum fluidization, and the bed is referred to as an incipiently fluidized bed.

Although in liquid-solid systems an increase in flow rate beyond minimum fluidization usually results in a homogeneously fluidized bed, in gas-solid systems the motion of solids becomes more vigorous and the expansion of the emulsion phase beyond its minimum fluidization volume is only very slight. In such systems, the excess gas flows through the fluidized bed in the form of gas voids and this system is referred to as a bubbling fluidized bed.

In a bubbling fluidized bed, the rising gas voids,

termed 'bubbles', dominate the behavior of the system. There are two distinguishing phases in such a system: the bubble phase which contains virtually no bed particles and the particulate phase, or the emulsion phase, consisting of particles fluidized by the interstitial gas. In a bubbling bed, the bubble phase is dispersed and the emulsion phase is continuous. At very high velocities, however, the volume occupied by the bubble phase is so high that the particulate phase no longer forms a continuous medium between discrete bubbles. Also, in this regime, the magnitude of the drag force is large enough to convey the solid particles out of the bed. This is known as pneumatic transport.

When bubbles erupt from the surface of a gas-fluidized bed, they push particles into the freeboard region. Some of these particles have large enough initial momentum to be carried from the bed with the aid of the upward gas motion.

Since their first commercially significant use for the gasification of powdered coal in 1922[1], fluidized beds have found diverse applications in industry ranging from synthesis reactions and cracking of hydrocarbons to carbonization of oil shale and solids transport.

2. LITERATURE REVIEW

The study of the behavior of single bubbles has been the subject of numerous investigations as it forms the fundamental step towards the understanding of bubbling fluidized beds.

X-ray photographs[2] of three dimensional bubbles show that the bubble is very close to spherical over the entire front surface and the rear portion is indented, forming what is known as the wake region.

The rise velocity of single bubbles was first studied by Davies and Taylor[3] who treated the emulsion phase as an incompressible inviscid fluid. They required the pressure to be constant in the vicinity of the bubble nose and showed that the rise velocity is given by

$$u_b = \frac{2}{3} (gR_n)^{1/2}$$

where R_n is the radius of curvature at the nose of the bubble.

Based on experimental observations the above equation is modified[4] as

$$u_b = 0.711(gd_b)^{1/2}$$

where d_b is the diameter of a sphere having the same volume as the spherical cap bubble.

Rowe[5] observed that bubbles, as they rise, carry

closed wakes of particulate phase, and there seems to be a continuous exchange of particles between the wake region and the surrounding solids. Davidson[6] treated the dense phase as an incompressible and inviscid fluid flowing around bubbles in irrotational motion and obtained expressions for the components of particle velocity.

As for the gas motion, Davidson made the earliest analysis by using Darcy's Law to establish a relation between the gas motion and the solids motion. An alternative approach for the gas flow was proposed by Murray[7] who employed a momentum equation for solids. Jackson[8] developed another model which allowed for voidage variations in the dense phase and obtained results similar to those of Murray.

Jackson[9] points out that the Davidson theory gives a more accurate prediction of the pressure field around the bubble than the model of Murray.

Collins[10] used conformal mapping techniques to obtain a two dimensional kidney shape for the bubble. His solutions indicated that the gas flow pattern is significantly altered close to the rear of the bubble and that under certain conditions a bubble moving on the axis of a bed of finite width is capable of capturing the

whole of the gas flow in the bed. Littman and Homolka[11] found that the pressure field is Laplacian upstream of bubble, confirming Davidson's theory in this region.

As a bubble approaches the free surface of a fluidized bed, it disturbs the surface and causes a dome to form. Eruption of bubbles at the free surface results in ejection of particles into the freboard region, which is the initial stage of particle entrainment. Do et al.[12] performed experiments and showed that the predominant mechanism for this phenomenon is the ejection of particles in the bulge region at the nose of the bursting bubbles. Chen and Saxena[13] proposed a model based on this mechanism. Levy et al.[14] identified three different wake ejection mechanisms. Pemberton and Davidson[15] carried out experiments using hot-wire anemometry and concluded that the gas within a bubble moves as an entity in the freeboard and the velocity of these "gas pockets" diminishes as they rise.

The above mentioned experimental results indicate that there is a need to take into account the dynamics of the free surface in the theoretical analysis of bubble motion, particularly near the top of a fluidized bed of finite dimensions. Radcliff[16] employed surface wave theory and a finite difference integration scheme to

handle the problem. Subsequently, Chen[17] computed the gas flow rates through the rising bubble and through the free surface. Both of these analyses involved the ideal spherical shape for the bubble. The present analysis extends Radcliff's model by incorporating a realistic kidney shape obtained from experimental video tapes. The flow rate of solid particles into and out of the wake of the bubble, as well as gas flow rates, are calculated. The results of this study, along with those from experimental investigations, are intended to contribute to the understanding of the behavior of gas and particle flow fields around a single rising bubble.

3. THEORETICAL APPROACH

This analysis is based on the model developed by Davidson[18] who made the first successful theoretical treatment for the calculation of emulsion and gas flow fields associated with the rise of single bubbles. His model, besides its simplicity, has been shown to yield essentially accurate results[1,9]. More complicated models were developed by Murray[7] and Jackson[8].

The Davidson model, which is able to handle both two and three dimensional bubbles, is based on the following three fundamental assumptions:

1. A gas bubble contains no solid particles and has a circular shape(i.e. cylindrical in the two dimensional case and spherical in the three dimensional case).

2. The solid particles move around the rising bubble as an inviscid incompressible fluid with a constant bulk density which is equal to the bulk density of the whole bed at minimum fluidization conditions.

3.The gas flow in the emulsion phase is that of a viscous incompressible fluid, thus the gas flow field obeys Darcy's law for flow through a porous medium.

The continuity equation for the particulate phase follows from assumption 2 above,

$$\nabla \cdot v_p = 0 \tag{1}$$

Also, a velocity potential for the particle motion exists and is given by

$$\nabla \phi = v_p \tag{2}$$

Combining (1) and (2) yields

$$\nabla \cdot \nabla \phi = \nabla^2 \phi = 0 \tag{3}$$

so that the particle velocity potential satisfies Laplace's equation.

As a consequence of assumption 3, the continuity equation for the interstitial gas flow is

$$\nabla \cdot u_g = 0 \tag{4}$$

Also, the relative velocity between solid particles and the gas phase is given by Darcy's law:

$$u_g - v_p = -k \nabla p \tag{5}$$

where k is a permeability constant which is a characteristic of the particles and of the fluidising fluid.

Taking the divergence of equation (5) and then substituting equations (1) and (4) leads to

$$\nabla \cdot \nabla p = \nabla^2 p = 0 \tag{6}$$

In other words, the pressure must also satisfy Laplace's equation. Equation (6) implies that the pressure

distribution is independent of the particle motion.

By further assuming that the pressure inside the bubble is constant and that far above and below the bubble the pressure gradient has a constant value, Davidson obtained an expression for the pressure distribution around a spherical void.

The equations presented so far complete the description of the model developed by Davidson. This analysis further involves the assumptions that the voidage of the bed remains constant at its minimum fluidization value(ϵ_{mf}) and that the bubble moves vertically upwards with a constant velocity. Also, any changes in bubble size with vertical position due to hydrostatic pressure variations were ignored.

The Davidson model was developed for an infinitely large bed. In order to adapt this model to a bed of finite dimensions it is necessary to account for the dynamics of the free surface due to the approach of the bubble. When a bubble rises towards the free surface, it will cause the surface to deform and the value of velocity potential at the surface to change.

The changing shape of the free surface can be calculated by applying dynamic and kinematic conditions at the surface. From surface wave theory[19] the equation

of the free surface, referring to Figure 1, is

$$z_f - \eta - z_o = 0 \tag{8}$$

where z_o is the level of the undeformed bed, z_f is the height of the deformed surface, and η is the deformation of the free surface.

Since the surface moves with the particles

$$\frac{D}{Dt} (z_f - z_o - \eta) = 0 \tag{9}$$

Noting that z_o is constant, equation (9) reduces to

$$\frac{Dz_f}{Dt} = \frac{D\eta}{Dt} \tag{10}$$

In equation (10), the term on the left hand side is the vertical component of velocity of particles on the free surface and the term on the right hand side may be expanded to give the following

$$v_z = \frac{\partial \eta}{\partial t} + v_r \frac{\partial \eta}{\partial r} \tag{11}$$

where v_z and v_r are the components of particle velocity at the free surface in the z and r directions.

Equation (11) is the statement of the kinematic condition at the free surface.

Another boundary condition to account for the surface dynamics is obtained by employing the unsteady Bernoulli equation which may be written as

$$p = \rho_s(1-\epsilon_{mf})\left\{ (\frac{\partial \phi}{\partial t} - gz_f - \frac{1}{2}v^2) + C(t) \right\} \tag{12}$$

where C(t) is a function of time only. Now, if the

transient part of C is incorporated into ϕ, then it is possible to replace C(t) by an absolute constant C. When the resulting expression is applied to the free surface

$$p_f = \rho_s(1-\epsilon_{mf})\left\{ \left(\frac{\partial\phi}{\partial t} - g(z_o+\eta) - \frac{1}{2}v^2\right) + C \right\} \qquad (13)$$

where p_f is the pressure at the surface.

Now, C can be evaluated using the initial condition which states that at the beginning of the process, the free surface is flat and at rest:

$$t = 0 \qquad \eta = 0 \quad , \quad \frac{\partial\phi}{\partial t} = 0, \quad v_p = 0$$

Then equation (13) gives

$$p_f = \rho_s(1-\epsilon_{mf})[- gz_o + C] \qquad (14)$$

Combining equations (13) and (14), and arranging, the dynamic boundary condition can be expressed as

$$\frac{\partial\phi}{\partial t} = g\eta + \frac{1}{2} v^2 \qquad (15)$$

In the foregoing analysis, the relations to describe the gas and particle motion associated with a single rising bubble were presented. Taking Davidson's model as the basis, and deriving the additional necessary equations, the complete set of equations governing the mechanics of the problem are written here altogether:

$$\nabla^2\phi = 0 \qquad (16)$$

$$\nabla\phi = \mathbf{v_p} \tag{17}$$

$$\nabla^2 p = 0 \tag{18}$$

$$\mathbf{u_g} - \mathbf{v_p} = -k\nabla p \tag{19}$$

$$v_z = \frac{\partial \eta}{\partial t} + v_r \frac{\partial \eta}{\partial r} \tag{20}$$

$$\frac{\partial \phi}{\partial t} = g\eta + \frac{1}{2} v^2 \tag{21}$$

Equations (16) through (21) may be rendered non-dimensional by using the following reference parameters:

u_b : bubble velocity

r_n : bubble nose radius (Figure 1)

$\rho_s(1-\epsilon_{mf})r_n g$: undisturbed pressure

Then, the dimensionless variables are

$$H = \frac{\eta}{r_n} \qquad Z = \frac{z}{r_n} \qquad R = \frac{r}{r_n}$$

$$V_r = \frac{v_r}{u_b} \qquad V_z = \frac{v_z}{u_b} \qquad T = \frac{t u_b}{r_n}$$

$$\Phi = \frac{\phi}{r_n u_b} \qquad P = \frac{p}{\rho_s(1-\epsilon_{mf})r_n g}$$

Substitution of these variables into the equations (16) through (21) yields the following non-dimensional equations:

$$\nabla^2 \Phi = 0 \tag{22}$$

$$\nabla^2 P = 0 \tag{23}$$

$$\mathbf{U_g} = \mathbf{V_p} - K\nabla P \tag{24}$$

$$\frac{\partial H}{\partial T} = V_z - V_r \frac{\partial H}{\partial R} \tag{25}$$

$$\frac{\partial \Phi}{\partial T} = \frac{H}{1.5828 Fr} + \frac{1}{2}\left(V_r^2 + V_z^2 \right) \tag{26}$$

where K is a dimensionless interstitial gas velocity,

$$K = \frac{u_{g\infty}}{u_b} \tag{27}$$

and Fr is the Froude number defined by

$$Fr = \frac{u_b^2}{g d_{eq}} \tag{28}$$

The constant in equation (26) comes from the relation between the nose radius and the equivalent diameter of the bubble. The derivation of the expression for K and the calculation of the equivalent diameter are given in detail in Appendices A and B, respectively.

For a freely bubbling bed, the rise velocity of bubbles is[20]

$$u_b = u_o - u_{mf} + 0.711 \ (g \ d_b)^{1/2} \tag{29}$$

where u_o is the superficial velocity of the fluidizing gas.

Substitution of (29) into (28) gives

$$Fr = \frac{\left\{ u_o - u_{mf} + 0.711 \ (g \ d_b)^{1/2} \right\}^2}{g \ d_b}$$

For conditions near minimum fluidization, the Froude number can be calculated as

$$Fr = (0.711)^2 = 0.50552$$

The flow rate of gas through the bubble is calculated from the basic equation

$$q_b = \int_{A_b} \epsilon_{mf} \; u_{gr} \cdot n \; dA_b \qquad (30)$$

where u_{gr} is the interstitial velocity of gas relative to the bubble and A_b is the surface area of the bubble over which gas flows out of the bubble.

Since the voidage is assumed to be constant

$$q_b = \epsilon_{mf} \int_{A_b} u_{gr} \cdot n \; dA_b \qquad (31)$$

Nondimensionalizing, this becomes

$$Q_b = \epsilon_{mf} \int_{A_b^*} U_{gr} \cdot n \; dA_b^* \qquad (32)$$

where

$$Q_b = \frac{q_b}{u_b \; r_n^2} \qquad \text{and} \qquad A_b^* = \frac{A_b}{u_b \; r_n^2} \qquad (33)$$

Similarly, the flow rate of solids through the wake of the bubble can be obtained from

$$q_s = \int_{A_w} (1-\epsilon_{mf}) v_{pr} \cdot n \; dA_w \tag{34}$$

where v_{pr} is the relative velocity of the particulate phase with respect to the bubble and A_w is the surface area of the wake over which particles flow out of the wake. In nondimensional terms,

$$Q_s = (1-\epsilon_{mf}) \int_{A_w^*} V_{pr} \cdot n \; dA_w^* \tag{35}$$

where

$$Q_s = \frac{q_s}{u_b \; r_n^2} \qquad \text{and} \qquad A_w^* = \frac{A_w}{u_b \; r_n^2} \tag{36}$$

4. NUMERICAL FORMULATIONS

The finite element method was selected in this study to solve the governing equations for the particle velocity potential and the pressure at every time step. This method suits well to the present problem which involves a domain whose shape is changing due to the deforming free surface and, also, due to the fact that the bubble is at a different vertical location at each time step.

A commercial finite element solver, called TWODEPEP, developed by International Mathematical and Statistical Libraries, Inc.(IMSL) was used[21]. This software uses triangular finite elements and is capable of generating a mesh once the user supplies an initial triangulation which involves just as many elements as necessary to define the domain. The fineness of the final mesh can be adjusted by specifying the number of triangles and an element density function. In addition, the aspect ratio of the triangles to be generated in the final mesh is controlled by a user-supplied function. The software provides the flexibility for the points at which the output will be generated by leaving the option to the user to specify the points in the domain at which the output is wanted. Therefore, it is possible to obtain the

solution at any desired point of the domain. Furthermore, a selection of quadratic, cubic and quartic elements, with which the accuracy of the solution increases in that order, is available for use.

For the case of Laplace's equation, the governing equation in this analysis, the solution includes the derivatives of the function in the horizontal and the vertical directions, as well as the value of the function.

To verify the accuracy of the software, numerous calculations were carried out for a spherical bubble deep in the bed, and the results were compared to those obtained from the Davidson model. It was observed that the results were not within the acceptable range. After a number of trials and examination of the solutions, it was concluded that the software-generated mesh was not able to yield sufficiently accurate solutions. Hence, the mesh generation option of the software had to be abandoned.

In subsequent investigation of the literature, it was found that for accuracy, the triangles should be close to the equilateral state and long narrow triangles should be avoided[22]. Based on this information, mesh generation was done manually so that full control of the shape of the triangles was possible. Table 1 gives a

comparison of the components of the particle velocity from finite element solution and from the Davidson model. Also, in Figures 2 and 3, the Davidson and the finite element solutions, respectively, are plotted in terms of vector fields in the vicinity of the spherical bubble.

At each time step, the triangulation was modified to adapt to the new shape of the domain due to both the deforming free surface and also the new elevation of the bubble within the domain.

The time dependent portion of the problem was solved by employing the finite difference technique. Time is contained in equations (25) and (26) which express, respectively, the rates of change of the height of the free surface and the value of the particle velocity potential at the surface. In order to advance the variables to the next time step, it is necessary to write the above mentioned equations in terms of finite differences.

For the deformation equation,

$$\frac{\partial H}{\partial T} + V_r \frac{\partial H}{\partial R} = V_z$$

a forward-time centered-space implicit scheme was applied to give

$$\frac{H_i^{n+1} - H_i^n}{\Delta T} + V_{r_i}^n \frac{H_{i+1}^{n+1} - H_{i-1}^{n+1}}{\Delta R} = V_{z_i}^n \qquad (37)$$

where subscript i stands for the spatial points and

superscript n refers to the levels of time separated by the interval ΔT. This scheme is first order accurate in time and second order accurate in space. The unknowns are the values of the dimensionless deformation H at the new time step n+1. The rest of the variables in equation (37) are known from the present time step.

Rearranging equation (37) and collecting the terms at the new time level results in

$$-\Delta T V_{r_i} H_{i-1}^{n+1} + 2\Delta R H_i^{n+1} + \Delta T V_{r_i} H_{i+1}^{n+1} = 2\Delta R H_i^n + 2\Delta T \Delta R V_{z_i} \qquad (38)$$

Defining

$$b_i = -\Delta T V_{r_i}$$

$$d_i = 2\Delta R$$

$$a_i = \Delta T V_{r_i}$$

$$c_i = 2\Delta R \left(H_i^n + \Delta T V_{z_i} \right)$$

equation (38) reduces to

$$b_i H_{i-1}^{n+1} + d_i H_i^{n+1} + a_i H_{i+1}^{n+1} = c_i \qquad (39)$$

In the above notation, i=0 is the left end of the free surface, or the axial centerline, and i=M refers to the right end of the surface. Due to symmetry, the zero slope condition is valid at the centerline, or

$$\frac{\partial H}{\partial R} = 0 \qquad \text{at } i = 0$$

The same condition applies to the right end, assuming that it is far enough from the bubble(this issue is discussed in Chapter 6). Then

$$\frac{\partial H}{\partial R} = 0 \qquad \text{at } i = M$$

These two conditions are satisfied provided that

$$a_0 = 0$$

$$b_M = 0$$

Now, equation (39) may be written in the form

$$\begin{bmatrix} d_0 & 0 & 0 & \cdot & \cdot & \cdot & 0 \\ b_1 & d_1 & a_1 & & & & \cdot \\ 0 & b_2 & d_2 & a_2 & & & \cdot \\ \cdot & & & & & & \cdot \\ \cdot & & & & & & 0 \\ \cdot & & & & & b_{M-1} & d_{M-1} & a_{M-1} \\ 0 & \cdot & \cdot & \cdot & 0 & 0 & d_M \end{bmatrix} \begin{bmatrix} H_0^{n+1} \\ H_1^{n+1} \\ H_2^{n+1} \\ \cdot \\ \cdot \\ H_{M-1}^{n+1} \\ H_M^{n+1} \end{bmatrix} = \begin{bmatrix} c_0 \\ c_1 \\ c_2 \\ \cdot \\ \cdot \\ c_{M-1} \\ c_M \end{bmatrix} \qquad (40)$$

where equation (40) represents a tridiagonal system of linear algebraic equations[22]. This system was solved by applying the Thomas algorithm.

For the velocity potential equation, a first order explicit scheme was employed:

$$\frac{\Phi_i^{n+1} - \Phi_i^n}{\Delta T} = \frac{H_i^n}{1.5828 Fr} + \frac{1}{2}\left\{ (V_{ri}^n)^2 + (V_{ri}^n)^2 \right\} \qquad (41)$$

Rearranging, this becomes,

$$\Phi_i^{n+1} = \Phi_i^n + \Delta T \left(\frac{H_i^n}{1.5828 Fr} + \frac{1}{2}\left\{ (V_{ri}^n)^2 + (V_{ri}^n)^2 \right\} \right) \qquad (42)$$

Solutions of equations (40) and (42) define, respectively, the shape of the free surface and the velocity potential at the surface, for the new time time step in terms of values at discrete points throughout the free surface. However, it is necessary to express these two variables as smooth continuous functions in order to implement them to the finite element software. Thus, there is a need to fit curves to the deformation and to the velocity potential.

Polynomials with degrees up to 11 were tried for this purpose, and it was observed that no single curve was able represent the variable all along the free surface. Hence, a combination of polynomials was used.

Going through an extensive trial procedure, polynomials with degrees ranging from three to nine were employed in order to cover the entire free surface. As shown in Figure 4 a ninth order polynomial was used for the region where the function has a steep gradient, a seventh order curve for the region where the function has its minimum, and a fourth order curve for the region where the function is relatively flat. These curves were smoothly connected by cubic polynomials satisfying the continuity of the function and the first derivative. It should be noted that the discontinuity of the curve in

Figure 4 is due to the fact that different magnification factors were employed to make the visualization of the sections away from the centerline easier. Care was taken to satisfy the zero slope condition at the ends and this is accomplished by excluding the first order terms in those polynomials.

5. SOLUTION ALGORITHM

The time dependent nature of the problem coupled with the fact that the solution domain does have a different shape at each time level, necessitates a step-by-step process. In other words, the results of any given time level will determine the shape of the domain and the boundary condition on the top edge for the next time step.

The outline of the solution algorithm follows.

1. Compute the particle velocity field.

At every time step, it was first necessary to create the domain using the information from the previous time step, and then generate the mesh. Here, care was taken to make the elements as close to equilateral as possible, a condition required for accuracy. Also, the mesh generation process was started at the bubble boundary with the element density decreasing radially outwards. In this way, the resulting mesh was finer in the vicinity of the bubble which increased the accuracy. Furthermore, as the bubble approached the free surface, the fine mesh region was extended towards the surface, eventually covering the entire bulge region in the last stages of calculations. The typical mesh dimension l at the bubble surface was of order $l/r_n \sim 1/2$ for a bubble deep in the

bed. The smallest mesh size was used in the bulge region for a bubble at the last stages of eruption. In this case $l/r_n \sim 1/8$. Shown in Figure 5 is the sketch of the finite element mesh in the vicinity of the bubble at the last stage of the computation.

Next, an input file to TWODEPEP was created to obtain the solution for the particle motion.

TWODEPEP then solves the governing equation

$$\nabla^2\Phi = 0$$

subject to the boundary conditions(shown in Fig.6)

free surface	:	$\Phi = \Phi^n$
surface of bubble	:	$\frac{\partial\Phi}{\partial n} = -\mathrm{Cos}\theta$
bottom edge	:	$\frac{\partial\Phi}{\partial Z} = 0$
centerline and right edge	:	$\frac{\partial\Phi}{\partial R} = 0$

The TWODEPEP solution includes the values of the velocity potential Φ, and the particle velocity in the R and Z directions.

2. Compute the pressure distribution.

The shape of the domain and the governing equation for the pressure field are the same as in the case of the velocity potential. Therefore, the same mesh may be used with proper replacement of the boundary conditions.

The governing equation is once again Laplace's

equation,

$$\nabla^2 P = 0$$

subject to the following boundary conditions:

free surface	:	$P = 0$
surface of bubble	:	$P = P_b$
centerline	:	$\frac{\partial P}{\partial R} = 0$
bottom and right edge	:	$P = Z_0 + H - Z$

where P_b is the constant pressure in the bubble. This is based on the assumption that at any instant of time the spatial variations of pressure within the bubble are very small compared to the variations in the surrounding emulsion phase. Hence, the pressure inside the bubble is only a function of time. The domain and the boundary conditions for pressure are shown in Figure 7, and the derivation of the boundary condition for the bottom and right edges is given in Appendix A.

The TWODEPEP solution contains the values of the pressure as well as the pressure gradients in the R and Z directions.

3. Calculate the gas velocity.

The interstitial gas velocity is now calculated by substituting the particle velocities from step(1) and the pressure gradients from step(2) into the expression for Darcy's law,

$$U_g = V_p - K\nabla P$$

The values of the dimensionless ratio K are chosen to cover both the slow bubble range(K>1) and the fast bubble range(K<1).

At this point it should be emphasized that, for a given value of K, the gas velocity obtained from the above equation must satisfy the principle of conservation of mass applied on the bubble. In other words, the gas flow rate into the bubble has to be equal to the gas flow rate out of the bubble. Hence, it is necessary to go through an iterative procedure to determine the bubble pressure P_b for which the resulting gas flow field yields a zero net gas flow through the bubble. Thus, at each time level, steps (2) and (3) are repeated for different values of P_b until conservation of mass is satisfied.

4. Advance deformation and velocity potential at the surface to the next time step n+1.

Finite difference equations (40) and (42) are now employed to calculate the shape of the free surface and the value of the velocity potential on the surface at the next time step n+1. The size of the time increment ΔT is selected based on Chen's analysis[17] in which he tried different ΔT values and determined the time step size which gave stable solutions. Taking into account that in

this analysis an implicit scheme is used for the deformation equation as opposed to the explicit scheme used by Chen, the same time increments, modified to include the effect of different reference length, were employed and the stability of the solutions was confirmed. Time increments, expressed in terms of the change in the dimensionless vertical position of the bubble, ranged from $\Delta Z_c=1.0$ for a bubble deep within the bed at $Z_c=34.0$, to $\Delta Z_c=0.1$ for a bubble at the last stages of eruption.

5. Fit curves to deformation and velocity potential.

Once the new values of the deformation and the velocity potential are obtained in step (4) at discrete points throughout the free surface, a least-square curve fitting method is then applied to express each of the two variables as a function consisting of a set of smoothly joined polynomials.

This step completes the information required to start the procedure at the new time level, for which the bubble is moved vertically upward a distance Δz given by

$$\Delta z = u_b \times \Delta t$$

or in dimensionless terms

$$\Delta Z = \Delta T$$

The starting point of the analysis was determined

based on Chen's[17] results. He started his calculations for a spherical bubble located midway between the bottom and top surfaces in a bed having a depth of 20 bubble diameters. His results did not indicate any significant effect of the bubble on the free surface until the bubble center was within 3 diameters of the free surface. In this study, the initial elevation of the bubble was taken as 34 r_n, or 6 r_n from the free surface which corresponds approximately to 17 d_b in Chen's analysis. Figure 8 shows the dimensions and the boundaries of the solution domain at the beginning of the calculations.

6. RESULTS AND DISCUSSION

In this study, a cylindrical domain with a diameter of 40 r_n and a depth of 40 r_n was selected. This selection is based on Radcliff's analysis[16] in which he carried out calculations with different domain sizes and compared the results to those obtained from the Davidson theory. The initial location of the bubble was taken as 6 r_n from the free surface of the bed(see Chapter 5). Bubble velocity was assumed to be constant with only a vertical component. Also, the size of the bubble was fixed all along its course of ascent. The value of the Froude number was 0.50552 which corresponds to conditions near minimum fluidization. The bubble was moved toward the free surface in 14 separate time steps of decreasing step size Δt.

The results presented here are identified with the instantaneous vertical position of the effective bubble center, Z_C. This characterizes the time-variable for the transient process. The calculations were started at Z_C=34.0 and terminated at Z_C=39.3.

In order to verify the accuracy of the finite element software, calculations were first carried out for a spherical bubble of radius r_b deep in the bed. The bed was 40 r_b in diameter and 40 r_b in depth. The bubble was

located on the centerline, midway between the top and the bottom surfaces. The components of the particle velocity were computed throughout the domain and the results were compared to the Davidson analytical solution. Figures 2 and 3 are the plots of the particle velocity in the vicinity of the bubble, obtained from the Davidson theory and the finite element method, respectively. The comparison is presented also in tabulated form in Tables 1 and 2. Table 1 lists the values of the components of the particle velocity for points located on the surface of the bubble. In Table 2, results at various points in the domain are compared. These Tables indicate that, with the exception of the points where there is a discontinuity in the boundary condition, the finite element solution approximates the Davidson theory with an error which is, in general, less than 5 %.

The region between the bubble and the free surface is critical in understanding the elutriation phenomenon. Figure 9 depicts the development of the dome at the free surface in relation to the location of the bubble. Once it starts, the deformation of the free surface progresses quite rapidly. Table 3 lists the location of the bubble and the corresponding deformation at the bubble centerline for all the computational time steps. It is

seen that the centerline deformation is less than 10 % of r_n until the effective center is within 2 r_n of the free surface. It should be noted that the undeformed position of the free surface corresponds to Z_C=40.0. The motion of the emulsion phase is illustrated in terms of vector fields in Figures 10 to 25. Figures 10-19 display the variation of the particle flow for five different locations of the bubble, Z_C=34.0, 37.0, 38.4, 39.0, 39.3. It is observed that the magnitude of the particle velocity diminishes rapidly with distance away from the bubble. At the nose of the bubble, the particles are pushed upward. In the region behind the bubble, the particulate phase moves to fill the space being displaced by the bubble. Another interesting feature of the particle motion is noticed when these sequential pictures are compared: the flow field exhibits a circulating pattern around the bubble when the bubble is relatively deep in the bed. As the bubble nears the free surface, however, the direction of the particle velocity turns toward the bubble in a region of radius of about R=3. The relative velocity of the emulsion phase with respect to the bubble is presented in Figures 20-25.

The behavior of the motion of the particulate phase at the free surface is examined in detail as it pertains

to the ejection of the bed material into the freeboard. As shown in Figure 26, there is a considerable increase in the vertical component of the particle velocity, especially when the bubble is within 2 r_n of the free surface. The maximum value occurs at the centerline and drops sharply with radial distance. Since the deformation is related to the particle velocity via equation (11), this figure implies a similar variation for the shape of the free surface. In fact, the deformation of the free surface, plotted in Figures 27 and 28, displays a very similar behavior. Hence, it can be concluded that the vertical component of the particle velocity is the dominant parameter governing the displacement of the free surface. As illustrated in Figures 27 and 28, the deformation, too, has a steep decrease until R=2, and soon after that it becomes negative. This is, clearly, necessary in order to satisfy the conservation of mass for the bed material across the undisturbed level of the surface of the bed. The characteristic shape of the free surface where the displacement is negative can be viewed from the magnified plot of Figure 4.

The gas flow is presented in Figures 29–52. These pictures display the relative gas velocity with respect to the bubble for three values of the bubble location,

Z_c=34.0,38.6,39.3 and four values of the interstitial gas velocity far from the bubble, ranging from K=0.01 to K=10.0. These figures indicate that the radial component of the gas velocity is significant only in the immediate vicinity of the bubble, hence, the vertical component, in general, dominates the gas flow field. In the case of a fast bubble(K < 1), Figures 29-40, the gas flow is downward with respect to the bubble throughout the flow field except in the region close to the bubble where it exhibits a recirculating pattern. For slow bubbles (K > 1), Figures 47-52, the gas flows upwards; it enters the bubble from below, and leaves around the top of the bubble. Another feature that can be noticed is that the magnitude of the gas velocity shows a drastic variation on the section of the bubble surface below the horizontal line passing through the effective bubble center(indicated in Figure 48 as the region between points A and B).

In order to illustrate the characteristics of the gas motion at the free surface more clearly, the spatial and time-wise variations of the vertical component of the absolute interstitial gas velocity is plotted in Figures 53-58 for all values of K used in this analysis. For K<1(fast bubble), the velocity profile has the

characteristic shape with the maximum at the centerline and decreasing smoothly with radial distance(Figures 53 and 54) except for the apparent shift of the peak value off the centerline for K=0.5 and Z_C=39.3(Figure 55). In the slow bubble regime(K>1), the velocity profile becomes more irregular. As shown in Figure 56, for K=1.1 the peak value for Z_C=39.3 is smaller than the maximum for Z_C=39.0, which is shifted off-centerline, as well. As K increases, the profiles for Z_C=39.3 and Z_C=39.0 begin to show an increasingly irregular behavior near the centerline before reaching an asymptotic value around R=3.0(Figures 57 and 58).

In order to be able to identify the reasons underlying this behavior of the gas velocity profile, it is necessary to consider the relative effects of the terms, in equation (24), which make up the gas velocity. For Z_C=39.3, the variation of the pressure gradient in the vertical direction at the free surface is plotted in Figures 59-61 for K=0.01, K=0.5 and K=10.0, respectively. Here, it should be stressed that the value of K affects the pressure gradient, indirectly, through the requirement of conservation of mass. It is observed that the pressure gradient follows essentially the same trend in both cases. However, the contribution of the

pressure gradient as compared to that of the particle velocity on the gas velocity is substantially different as demonstrated in Tables 4-6, which list the magnitudes of the terms in equation (24) at radial positions up to R=5.0, for K=0.01, K=0.5 and K=10.0, respectively. The columns, from left to right, are the radial distance from centerline, the vertical component of the particle velocity, the pressure gradient term(i.e. the product of $-K$ and $\partial P/\partial Z$), and the vertical component of the gas velocity. These Tables indicate that for K=0.01(Table 4), the gas velocity is determined primarily by the particle velocity, whereas for K=10.0(Table 6), the pressure gradient is the dominant term. For K=0.5, the two terms have comparable contributions(Table 5). Therefore, it follows that it is the pressure gradient which is responsible for the behavior of the gas velocity in Figure 58. The profile in Figure 53, on the other hand, is very similar to the behavior of the vertical particle velocity in Figure 26, as expected.

In the calculation of the gas flow field, the bubble pressure was selected so as to satisfy the conservation of mass through the bubble. The proper value of the bubble pressure was determined in an iterative procedure. The gas flow rates into and out of the bubble were

calculated for different values of the bubble pressure, and the iterations were continued until the difference between the two flow rates dropped to less than 1 % of the mean value. The pressures for which the conservation of mass is satisfied are tabulated in Table 7.

The flow rate of gas through the bubble was then calculated using the proper value of the pressure inside the bubble. The values of the gas velocity at 226 points (equally spaced on each of the 5 arcs of the bubble, by an angular interval of 1°, ensuring smaller area elements in the regions of sharp variations) on the boundary of the bubble were used in the numerical integration. The results are listed in Table 8. For the course of the motion of the bubble considered in this study, the gas flow rate first increases as the bubble approaches the free surface, and then decreases. This is the case for all values of K. These results combined with those regarding the behavior of the gas velocity at the surface in the vicinity of the bubble centerline suggest that the resistance to the gas flow of the bed material in the bulge region starts to increase after the bubble passes a certain elevation along its course of rise.

Figure 62 shows the symmetric portion of the boundary of the wake, in relation to the bubble, used as

the control volume in the calculation of the flow rate of solid particles through the wake. The volume fraction of the wake is 17.6 %(See Appendix B). 54 equally spaced points were employed in the numerical integration. Table 9 shows the results in the form of $Q_s/(1-\epsilon_{mf})$ as a function of the bubble location. Figure 63 illustrates the vectors of particle velocity relative to the bubble on the boundary of the wake. There is a total decrease of approximately 10 % between the lowest and the highest elevations of the bubble. Hence, it seems that the presence of the free surface has only a slight effect in the wake region even when the bubble is very close to the surface.

7. CONCLUSIONS AND RECOMMENDATIONS

The shape of the free surface, gas flow rates through the bubble and the flow rate of solid particles through the wake of the bubble were calculated as a kidney-shaped bubble was moved upward in a gas-fluidized fluidized bed. The analysis was performed assuming an incompressible inviscid particle phase and an incompressible gas phase, and using Darcy's law to relate the two phases. The resulting equations were solved by a combination of finite element and finite difference methods.

In summary, the following conclusions can be drawn from the results:

- The gas flow rate through the bubble first increases and when the bubble reaches a certain elevation, it starts to decrease.
- Drastic changes in the behavior of the gas flow in the bulge region occurs when the bubble is very close to the free surface.
- The gas flow field is a strong function of the value of K.
- The flow rate of solid particles through the wake decreases only slightly as the bubble rises.

The results presented here are based on several simplifying assumptions. Improvements can be made to build a more realistic model. Recommendations for future work may be listed as:

1. Allow the shape and the size of the bubble to vary,
2. Use different wake fractions to determine its effect on the solids flow rate,
3. Consider variations in voidage, particularly in the bulge region,

Also, experimental work is needed in order to verify these results.

Table 1. Comparison of the finite element solution for the components of particle velocity with the Davidson solution for points on the bubble.

R	Z	VPR		VPZ	
COORD	COORD	DAVIDSON	NUMERIC	DAVIDSON	NUMERIC
.0000E+00	.1000E+01	.0000E+00	-.2974E-02	.1000E+01	.9968E+00
.1305E+00	.9914E+00	.1941E+00	.1896E+00	.9744E+00	.9785E+00
.2588E+00	.9659E+00	.3750E+00	.3779E+00	.8995E+00	.9051E+00
.3827E+00	.9239E+00	.5303E+00	.5364E+00	.7803E+00	.7804E+00
.5000E+00	.8660E+00	.6495E+00	.6496E+00	.6250E+00	.6273E+00
.6088E+00	.7934E+00	.7244E+00	.7198E+00	.4441E+00	.4451E+00
.7071E+00	.7071E+00	.7500E+00	.7550E+00	.2500E+00	.2507E+00
.7934E+00	.6088E+00	.7244E+00	.7307E+00	.5589E-01	.5516E-01
.8660E+00	.5000E+00	.6495E+00	.6587E+00	-.1250E+00	-.1144E+00
.9239E+00	.3827E+00	.5303E+00	.5258E+00	-.2803E+00	-.2802E+00
.9659E+00	.2588E+00	.3750E+00	.3770E+00	-.3995E+00	-.4028E+00
.9914E+00	.1305E+00	.1941E+00	.1980E+00	-.4744E+00	-.4758E+00
.1000E+01	.1327E-05	.1990E-05	.1839E-01	-.5000E+00	-.4938E+00
.9915E+00	-.1305E+00	-.1941E+00	-.1980E+00	-.4744E+00	-.4758E+00
.9659E+00	-.2588E+00	-.3750E+00	-.3770E+00	-.3995E+00	-.4028E+00
.9239E+00	-.3827E+00	-.5303E+00	-.5258E+00	-.2803E+00	-.2802E+00
.8660E+00	-.5000E+00	-.6495E+00	-.6253E+00	-.1250E+00	-.1291E+00
.7934E+00	-.6088E+00	-.7244E+00	-.7307E+00	.5588E-01	.5515E-01
.7071E+00	-.7071E+00	-.7500E+00	-.7550E+00	.2500E+00	.2507E+00
.6088E+00	-.7934E+00	-.7245E+00	-.7198E+00	.4441E+00	.4451E+00
.5000E+00	-.8660E+00	-.6495E+00	-.6336E+00	.6250E+00	.6131E+00
.3827E+00	-.9239E+00	-.5303E+00	-.5364E+00	.7803E+00	.7804E+00
.2588E+00	-.9659E+00	-.3750E+00	-.3780E+00	.8995E+00	.9051E+00
.1305E+00	-.9914E+00	-.1941E+00	-.1896E+00	.9744E+00	.9785E+00
.2654E-05	-.1000E+01	-.3980E-05	.2970E-02	.1000E+01	.9968E+00

Table 2. Comparison of the finite element solution for the components of particle velocity with the Davidson solution for various points in the domain.

R	Z	VPR		VPZ	
COORD	COORD	DAVIDSON	NUMERIC	DAVIDSON	NUMERIC
.6945E+00	.1039E+01	.3548E+00	.3487E+00	.2750E+00	.2727E+00
.1121E+01	-.5529E+00	-.3047E+00	-.2997E+00	-.1058E+00	-.1050E+00
.5740E+00	.1386E+01	.1571E+00	.1528E+00	.2312E+00	.2198E+00
.1449E+01	-.3882E+00	-.1111E+00	-.9880E-01	-.1184E+00	-.1202E+00
.3902E+00	.1962E+01	.3588E-01	.3635E-01	.1179E+00	.1154E+00
.1996E+01	-.1308E+00	-.1224E-01	-.1272E-01	-.6170E-01	-.6084E-01
.1308E+00	-.1996E+01	-.1224E-01	-.8902E-02	.1242E+00	.1246E+00
.2479E+01	.3263E+00	.1242E-01	.1387E-01	-.3036E-01	-.3038E-01
.6471E+00	-.2415E+01	-.2400E-01	-.2341E-01	.5757E-01	.5413E-01
.2841E+01	.9643E+00	.1691E-01	.1794E-01	-.1278E-01	-.1303E-01
.1327E+01	-.2691E+01	-.2204E-01	-.2357E-01	.2617E-01	.2635E-01
.3464E+01	.2000E+01	.1015E-01	.9723E-02	-.1953E-02	-.2001E-02
.2435E+01	-.3173E+01	-.1132E-01	-.1097E-01	.6939E-02	.6160E-02
.3759E+01	.3297E+01	.5949E-02	.5938E-02	.1217E-02	.1389E-02
.3759E+01	-.3297E+01	-.5949E-02	-.5940E-02	.1217E-02	.1386E-02
.3653E+01	.4760E+01	.3354E-02	.3388E-02	.2056E-02	.1920E-02
.5196E+01	-.3000E+01	-.3007E-02	-.3004E-02	-.5787E-03	-.7039E-03
.3538E+01	.7175E+01	.1162E-02	.1211E-02	.1380E-02	.1292E-02
.7575E+01	-.2572E+01	-.8917E-03	-.9205E-03	-.6739E-03	-.7897E-03
.2588E+01	.9659E+01	.3750E-03	.3692E-03	.8995E-03	.7972E-03
.9915E+01	-.1305E+01	-.1941E-03	-.2043E-03	-.4744E-03	-.5776E-03
.7848E+00	.1197E+02	.5665E-04	.5535E-04	.5750E-03	.5158E-03
.1197E+02	.7849E+00	.5665E-04	.5509E-04	-.2856E-03	-.4025E-03
.2341E+01	-.1177E+02	-.1661E-03	-.1652E-03	.5457E-03	.4523E-03
.1352E+02	.3624E+01	.1367E-03	.1229E-03	-.1456E-03	-.2653E-03

Table 3. The Deformation of the Free Surface at the Bubble Centerline as a Function of the Position of the Bubble.

position of bubble, Z_c	centerline deformation, H_{cl}
34.0	0.0000
35.0	0.0058
36.0	0.0160
37.0	0.0402
37.5	0.0721
38.0	0.1295
38.2	0.1727
38.4	0.2297
38.6	0.3044
38.8	0.4011
39.0	0.5225
39.1	0.5957
39.2	0.6754
39.3	0.7614

Table 4. Effects of the particle velocity and the pressure gradient on the gas velocity for K=0.01

R	VY	-K*PY	UY
.0000E+00	.9192E+00	.5305E-02	.9245E+00
.1000E+00	.9167E+00	.5511E-02	.9222E+00
.2000E+00	.9083E+00	.5796E-02	.9141E+00
.3000E+00	.8960E+00	.6192E-02	.9022E+00
.4000E+00	.8767E+00	.6597E-02	.8833E+00
.5000E+00	.8490E+00	.6857E-02	.8559E+00
.6000E+00	.8120E+00	.7037E-02	.8190E+00
.7000E+00	.7626E+00	.7070E-02	.7697E+00
.8000E+00	.7027E+00	.7003E-02	.7097E+00
.9000E+00	.6298E+00	.6796E-02	.6366E+00
.1000E+01	.5532E+00	.6626E-02	.5598E+00
.1100E+01	.4767E+00	.6561E-02	.4833E+00
.1200E+01	.4018E+00	.6607E-02	.4084E+00
.1300E+01	.3298E+00	.6766E-02	.3366E+00
.1400E+01	.2650E+00	.6971E-02	.2719E+00
.1500E+01	.2069E+00	.7277E-02	.2141E+00
.1600E+01	.1552E+00	.7631E-02	.1629E+00
.1700E+01	.1127E+00	.8020E-02	.1207E+00
.1800E+01	.8028E-01	.8395E-02	.8867E-01
.1900E+01	.5403E-01	.8745E-02	.6278E-01
.2000E+01	.3289E-01	.9043E-02	.4194E-01
.2100E+01	.1512E-01	.9306E-02	.2442E-01
.2200E+01	.9470E-03	.9528E-02	.1048E-01
.2300E+01	-.9515E-02	.9709E-02	.1943E-03
.2400E+01	-.1653E-01	.9867E-02	-.6666E-02
.2500E+01	-.1982E-01	.9932E-02	-.9883E-02
.2600E+01	-.2185E-01	.9964E-02	-.1189E-01
.2700E+01	-.2319E-01	.9983E-02	-.1321E-01
.2800E+01	-.2383E-01	.9990E-02	-.1384E-01
.2900E+01	-.2378E-01	.9983E-02	-.1379E-01
.3000E+01	-.2304E-01	.9965E-02	-.1307E-01
.3100E+01	-.2162E-01	.9935E-02	-.1169E-01
.3200E+01	-.2026E-01	.9918E-02	-.1034E-01
.3300E+01	-.2126E-01	.9962E-02	-.1130E-01
.3400E+01	-.2157E-01	.9979E-02	-.1159E-01
.3500E+01	-.2178E-01	.9993E-02	-.1179E-01
.3600E+01	-.2190E-01	.1001E-01	-.1190E-01
.3700E+01	-.2193E-01	.1002E-01	-.1191E-01
.3800E+01	-.2186E-01	.1003E-01	-.1184E-01
.3900E+01	-.2170E-01	.1003E-01	-.1166E-01
.4000E+01	-.2144E-01	.1004E-01	-.1140E-01
.4100E+01	-.2108E-01	.1004E-01	-.1104E-01
.4200E+01	-.2064E-01	.1004E-01	-.1060E-01
.4300E+01	-.2010E-01	.1004E-01	-.1006E-01
.4400E+01	-.1967E-01	.1004E-01	-.9631E-02
.4500E+01	-.1920E-01	.1004E-01	-.9155E-02
.4600E+01	-.1874E-01	.1004E-01	-.8703E-02
.4700E+01	-.1828E-01	.1004E-01	-.8240E-02
.4800E+01	-.1781E-01	.1004E-01	-.7766E-02
.4900E+01	-.1732E-01	.1004E-01	-.7282E-02
.5000E+01	-.1683E-01	.1004E-01	-.6787E-02

Table 5. Effects of the particle velocity and the pressure gradient on the gas velocity for K=0.5

R	VY	-K*PY	UY
.0000E+00	.9192E+00	.3414E+00	.1261E+01
.1000E+00	.9167E+00	.3546E+00	.1271E+01
.2000E+00	.9083E+00	.3729E+00	.1281E+01
.3000E+00	.8960E+00	.3984E+00	.1294E+01
.4000E+00	.8767E+00	.4242E+00	.1301E+01
.5000E+00	.8490E+00	.4405E+00	.1290E+01
.6000E+00	.8120E+00	.4515E+00	.1263E+01
.7000E+00	.7626E+00	.4524E+00	.1215E+01
.8000E+00	.7027E+00	.4458E+00	.1149E+01
.9000E+00	.6298E+00	.4293E+00	.1059E+01
.1000E+01	.5532E+00	.4134E+00	.9666E+00
.1100E+01	.4767E+00	.4025E+00	.8792E+00
.1200E+01	.4018E+00	.3970E+00	.7988E+00
.1300E+01	.3298E+00	.3972E+00	.7270E+00
.1400E+01	.2650E+00	.3995E+00	.6644E+00
.1500E+01	.2069E+00	.4078E+00	.6147E+00
.1600E+01	.1552E+00	.4192E+00	.5744E+00
.1700E+01	.1127E+00	.4332E+00	.5459E+00
.1800E+01	.8028E-01	.4475E+00	.5278E+00
.1900E+01	.5403E-01	.4613E+00	.5154E+00
.2000E+01	.3289E-01	.4729E+00	.5058E+00
.2100E+01	.1512E-01	.4831E+00	.4982E+00
.2200E+01	.9470E-03	.4917E+00	.4926E+00
.2300E+01	-.9515E-02	.4986E+00	.4890E+00
.2400E+01	-.1653E-01	.5048E+00	.4882E+00
.2500E+01	-.1982E-01	.5067E+00	.4869E+00
.2600E+01	-.2185E-01	.5071E+00	.4852E+00
.2700E+01	-.2319E-01	.5069E+00	.4837E+00
.2800E+01	-.2383E-01	.5063E+00	.4824E+00
.2900E+01	-.2378E-01	.5052E+00	.4814E+00
.3000E+01	-.2304E-01	.5035E+00	.4805E+00
.3100E+01	-.2162E-01	.5014E+00	.4798E+00
.3200E+01	-.2026E-01	.5001E+00	.4798E+00
.3300E+01	-.2126E-01	.5020E+00	.4807E+00
.3400E+01	-.2157E-01	.5025E+00	.4809E+00
.3500E+01	-.2178E-01	.5029E+00	.4811E+00
.3600E+01	-.2190E-01	.5033E+00	.4813E+00
.3700E+01	-.2193E-01	.5035E+00	.4816E+00
.3800E+01	-.2186E-01	.5037E+00	.4818E+00
.3900E+01	-.2170E-01	.5039E+00	.4822E+00
.4000E+01	-.2144E-01	.5039E+00	.4825E+00
.4100E+01	-.2108E-01	.5039E+00	.4828E+00
.4200E+01	-.2064E-01	.5038E+00	.4832E+00
.4300E+01	-.2010E-01	.5037E+00	.4836E+00
.4400E+01	-.1967E-01	.5036E+00	.4839E+00
.4500E+01	-.1920E-01	.5035E+00	.4843E+00
.4600E+01	-.1874E-01	.5034E+00	.4846E+00
.4700E+01	-.1828E-01	.5033E+00	.4850E+00
.4800E+01	-.1781E-01	.5032E+00	.4853E+00
.4900E+01	-.1732E-01	.5031E+00	.4857E+00
.5000E+01	-.1683E-01	.5030E+00	.4861E+00

Table 6. Effects of the particle velocity and the pressure gradient on the gas velocity for K=10.0

R	VY	-K*PY	UY
.0000E+00	.9192E+00	.6861E+01	.7780E+01
.1000E+00	.9167E+00	.7127E+01	.8044E+01
.2000E+00	.9083E+00	.7495E+01	.8403E+01
.3000E+00	.8960E+00	.8006E+01	.8902E+01
.4000E+00	.8767E+00	.8525E+01	.9401E+01
.5000E+00	.8490E+00	.8854E+01	.9703E+01
.6000E+00	.8120E+00	.9074E+01	.9886E+01
.7000E+00	.7626E+00	.9092E+01	.9855E+01
.8000E+00	.7027E+00	.8959E+01	.9661E+01
.9000E+00	.6298E+00	.8626E+01	.9255E+01
.1000E+01	.5532E+00	.8304E+01	.8857E+01
.1100E+01	.4767E+00	.8083E+01	.8559E+01
.1200E+01	.4018E+00	.7970E+01	.8371E+01
.1300E+01	.3298E+00	.7970E+01	.8300E+01
.1400E+01	.2650E+00	.8012E+01	.8277E+01
.1500E+01	.2069E+00	.8175E+01	.8382E+01
.1600E+01	.1552E+00	.8400E+01	.8555E+01
.1700E+01	.1127E+00	.8679E+01	.8791E+01
.1800E+01	.8028E-01	.8962E+01	.9043E+01
.1900E+01	.5403E-01	.9237E+01	.9291E+01
.2000E+01	.3289E-01	.9468E+01	.9500E+01
.2100E+01	.1512E-01	.9670E+01	.9685E+01
.2200E+01	.9470E-03	.9840E+01	.9841E+01
.2300E+01	-.9515E-02	.9977E+01	.9967E+01
.2400E+01	-.1653E-01	.1010E+02	.1008E+02
.2500E+01	-.1982E-01	.1014E+02	.1012E+02
.2600E+01	-.2185E-01	.1015E+02	.1012E+02
.2700E+01	-.2319E-01	.1014E+02	.1012E+02
.2800E+01	-.2383E-01	.1013E+02	.1010E+02
.2900E+01	-.2378E-01	.1011E+02	.1008E+02
.3000E+01	-.2304E-01	.1007E+02	.1005E+02
.3100E+01	-.2162E-01	.1003E+02	.1001E+02
.3200E+01	-.2026E-01	.1000E+02	.9984E+01
.3300E+01	-.2126E-01	.1004E+02	.1002E+02
.3400E+01	-.2157E-01	.1005E+02	.1003E+02
.3500E+01	-.2178E-01	.1006E+02	.1004E+02
.3600E+01	-.2190E-01	.1007E+02	.1004E+02
.3700E+01	-.2193E-01	.1007E+02	.1005E+02
.3800E+01	-.2186E-01	.1008E+02	.1005E+02
.3900E+01	-.2170E-01	.1008E+02	.1006E+02
.4000E+01	-.2144E-01	.1008E+02	.1006E+02
.4100E+01	-.2108E-01	.1008E+02	.1006E+02
.4200E+01	-.2064E-01	.1008E+02	.1006E+02
.4300E+01	-.2010E-01	.1007E+02	.1005E+02
.4400E+01	-.1967E-01	.1007E+02	.1005E+02
.4500E+01	-.1920E-01	.1007E+02	.1005E+02
.4600E+01	-.1874E-01	.1007E+02	.1005E+02
.4700E+01	-.1828E-01	.1007E+02	.1005E+02
.4800E+01	-.1781E-01	.1006E+02	.1005E+02
.4900E+01	-.1732E-01	.1006E+02	.1004E+02
.5000E+01	-.1683E-01	.1006E+02	.1004E+02

Table 7. Bubble Pressure for Which Conservation of Mass is Satisfied through the Bubble.

	P_b					
Z_c	K=0.01	K=0.1	K=0.5	K=1.1	K=3.0	K=10.0
34.0	5.910	5.846	5.839	5.839	5.839	5.839
37.0	2.120	2.680	2.730	2.738	2.741	2.742
38.4	1.030	1.550	1.598	1.604	1.606	1.610
38.6	1.192	1.183	1.183	1.183	1.183	1.183
39.0	0.770	0.829	0.834	0.835	0.835	0.835
39.3	0.473	0.600	0.609	0.610	0.611	0.612

Table 8. Gas Flow Rate Through the Bubble as a function of the Bubble Position and K

Z_c	Q_b/ϵ_{mf}					
	K=0.01	K=0.1	K=0.5	K=1.1	K=3.0	K=10.0
34.0	0.112	0.643	3.114	6.821	18.56	61.80
37.0	0.190	0.639	3.062	6.700	18.23	60.72
38.4	0.196	0.719	3.465	7.588	20.64	68.75
38.6	0.135	0.575	2.907	6.411	17.50	58.38
39.0	0.139	0.560	2.813	6.197	16.91	56.39
39.3	0.116	0.524	2.644	5.825	15.90	53.05

Table 9. The Flow Rate of Solids Through the Wake of the Bubble.

position of bubble, Z_c	solids flow rate, $Q_s/(1-\epsilon_{mf})$
34.0	0.26763
35.0	0.26526
36.0	0.26508
37.0	0.26447
37.5	0.26370
38.0	0.26216
38.2	0.26111
38.4	0.25951
38.6	0.25786
38.8	0.25540
39.0	0.25285
39.1	0.25014
39.2	0.24778
39.3	0.24453

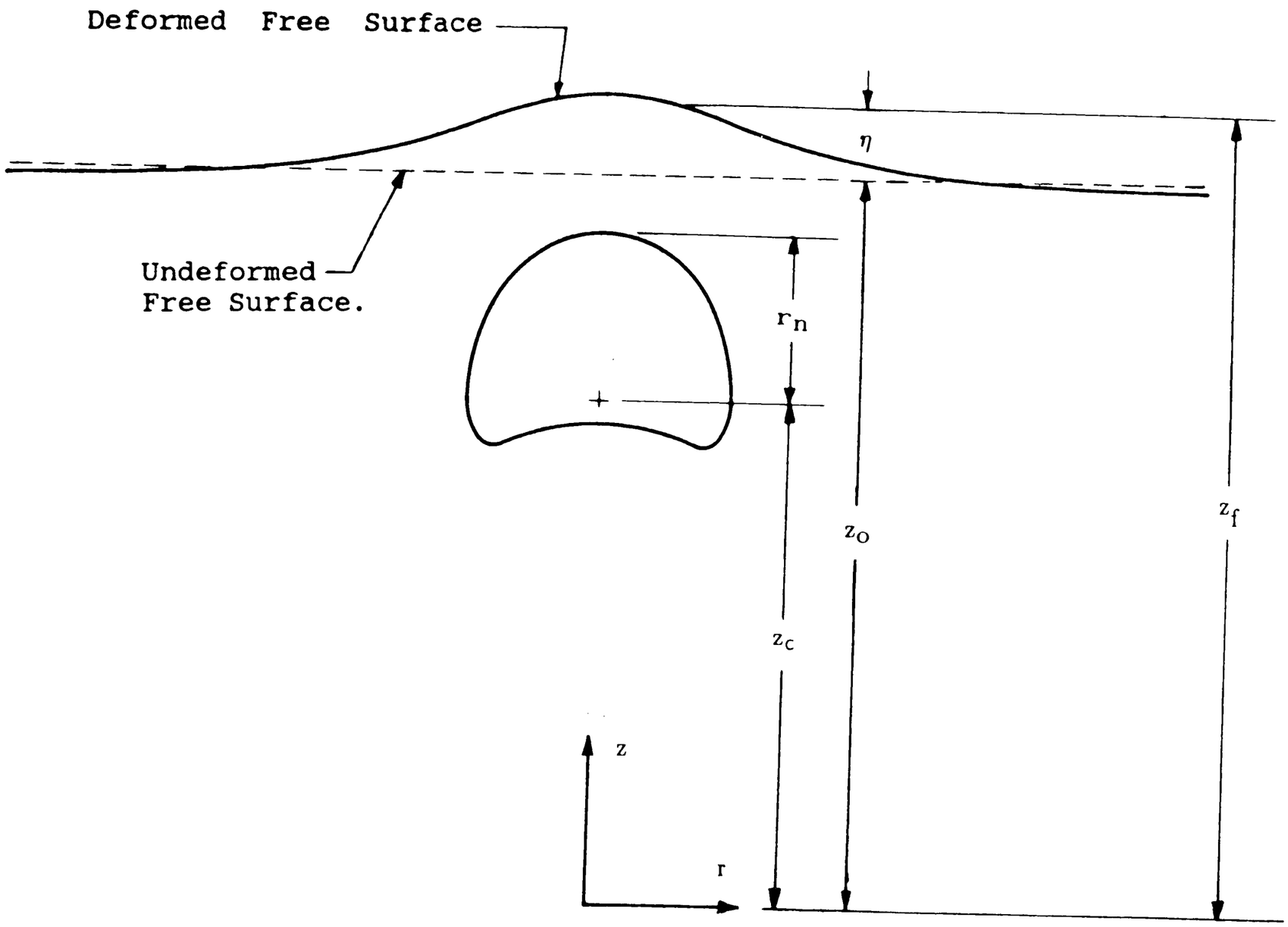

Figure 1. Coordinate system and parameters used in governing equations.

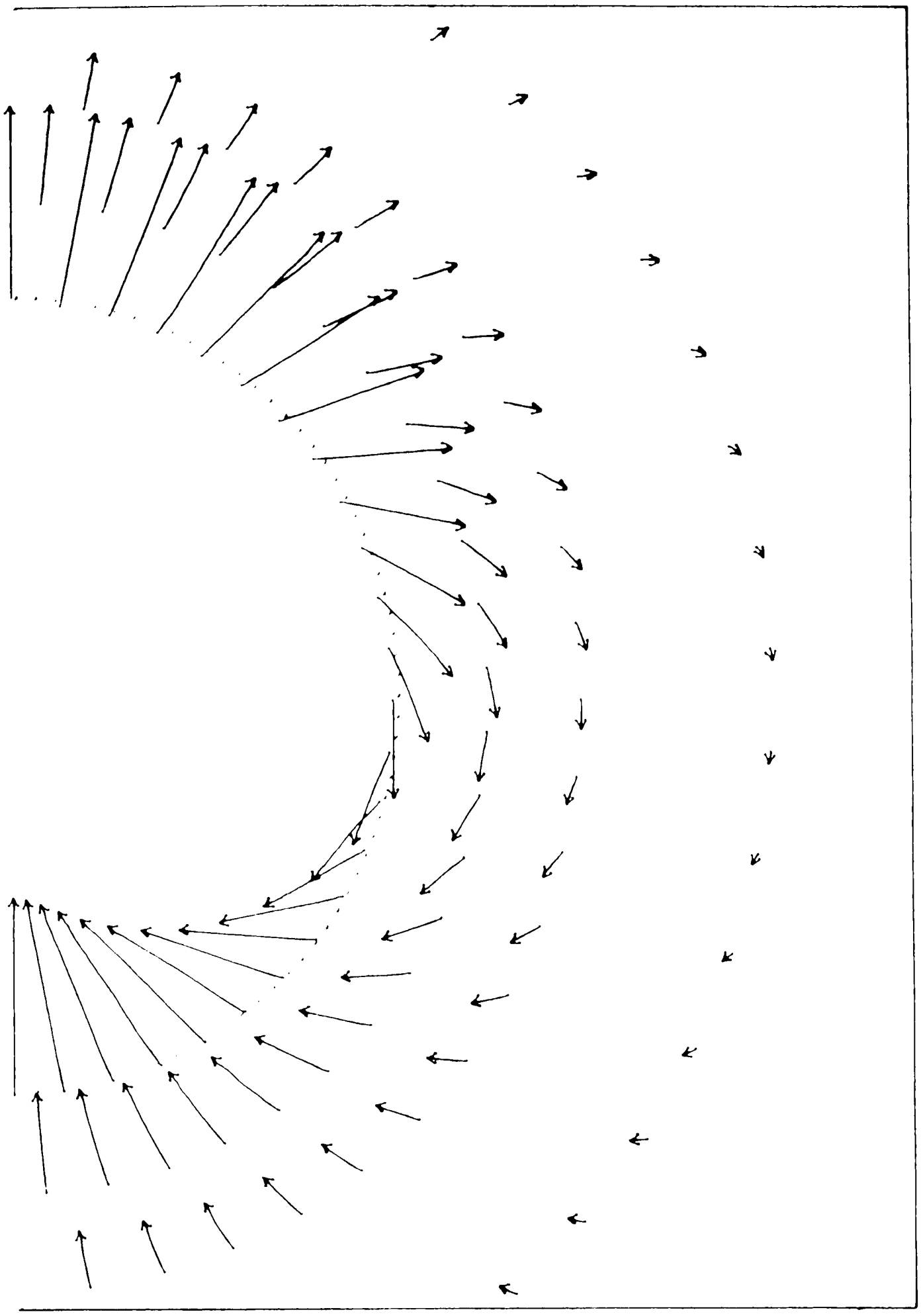

Figure 2. The Davidson solution for the particle velocity in the vicinity of the bubble.

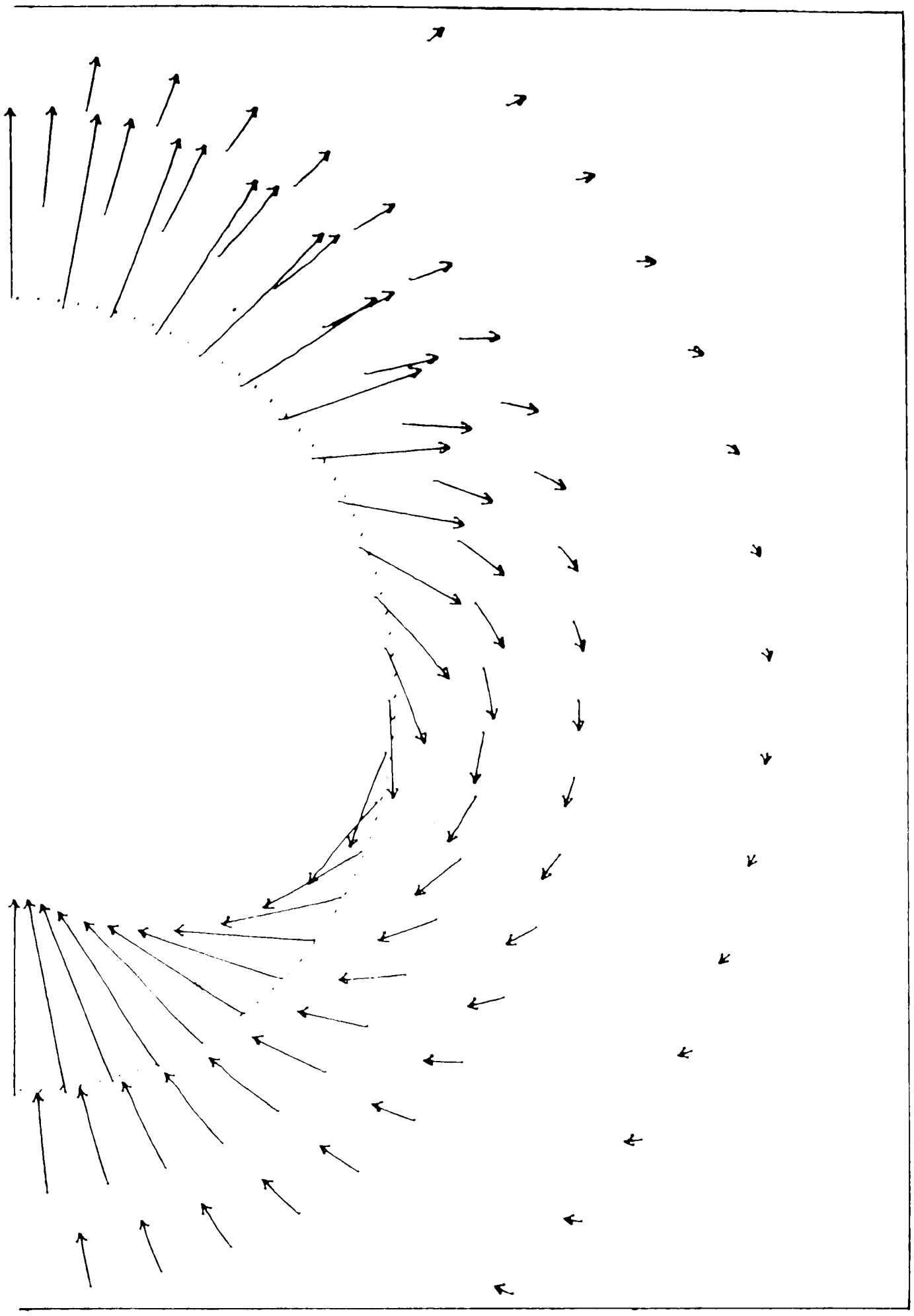

Figure 3. The finite element solution for the particle velocity in the vicinity of the bubble.

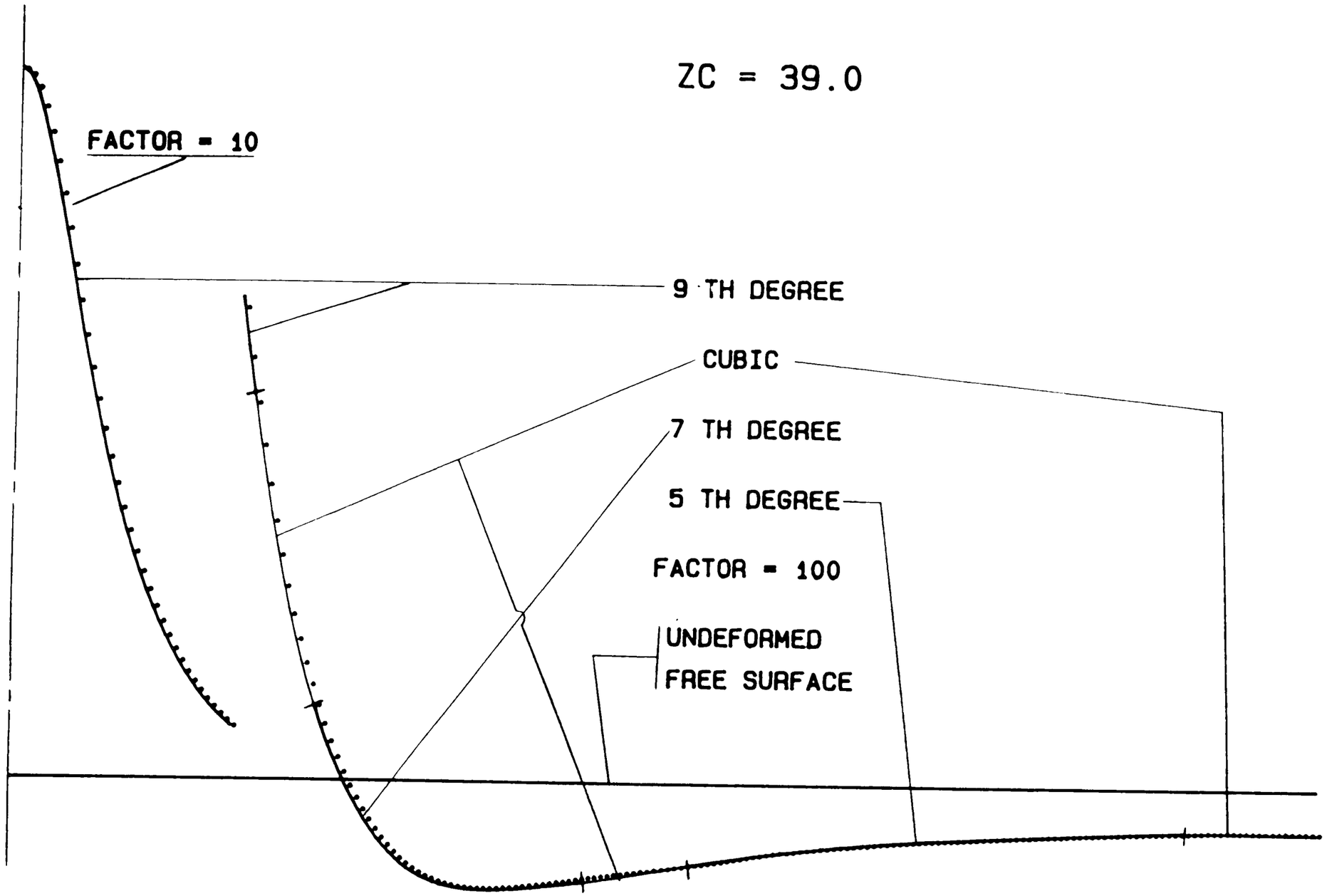

Figure 4. Sample sketch illustrating the curve-fitting procedure for the free surface and the velocity potential.

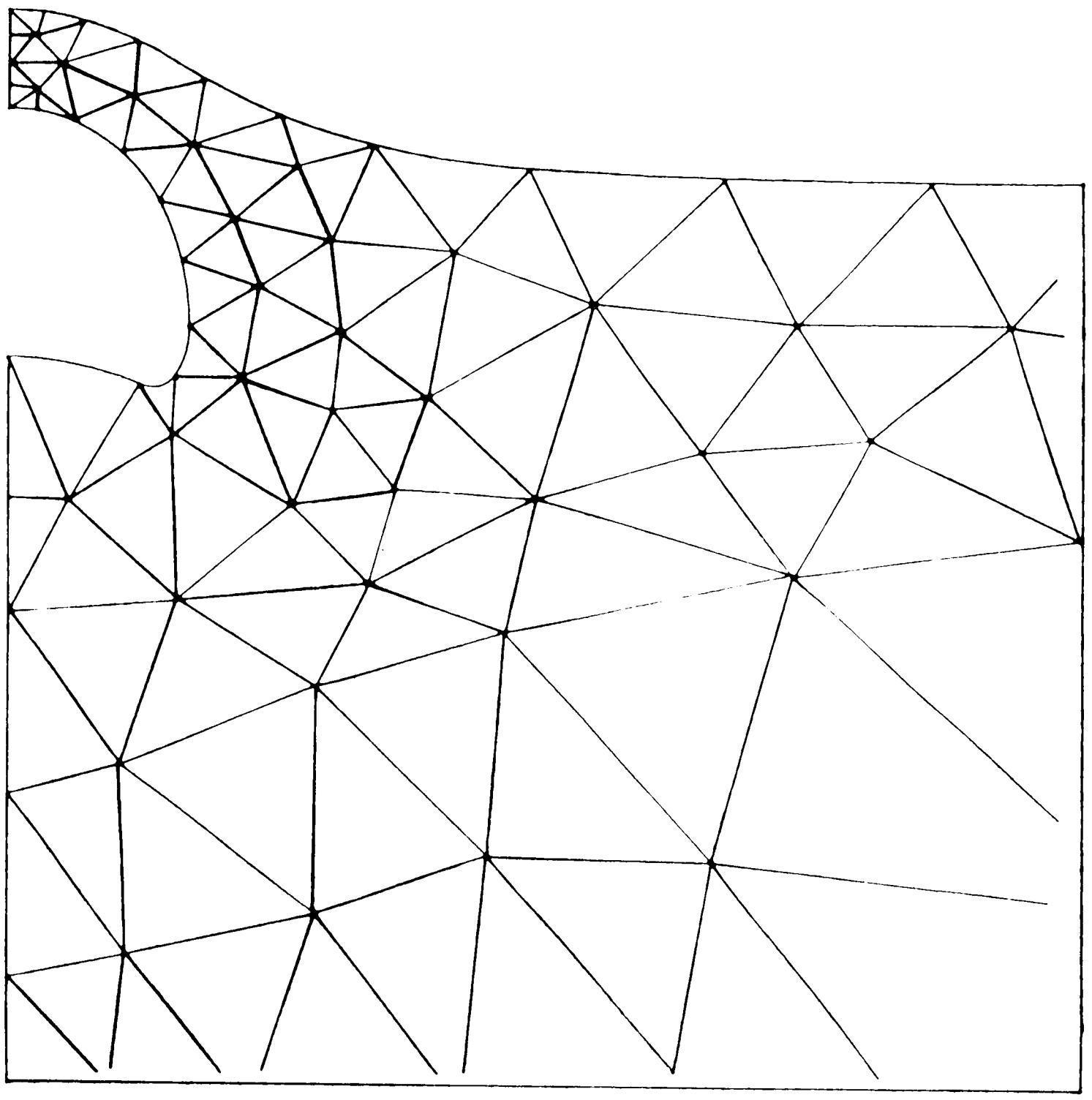

Figure 5. The finite element mesh in the vicinity of the bubble for the last stages of the computation.

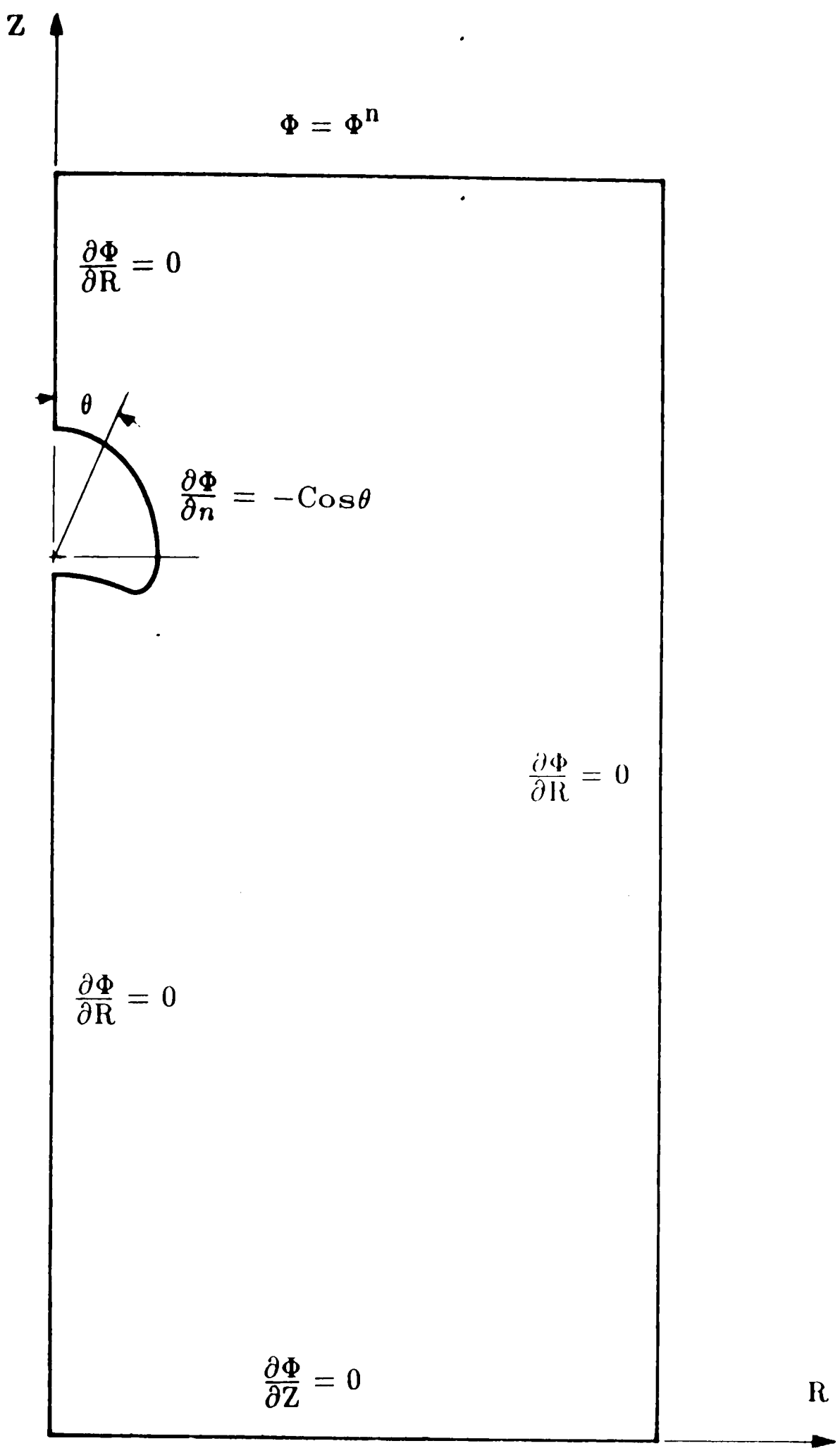

Figure 6. Axes, solution domain and boundary conditions for particle velocity potential.

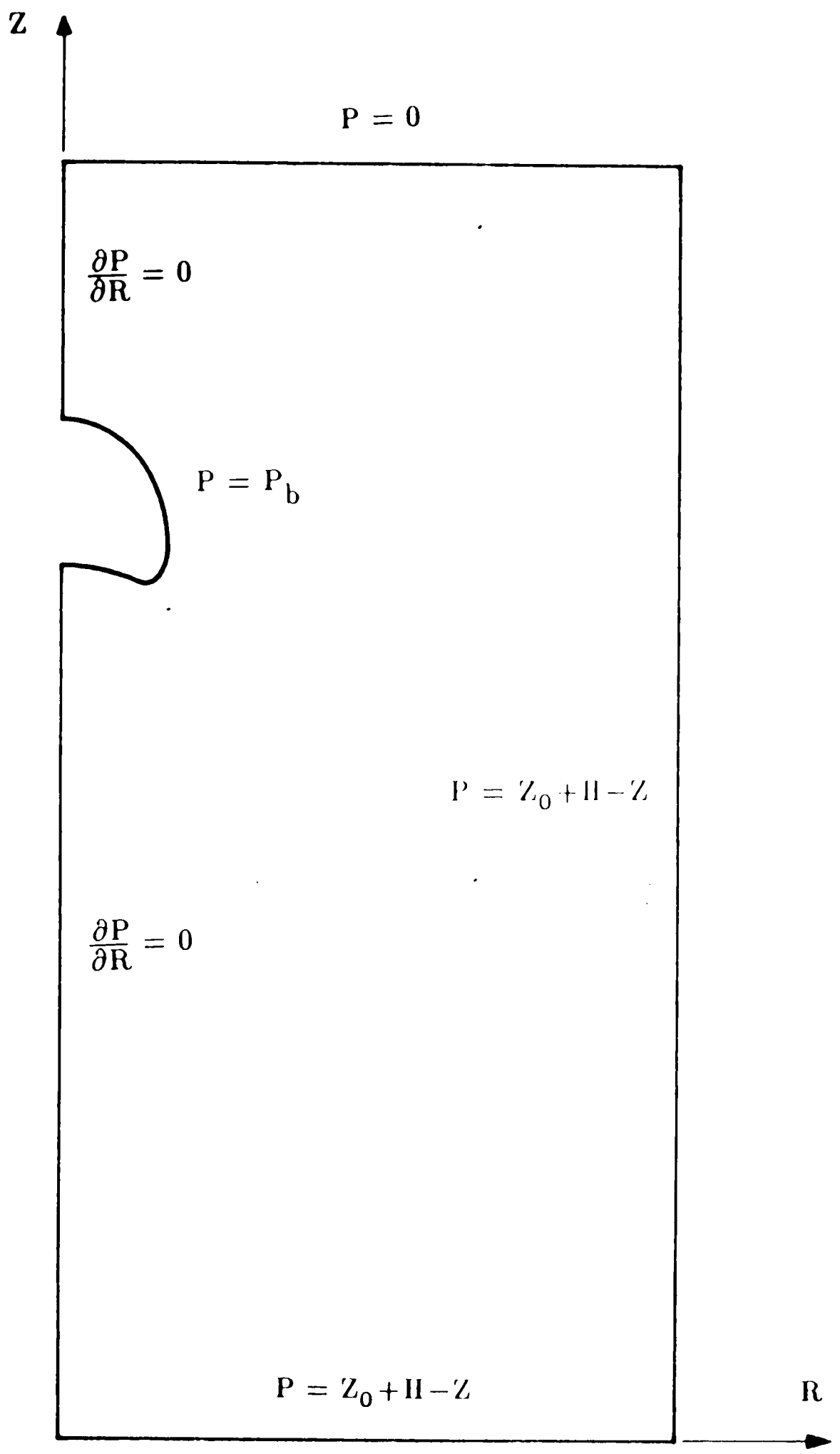

Figure 7. Axes, solution domain and boundary conditions for pressure.

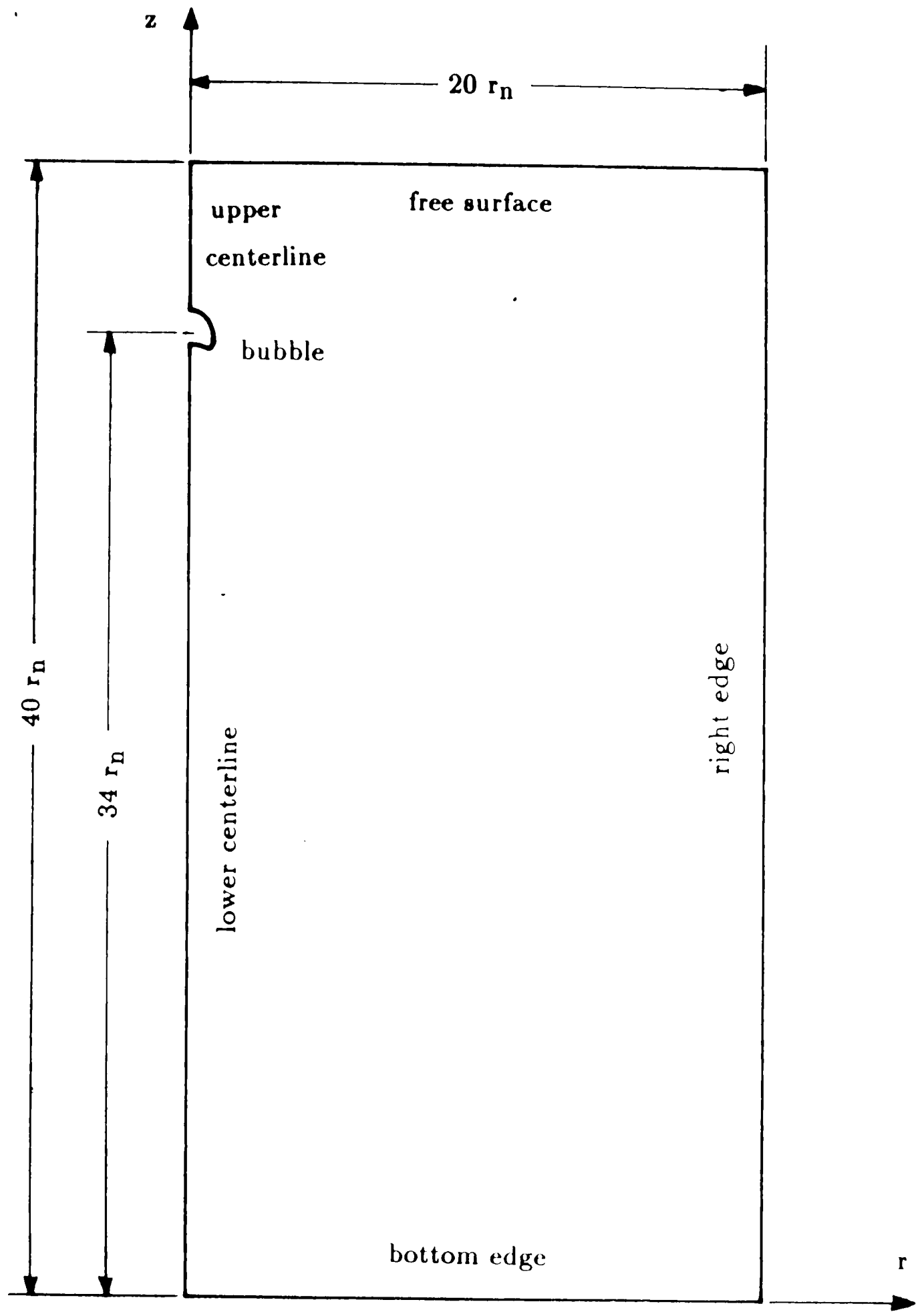

Figure 8. Dimensions and boundaries of the axisymmetric domain.

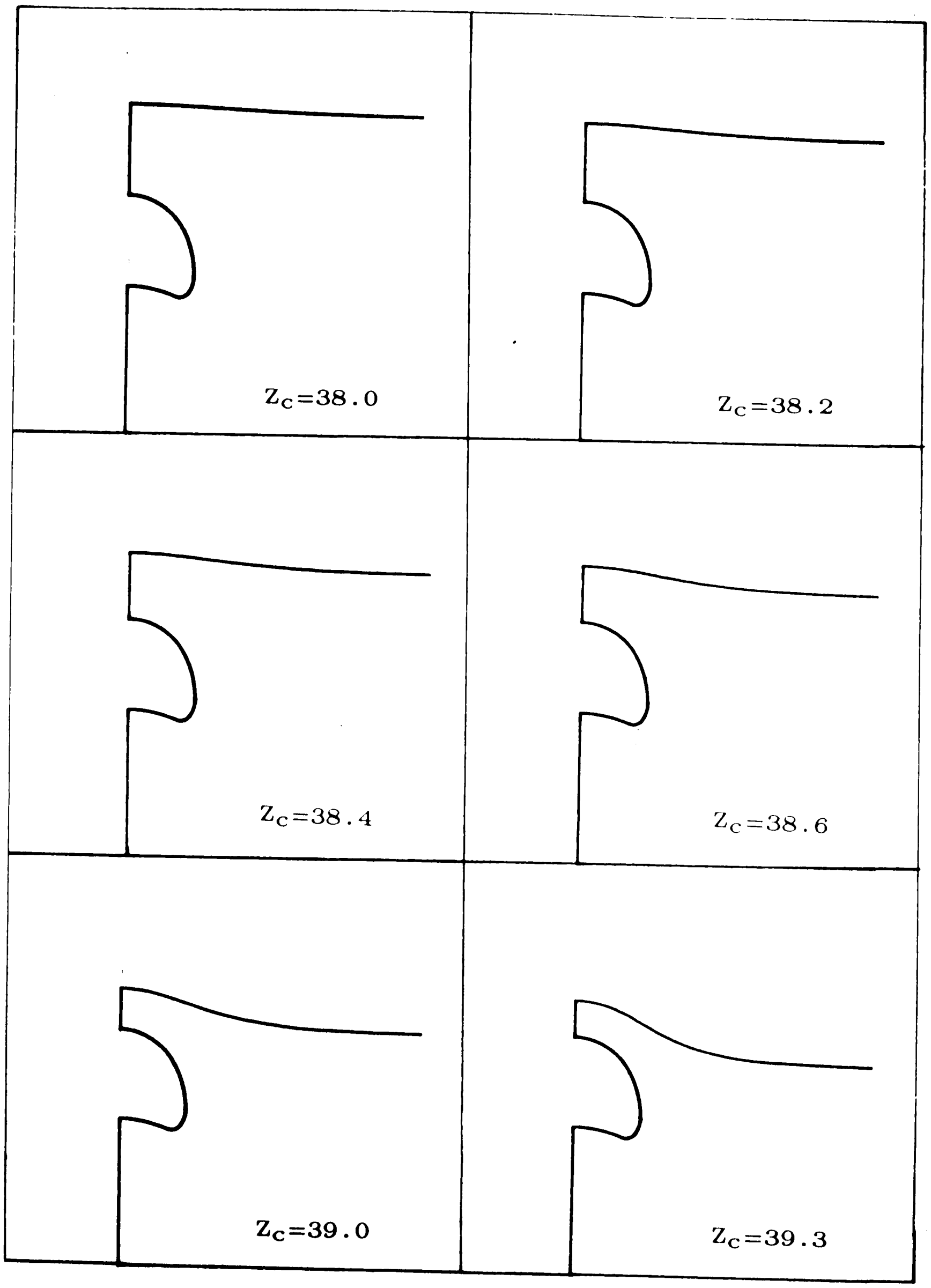

Figure 9. Shape of the free surface during bubble rise.

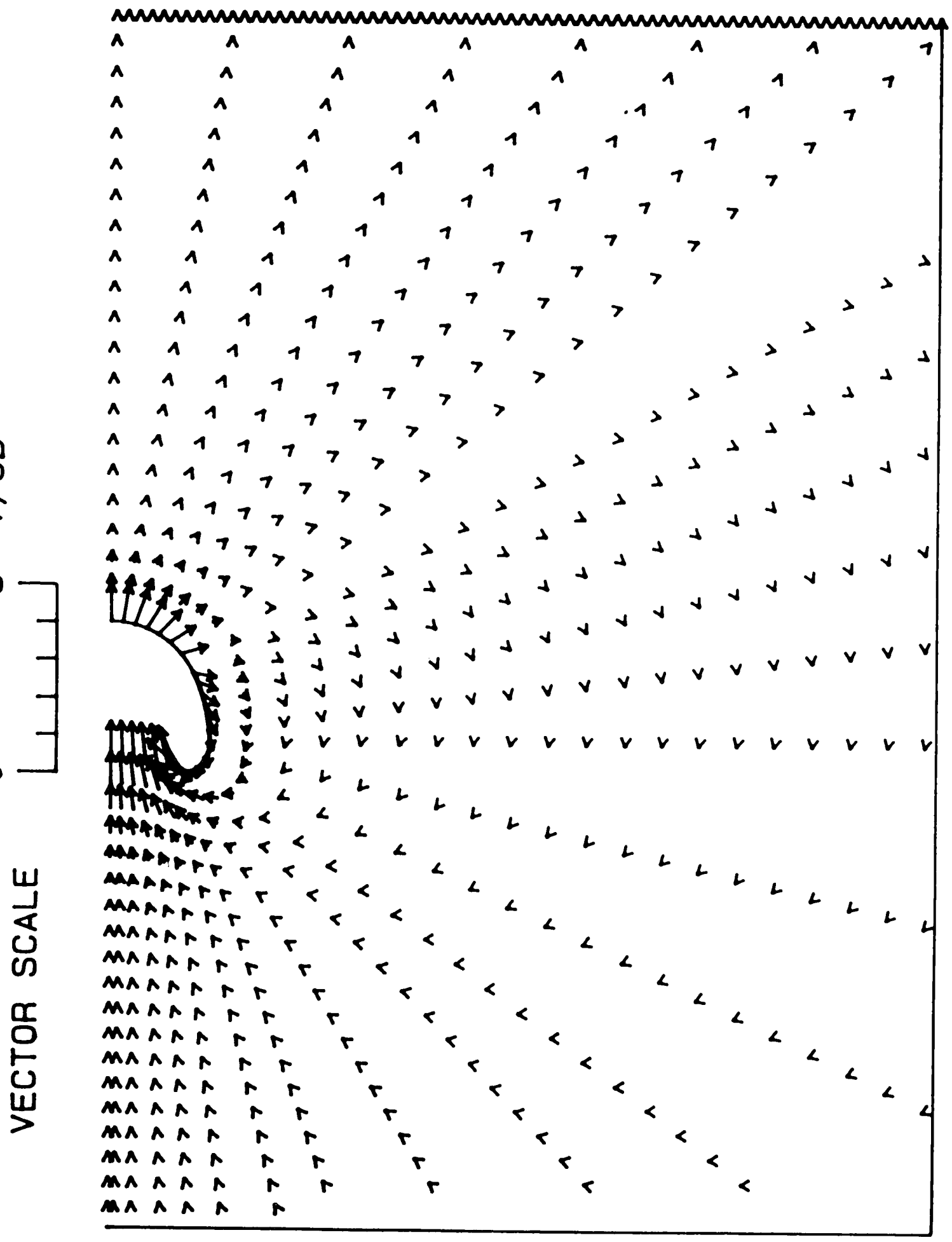

Figure 10. Vector field of absolute particle velocity for $Z_c = 34.0$

PARTICLE VELOCITY
ZC = 34.0

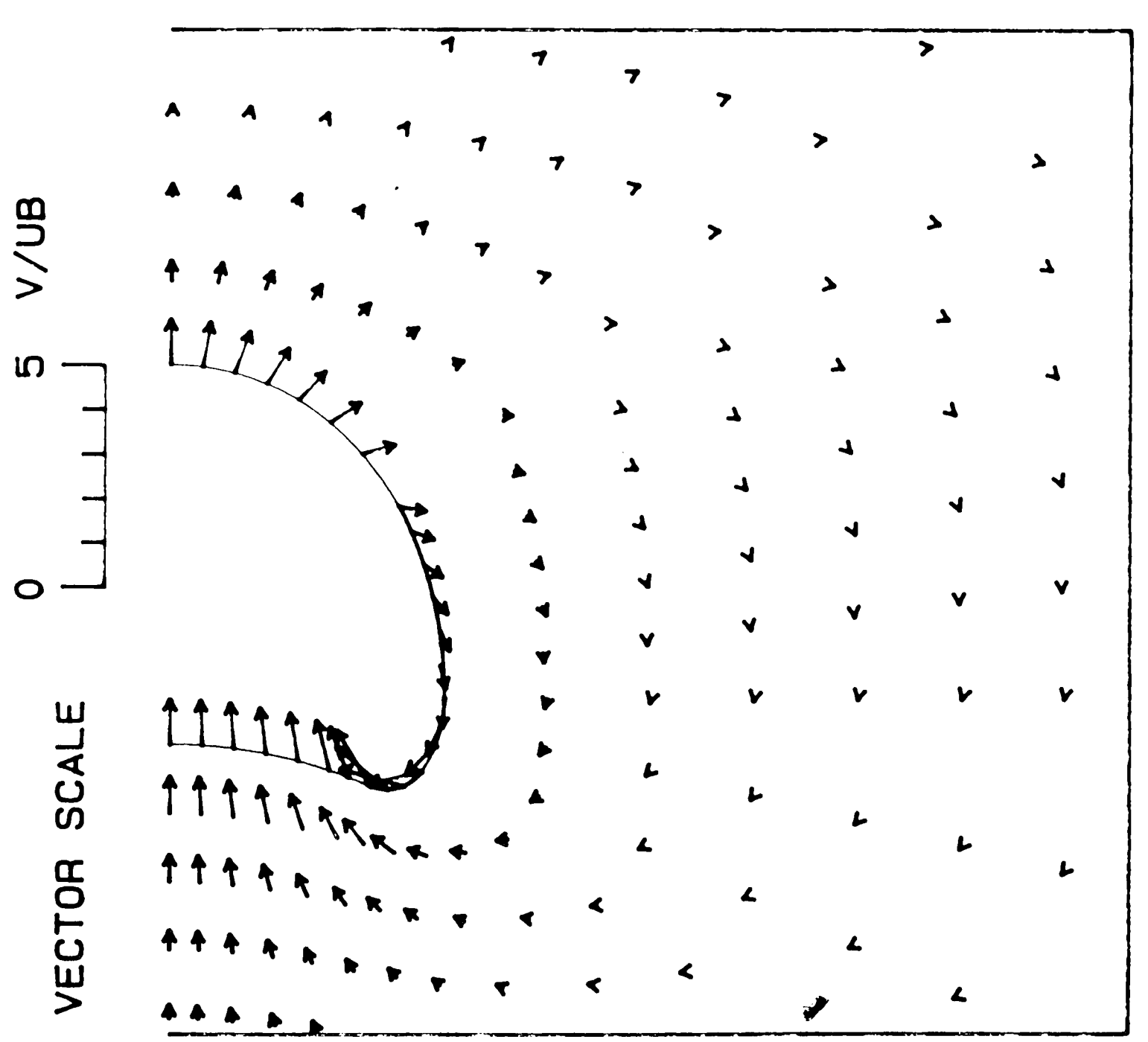

Figure 11. Vector field of absolute particle velocity highlighting area near bubble for Z_C = 34.0

PARTICLE VELOCITY
ZC = 37.0

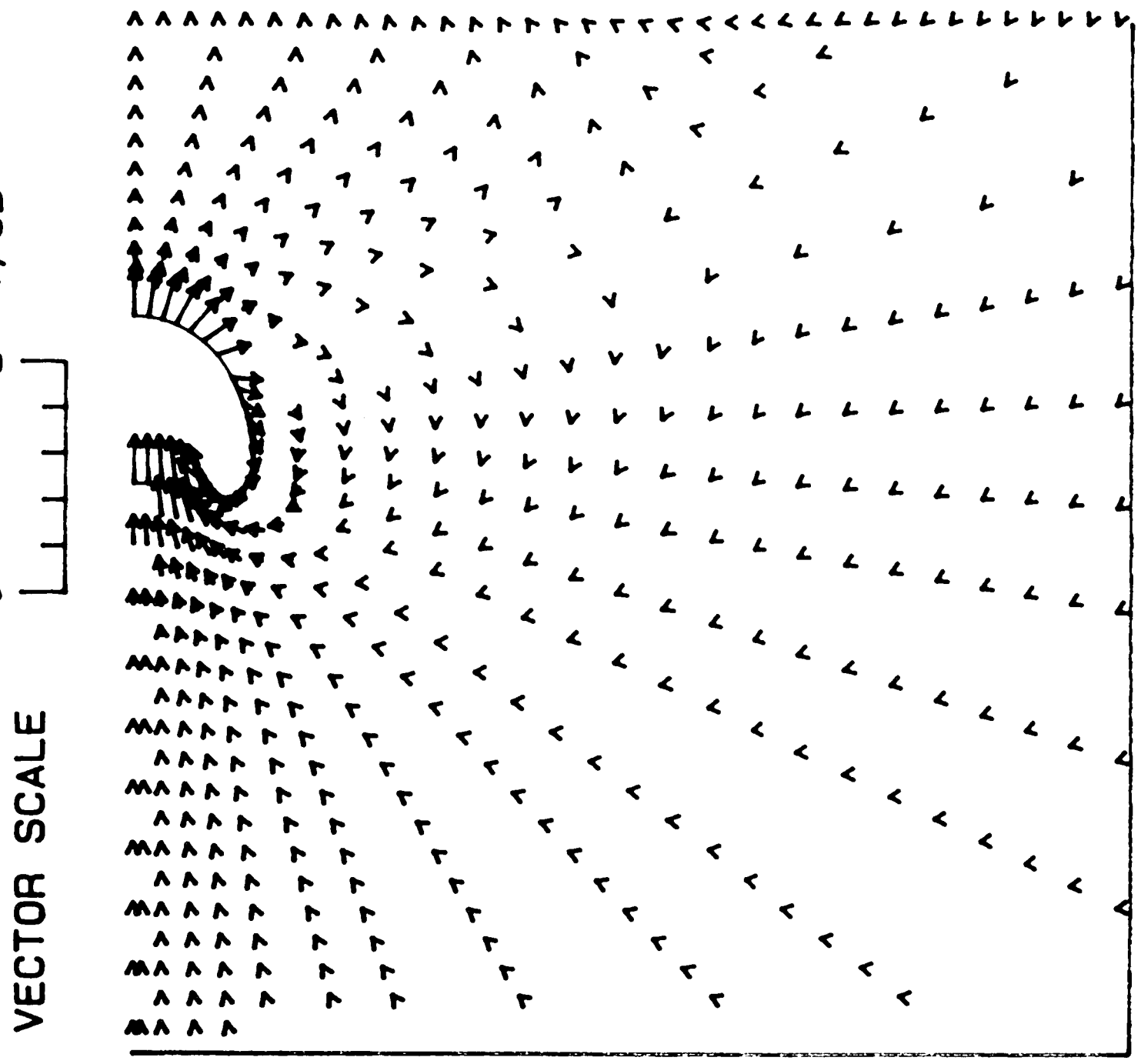

Figure 12. Vector field of absolute particle velocity for Z_c = 37.0

PARTICLE VELOCITY
ZC = 37.0

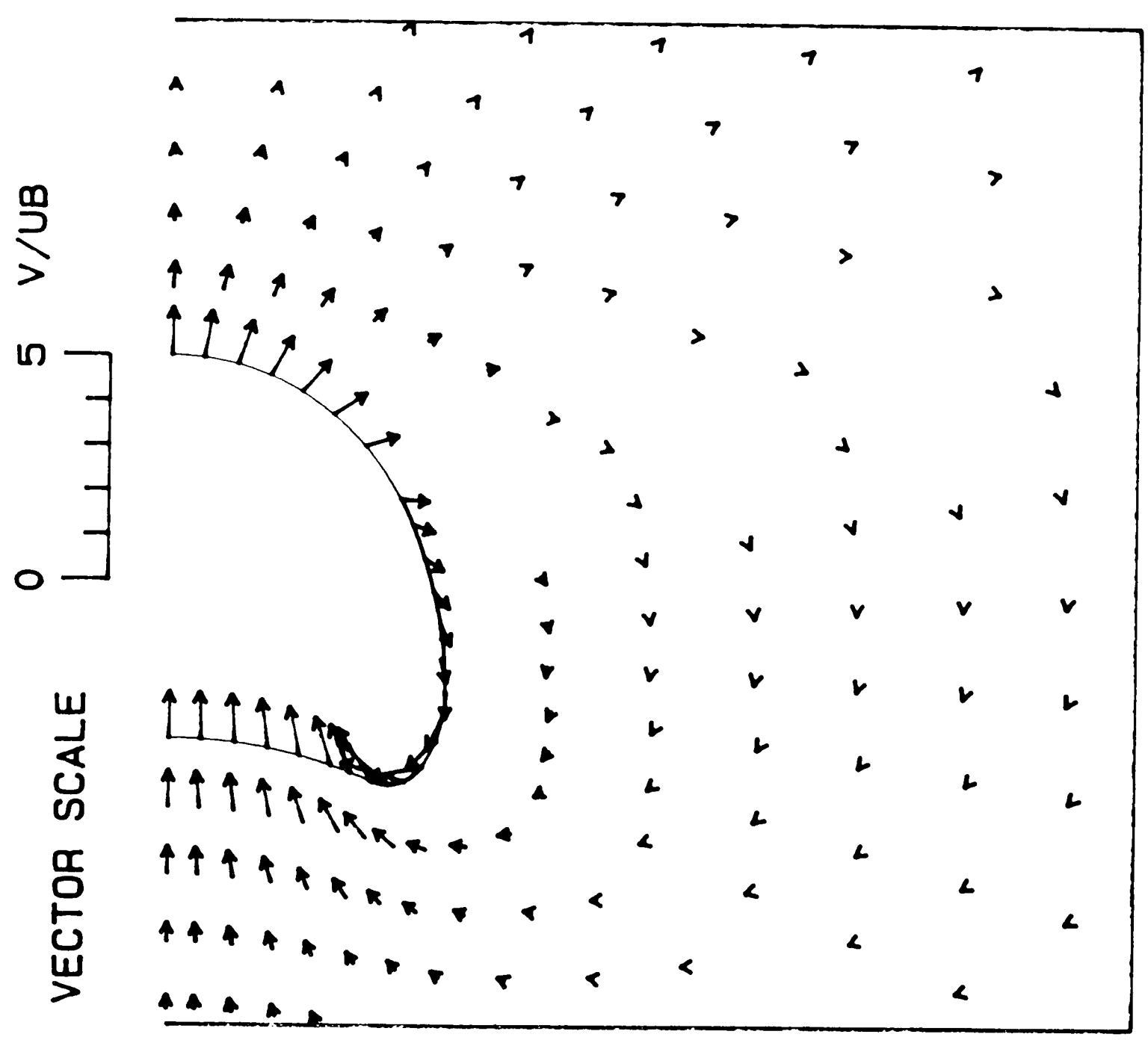

Figure 13. Vector field of absolute particle velocity highlighting area near bubble for Z_c = 37.0

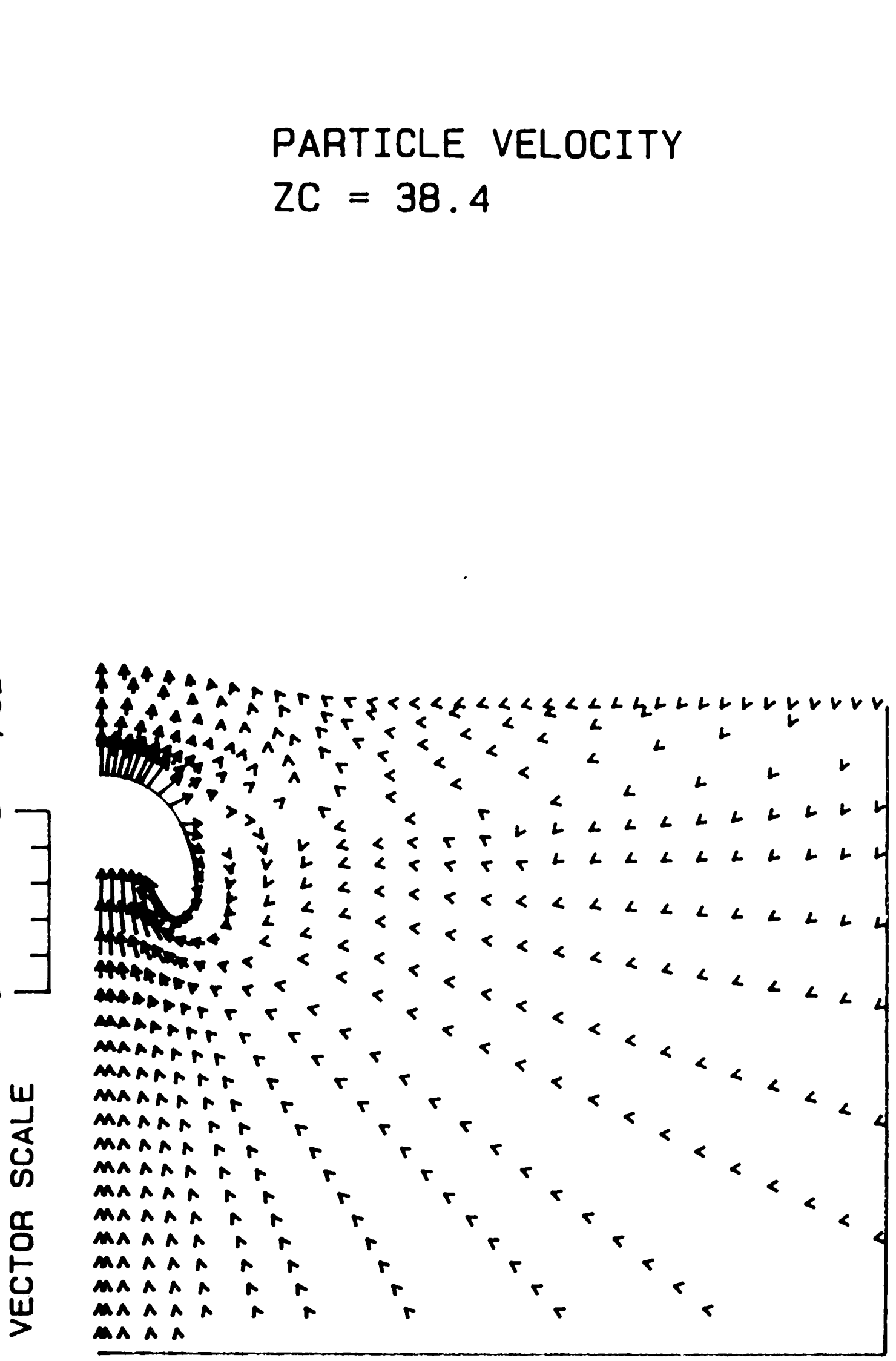

Figure 14. Vector field of absolute particle velocity for Z_c = 38.4

PARTICLE VELOCITY
ZC = 38.4

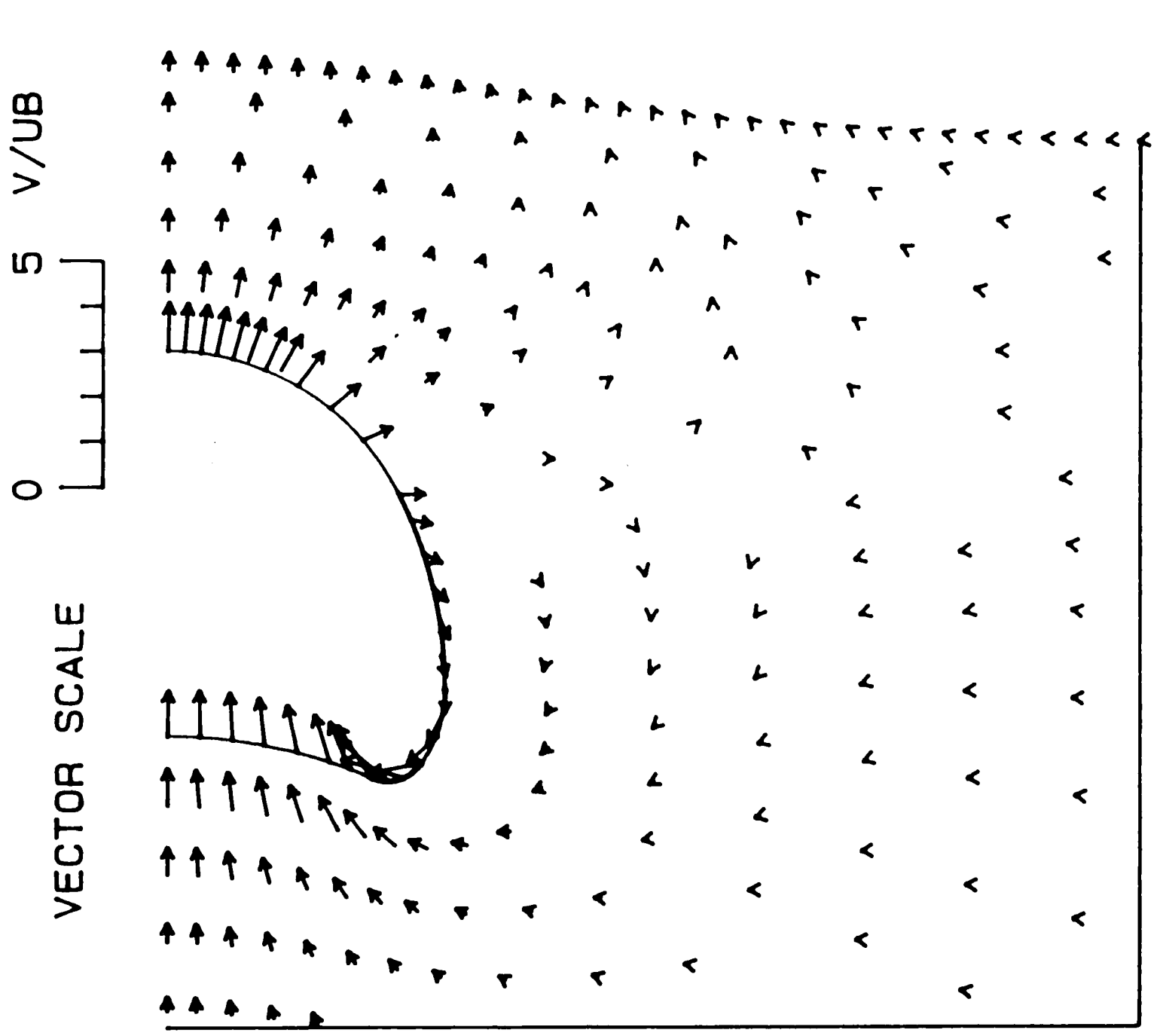

Figure 15. Vector field of absolute particle velocity highlighting area near bubble for Z_C = 38.4

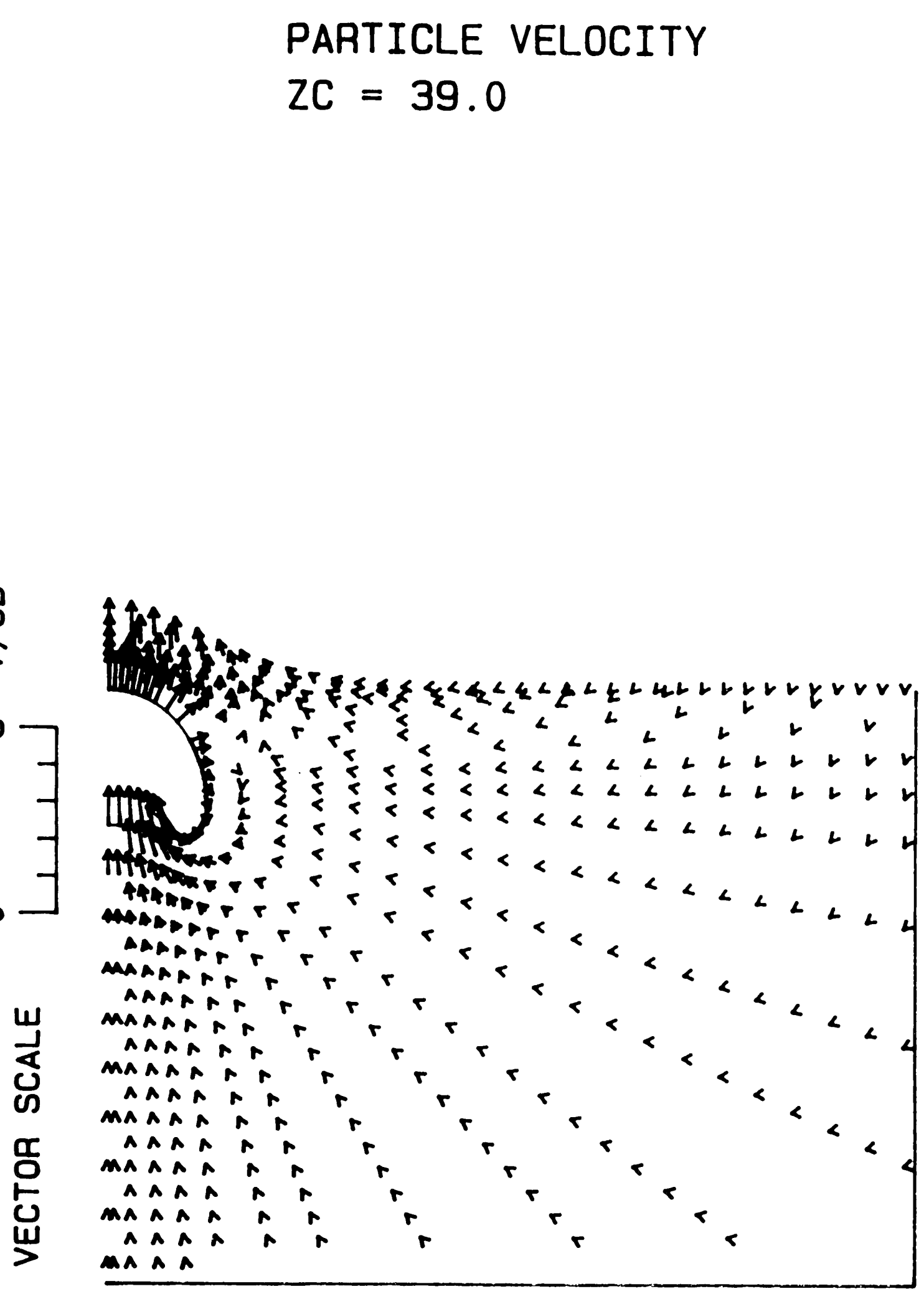

Figure 16. Vector field of absolute particle velocity for $Z_c = 39.0$

PARTICLE VELOCITY
ZC = 39.0

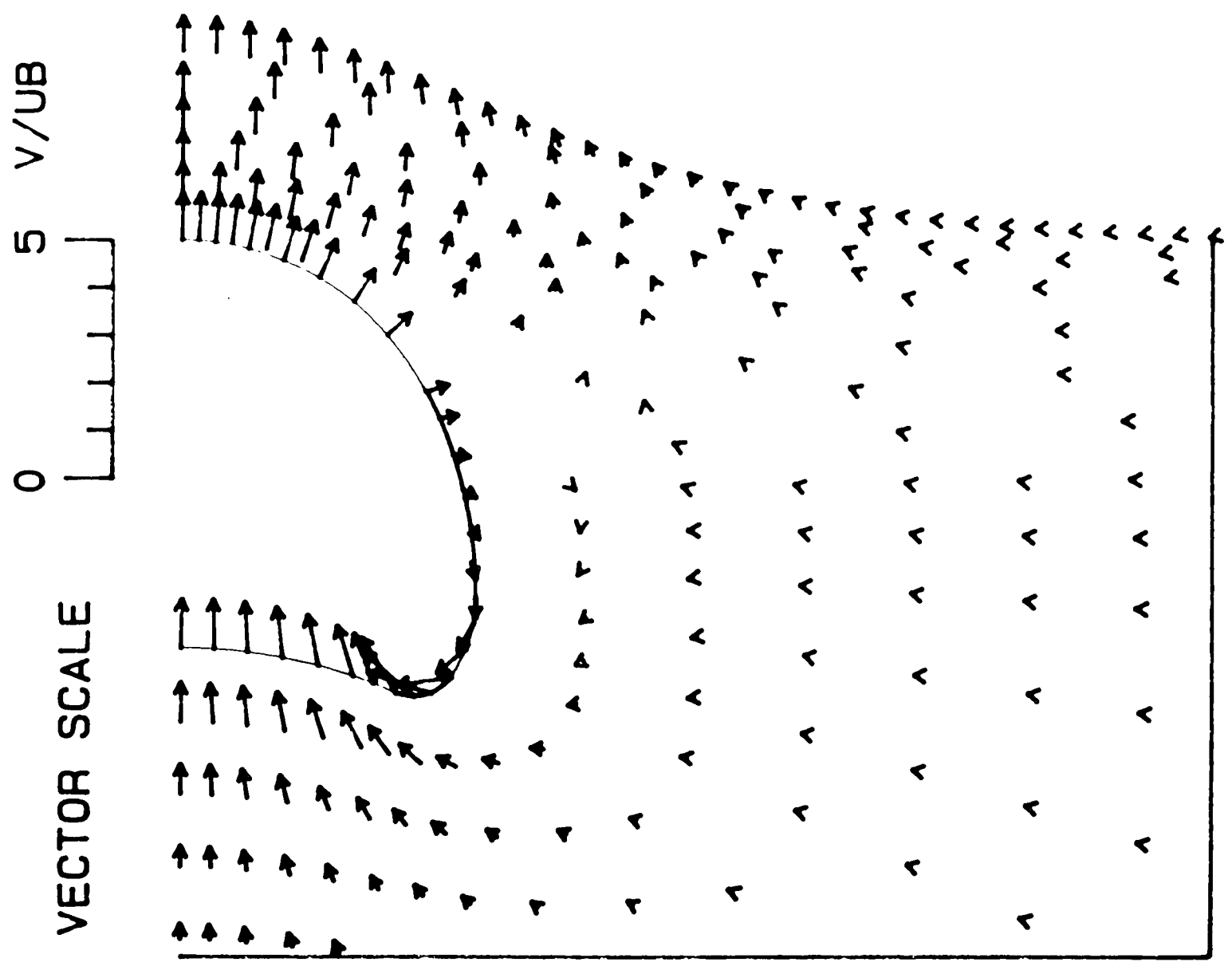

Figure 17. Vector field of absolute particle velocity highlighting area near bubble for Z_C = 39.0

PARTICLE VELOCITY
ZC = 39.3

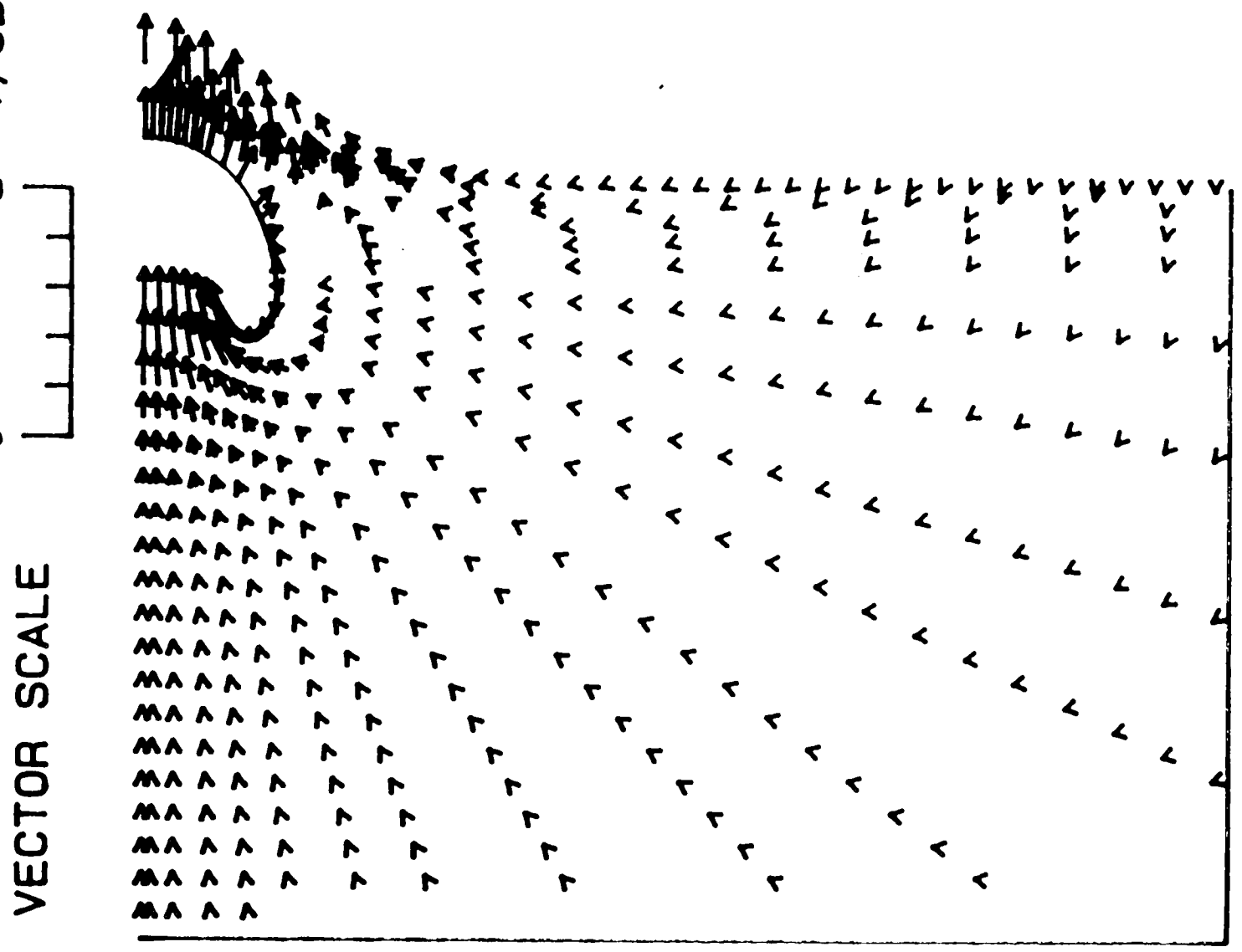

Figure 18. Vector field of absolute particle velocity for Z_c = 39.3

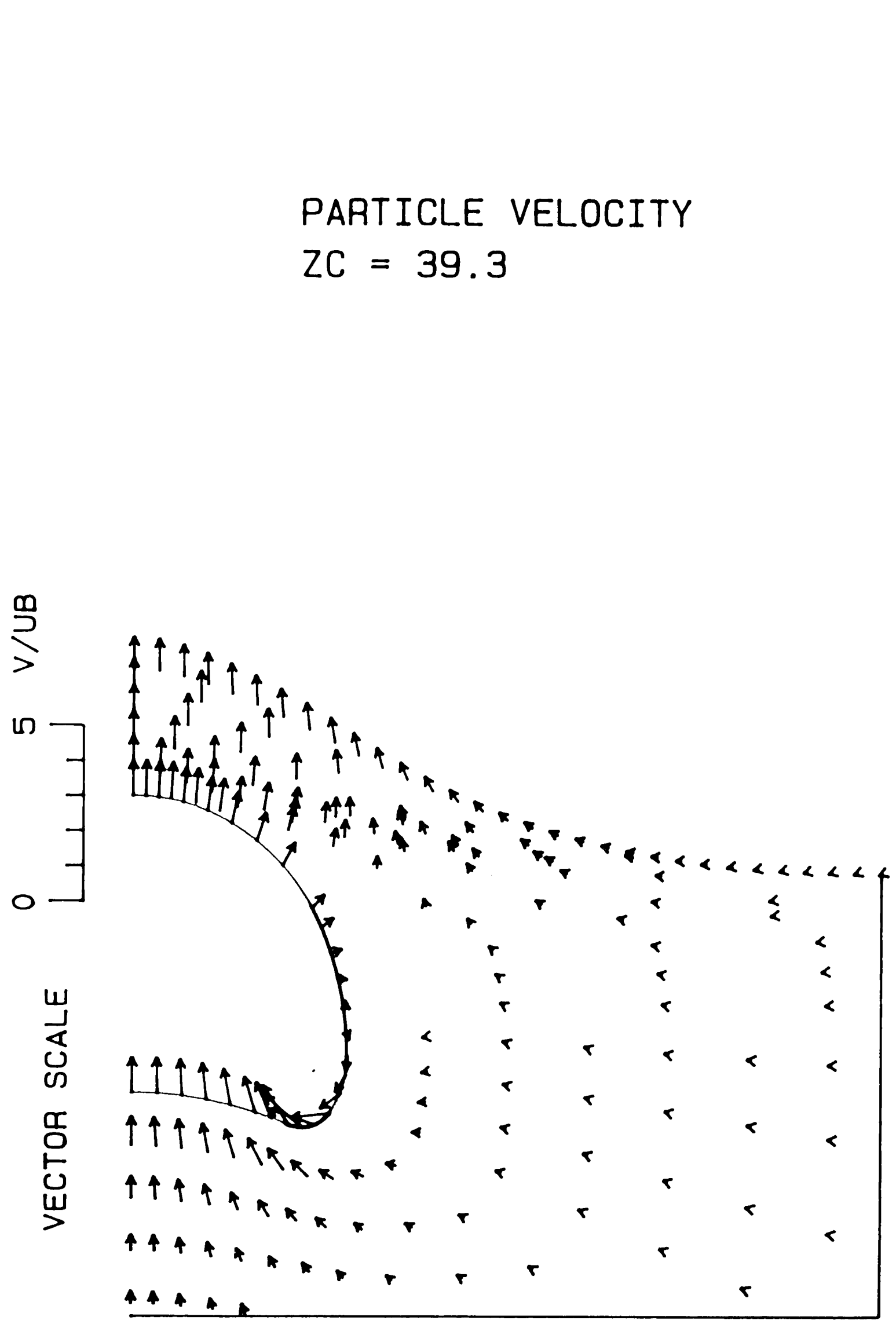

Figure 19. Vector field of absolute particle velocity highlighting area near bubble for Z_C = 39.3

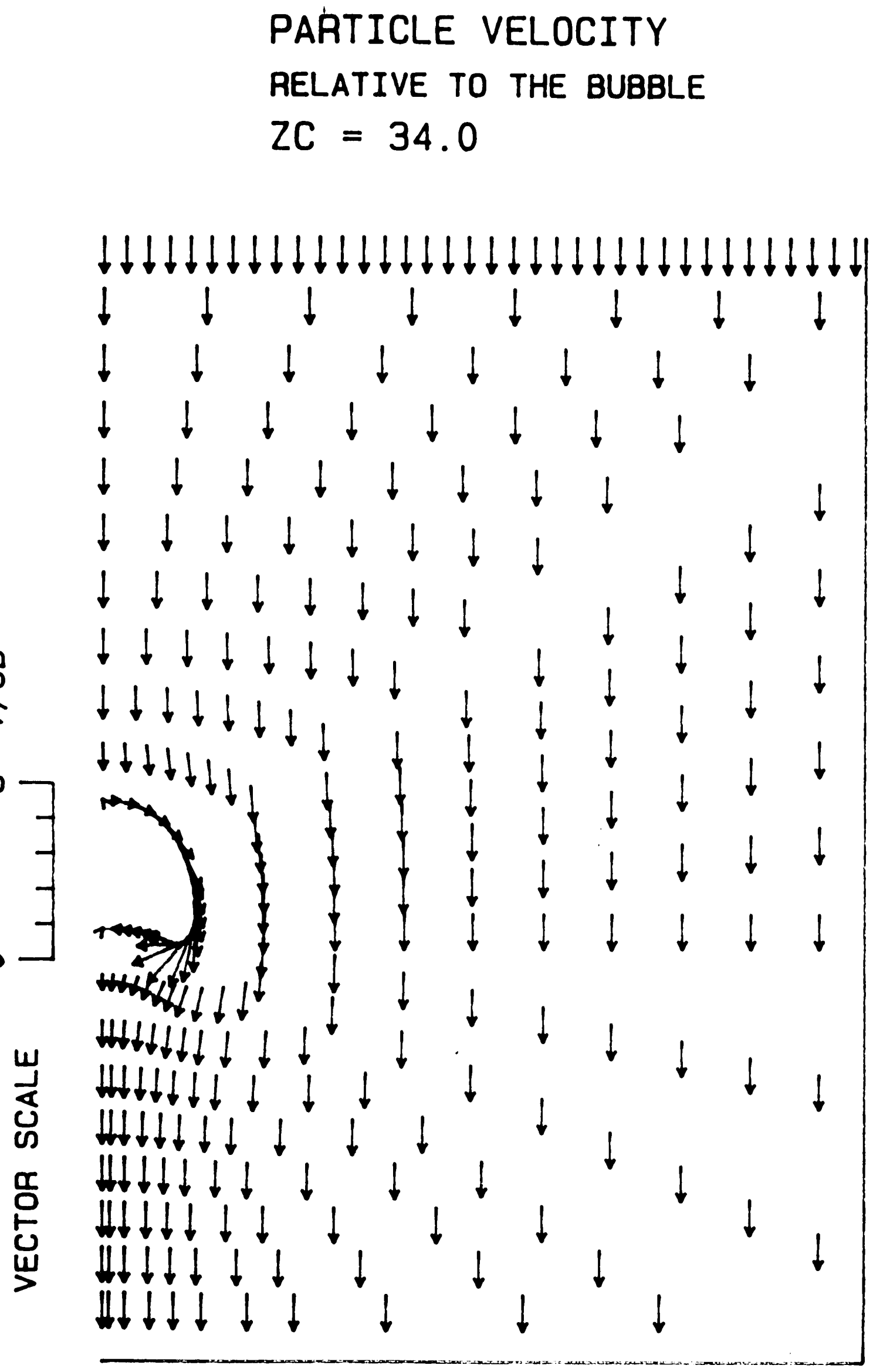

Figure 20. Vector field of particle velocity relative to bubble for $Z_c = 34.0$

PARTICLE VELOCITY

RELATIVE TO BUBBLE

ZC = 34.0

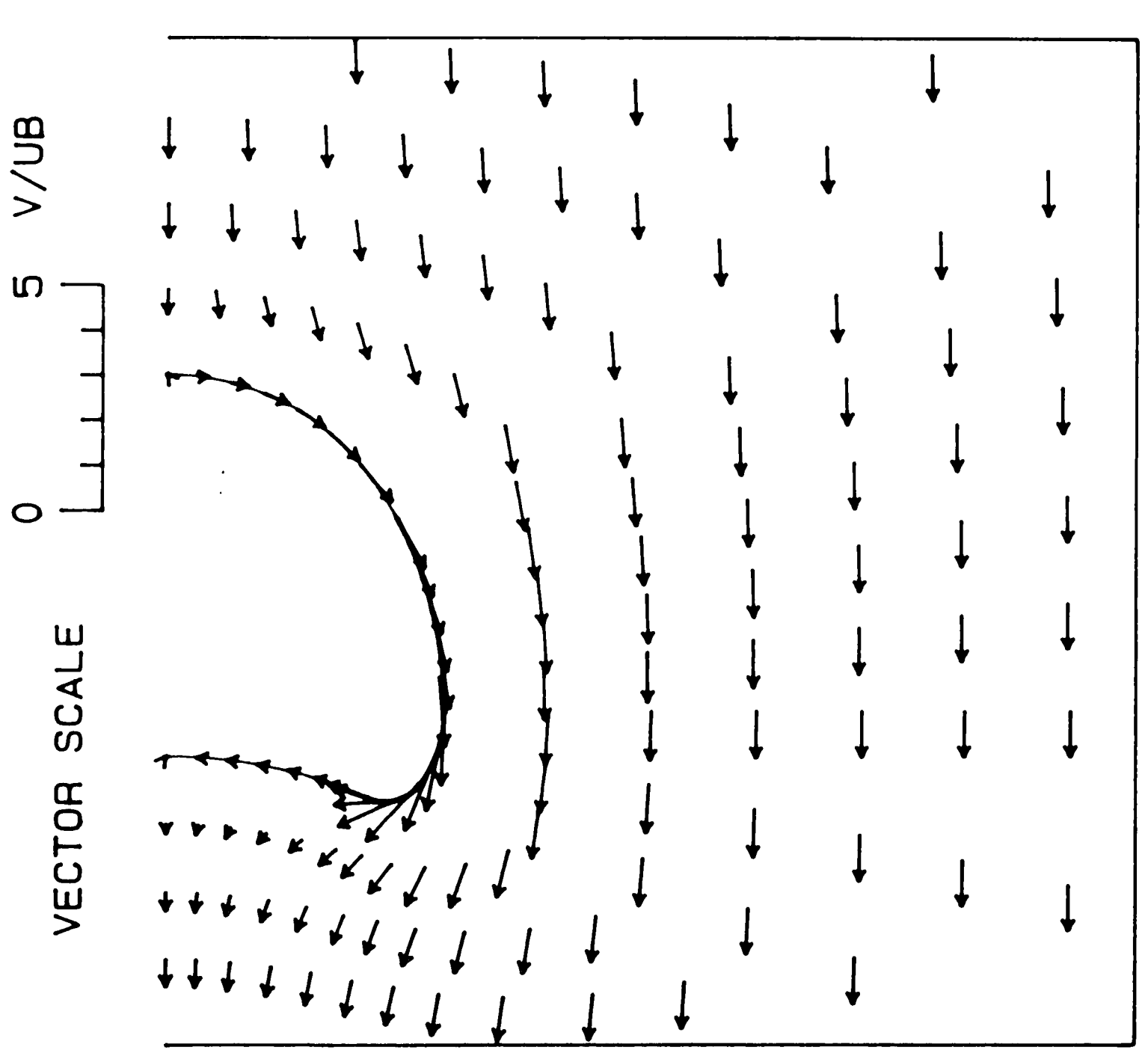

Figure 21. Vector field of particle velocity relative to bubble highlighting area near bubble for Z_c = 34.0

PARTICLE VELOCITY
RELATIVE TO BUBBLE
ZC = 37.0

Figure 22. Vector field of particle velocity relative to bubble highlighting area near bubble for Z_c = 37.0

PARTICLE VELOCITY
RELATIVE TO BUBBLE
ZC = 38.4

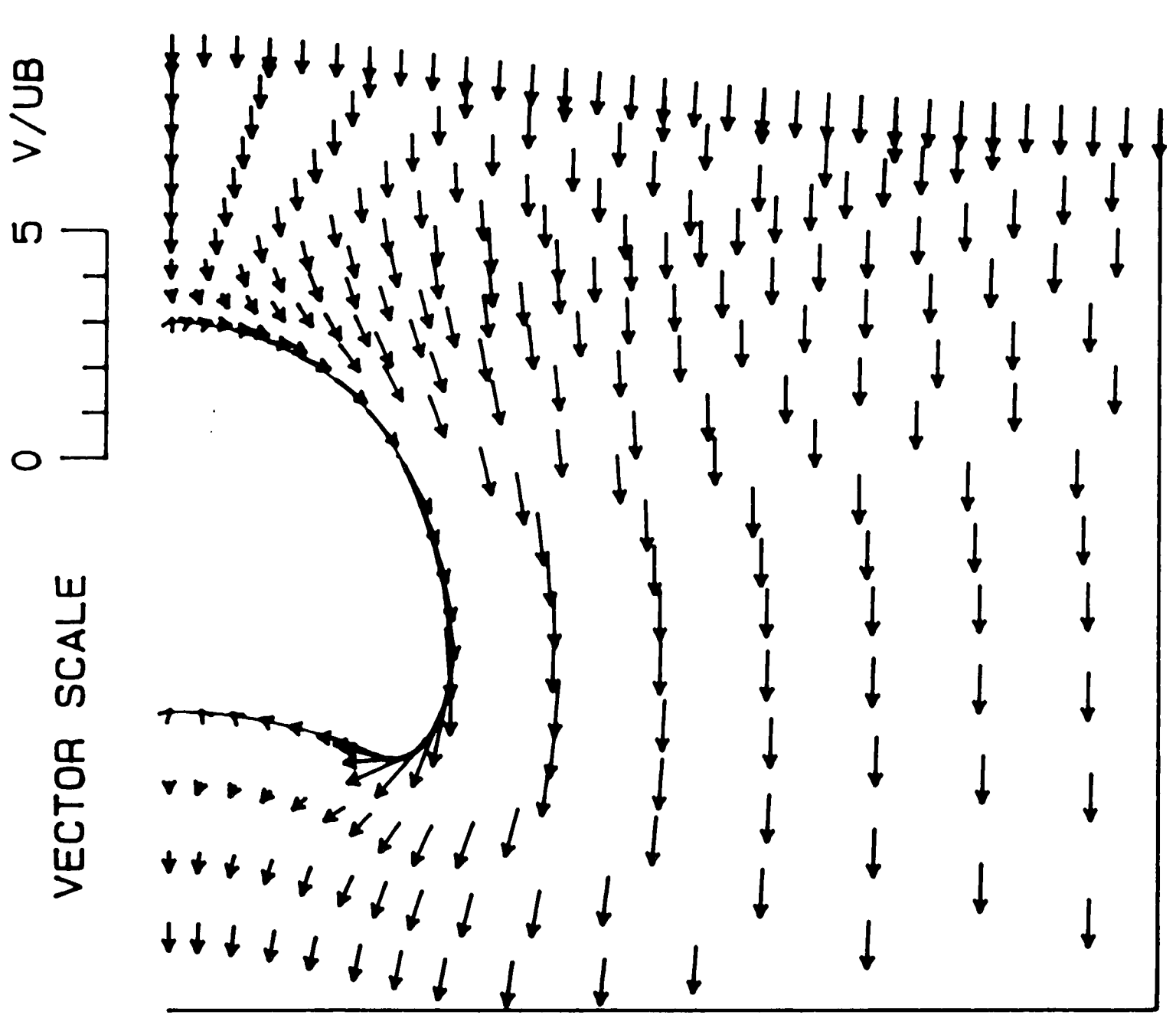

Figure 23. Vector field of particle velocity relative to bubble highlighting area near bubble for Z_c = 38.4

PARTICLE VELOCITY
RELATIVE TO BUBBLE
ZC = 39.0

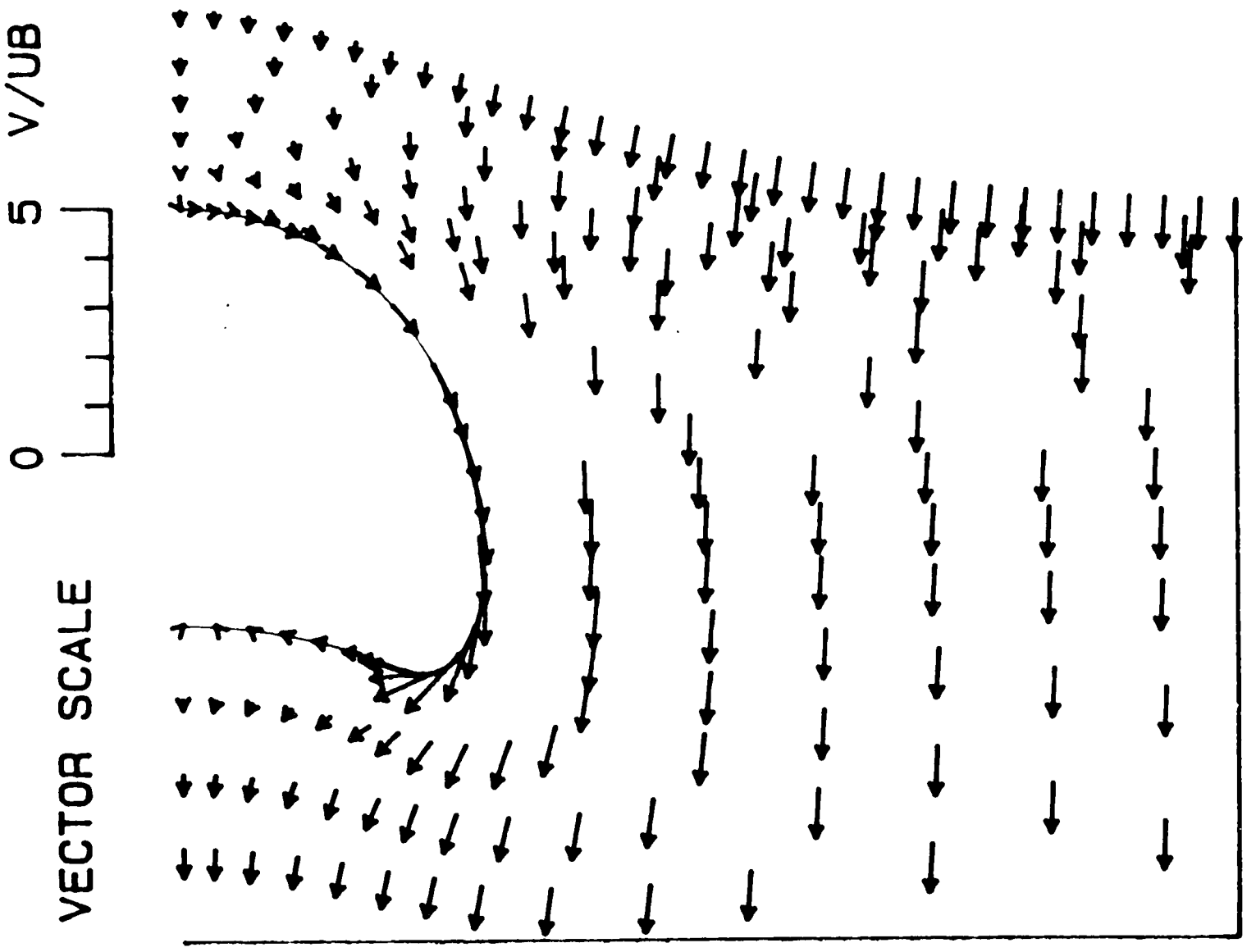

Figure 24. Vector field of particle velocity relative to bubble highlighting area near bubble for Z_c = 39.0

PARTICLE VELOCITY
RELATIVE TO BUBBLE
ZC = 39.3

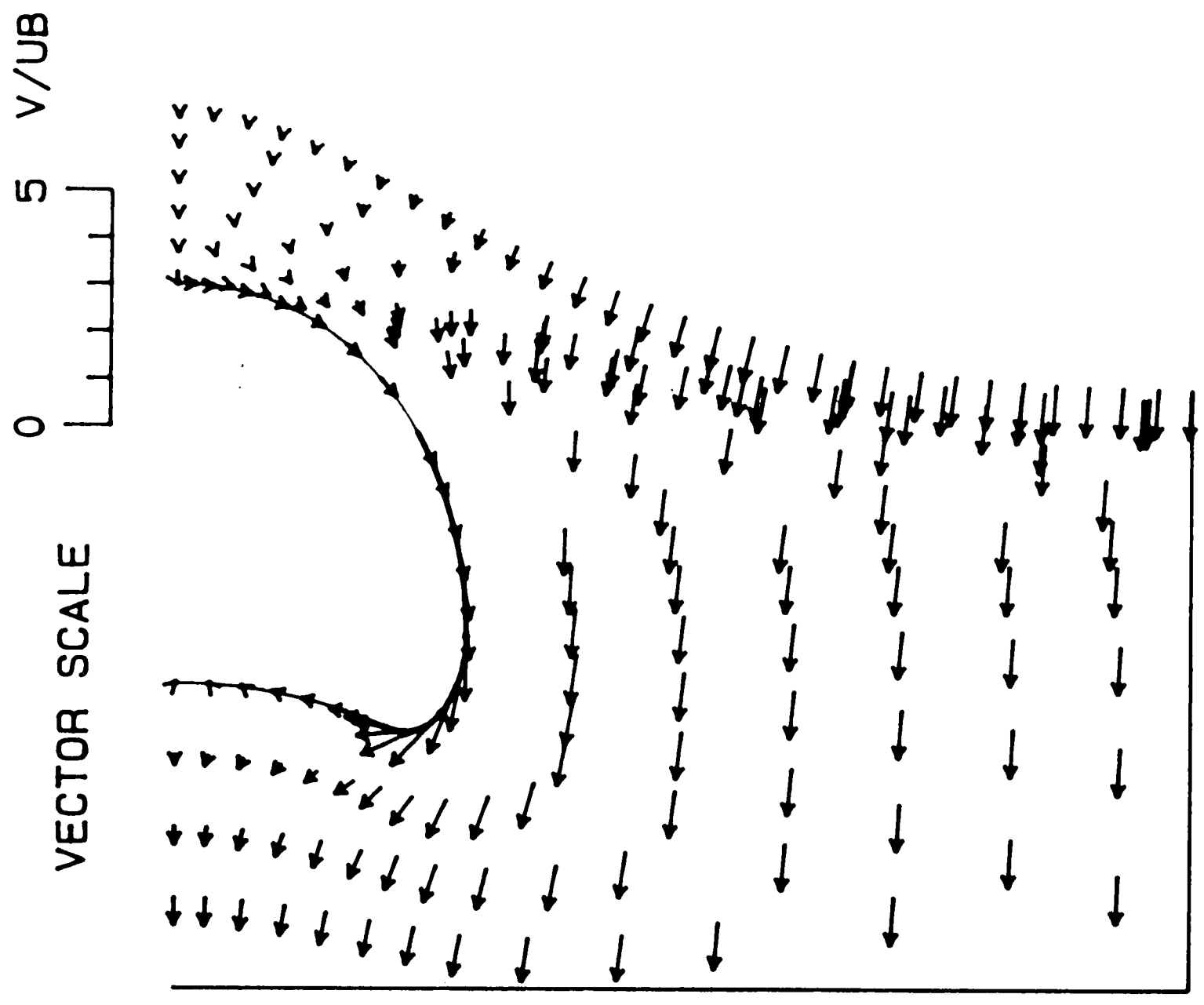

Figure 25. Vector field of particle velocity relative to bubble highlighting area near bubble for Z_c = 39.3

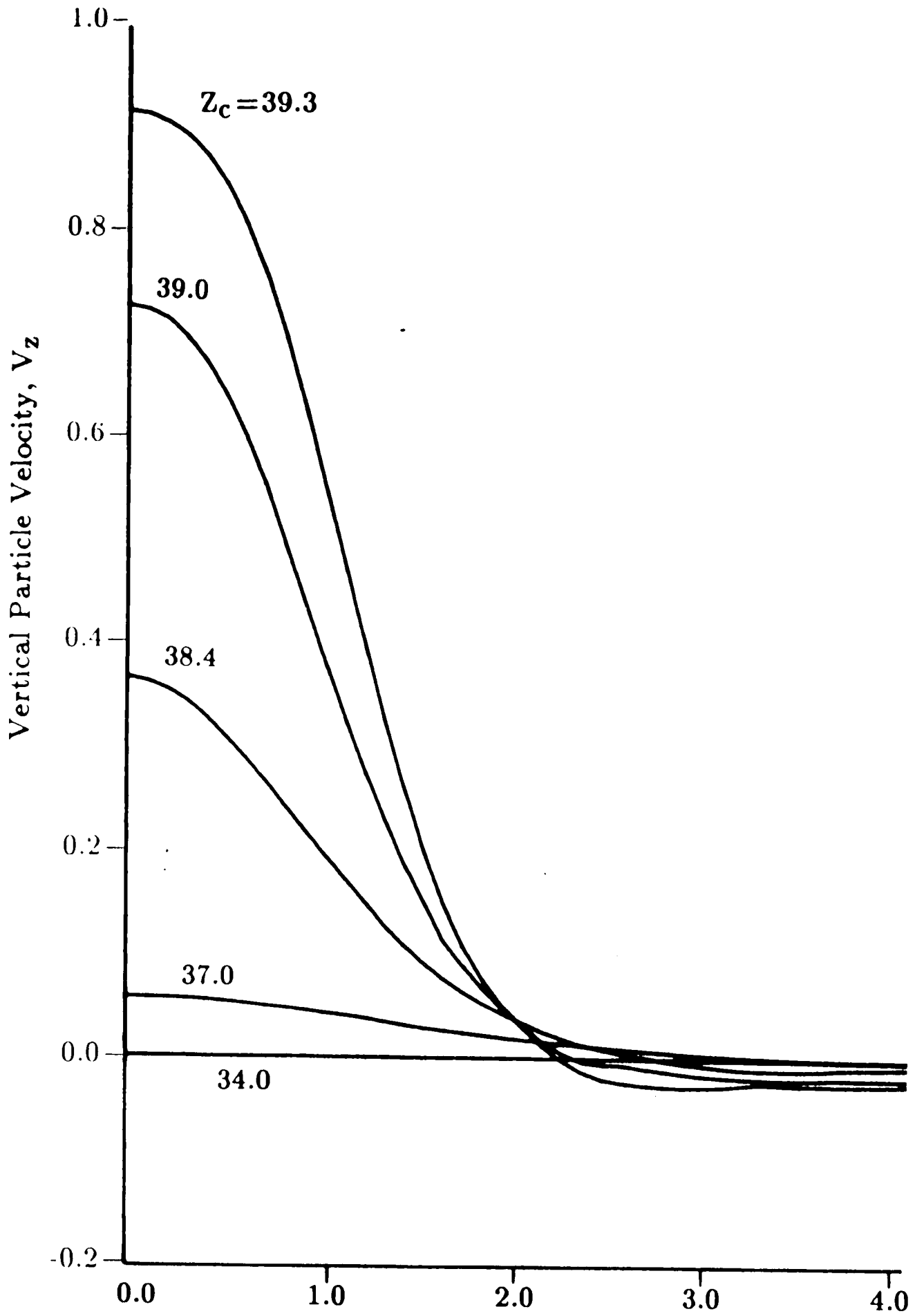

Figure 26. Vertical component of absolute particle velocity at the free surface.

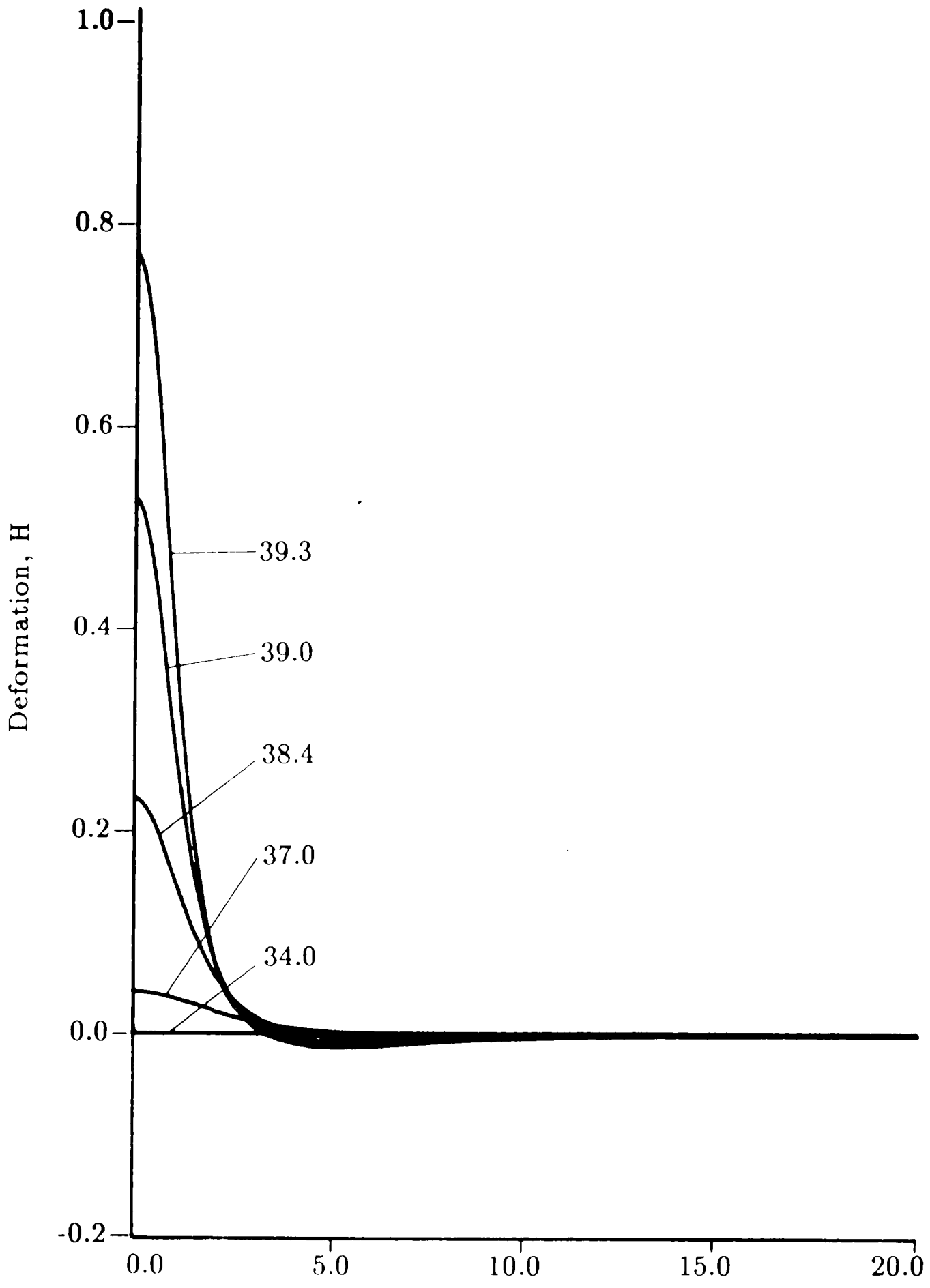

Figure 27. Deformation of free surface.

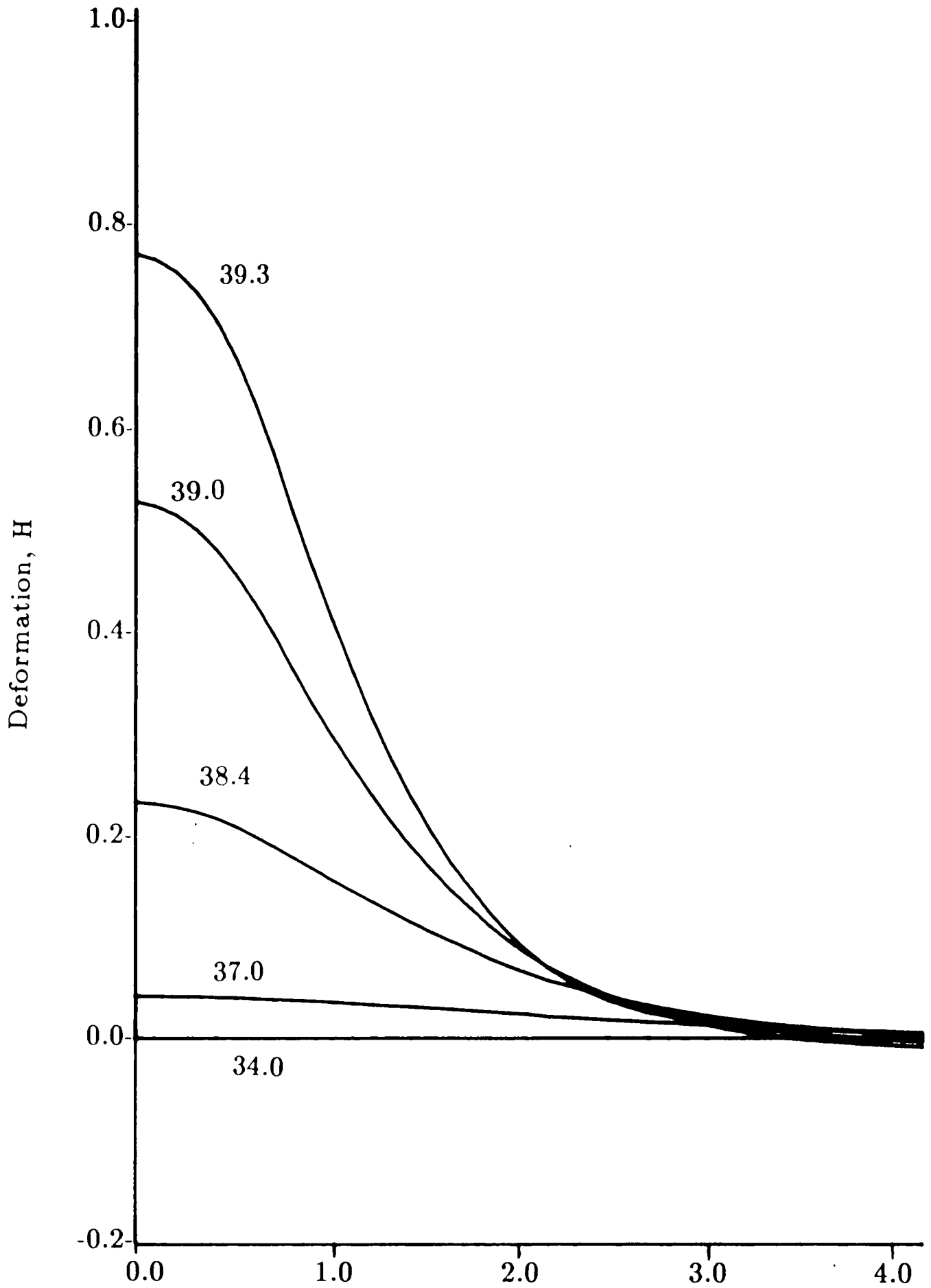

Figure 28. Deformation of free surface highlighting area in the vicinity of bubble centerline.

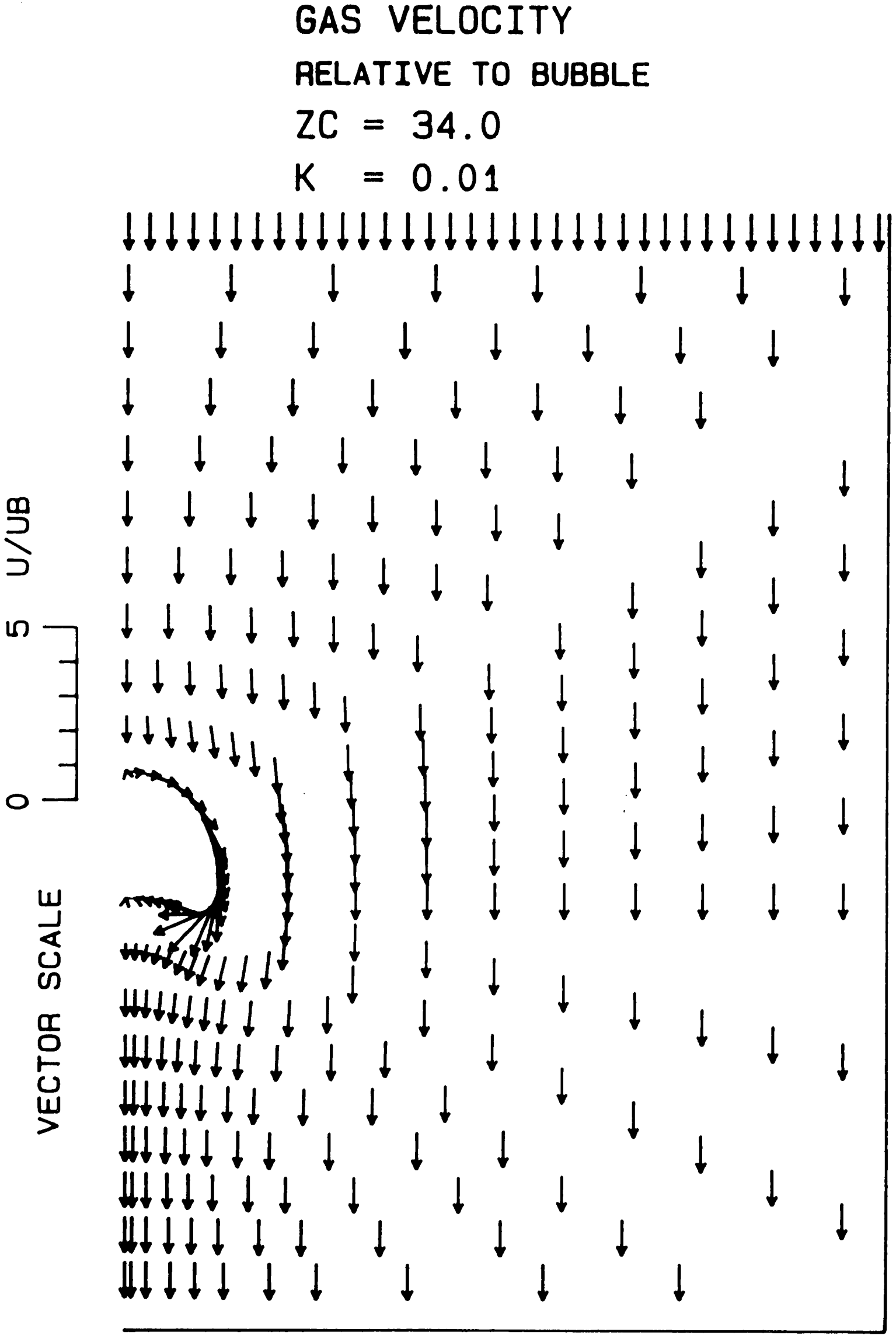

Figure 29. Vector field of interstitial gas velocity relative to bubble for Z_C = 34.0 and K = 0.01.

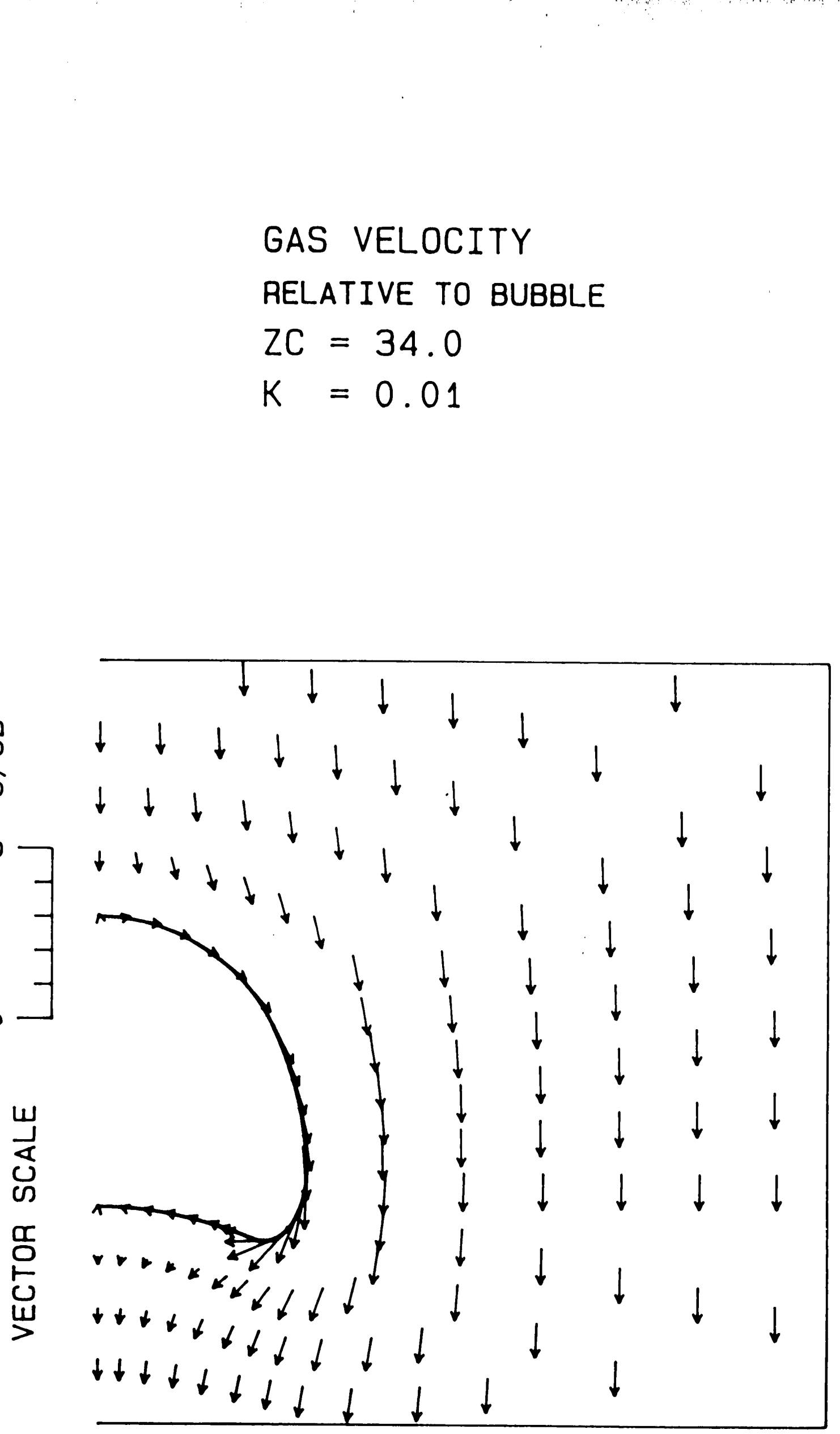

Figure 30. Vector field of interstitial gas velocity relative to bubble highlighting area near bubble for Z_C = 34.0 and K = 0.01.

GAS VELOCITY

RELATIVE TO BUBBLE

ZC = 38.6

K = 0.01

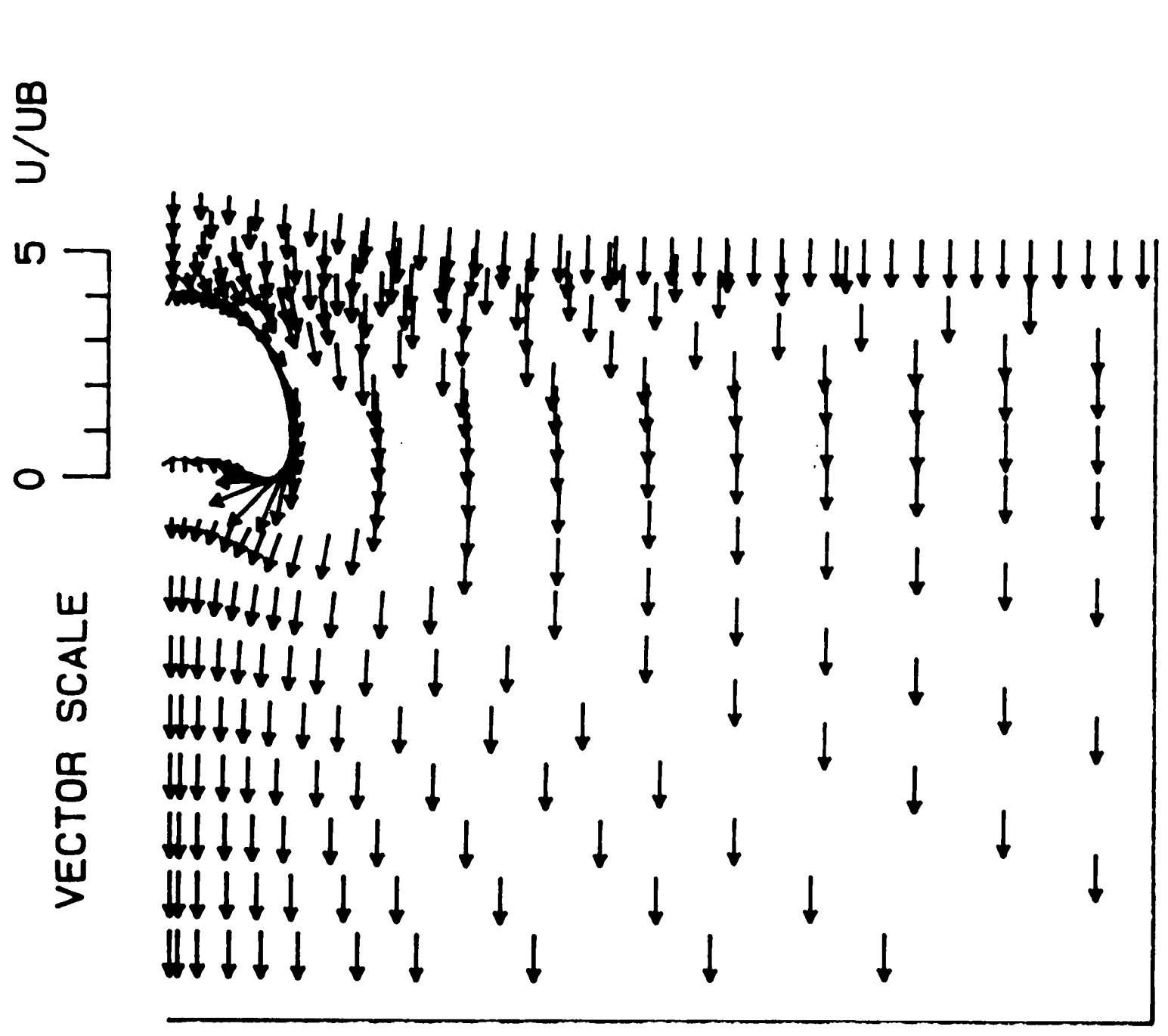

Figure 31. Vector field of interstitial gas velocity relative to bubble for Z_C = 38.6 and K = 0.01.

GAS VELOCITY

RELATIVE TO BUBBLE

ZC = 38.6

K = 0.01

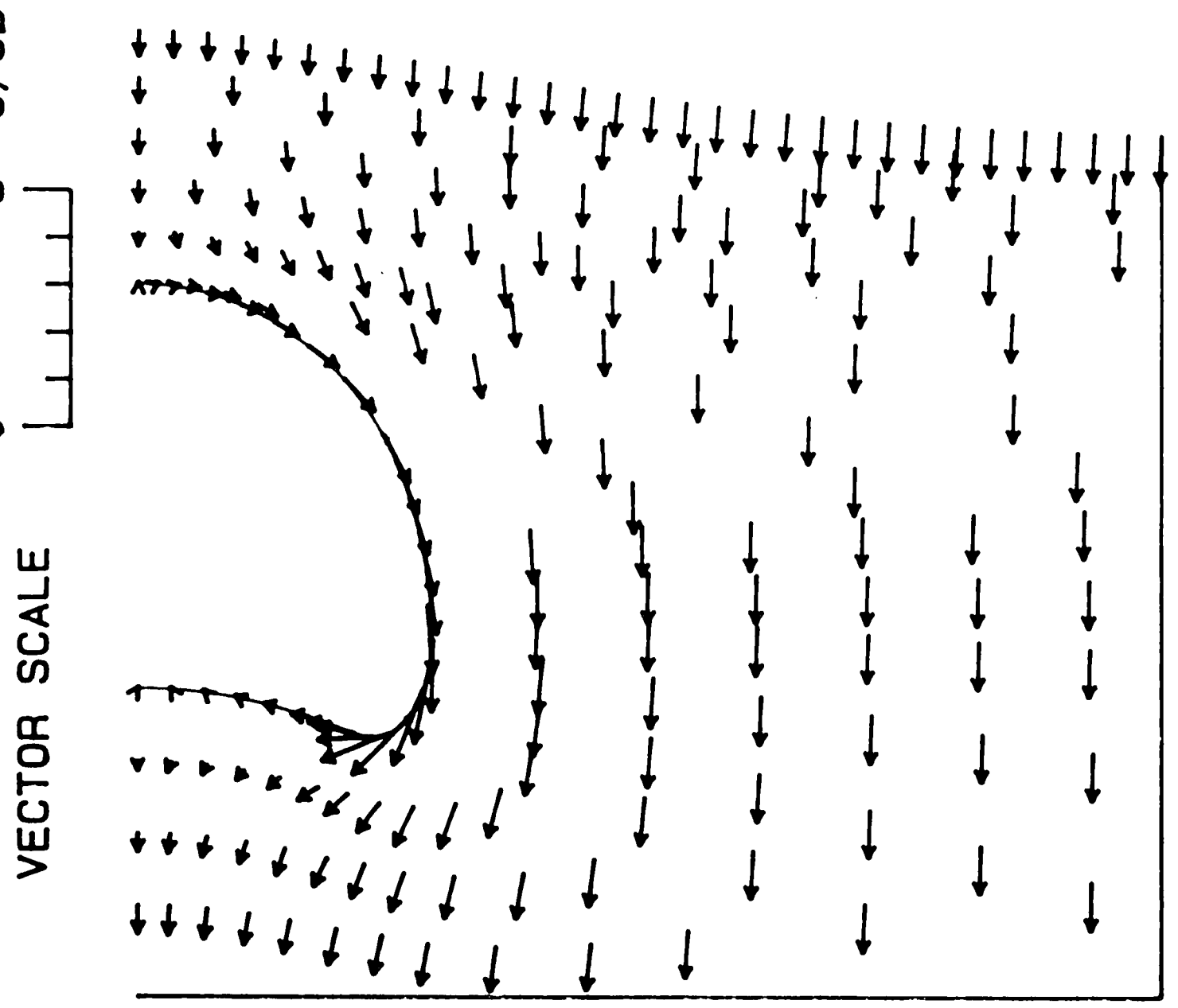

Figure 32. Vector field of interstitial gas velocity relative to bubble highlighting area near bubble for Z_C = 38.6 and K = 0.01.

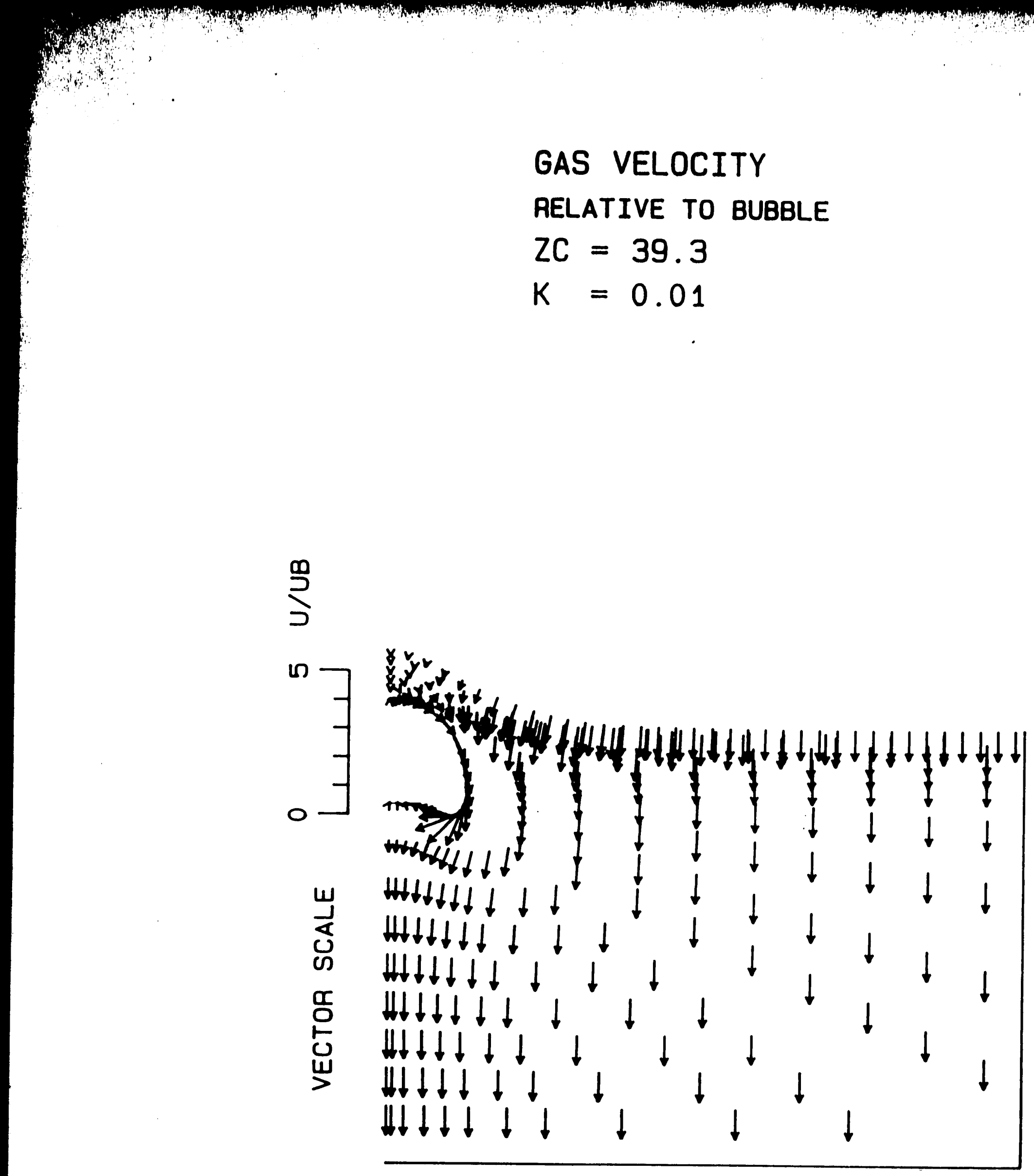

Figure 33. Vector field of interstitial gas velocity relative to bubble for Z_c = 39.3 and K = 0.01.

GAS VELOCITY

RELATIVE TO BUBBLE

ZC = 39.3

K = 0.01

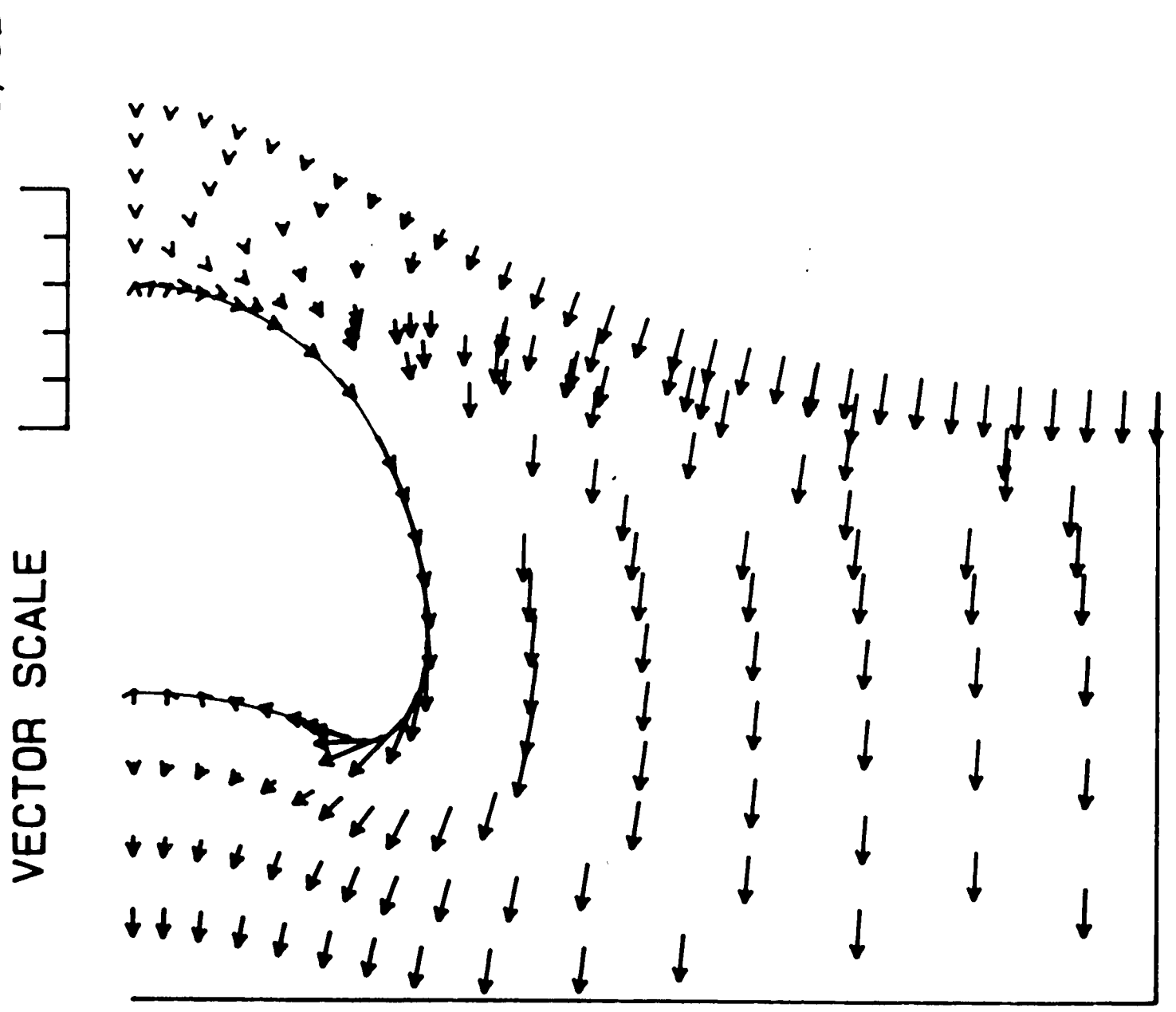

Figure 34. Vector field of interstitial gas velocity relative to bubble highlighting area near bubble for Z_C = 39.3 and K = 0.01.

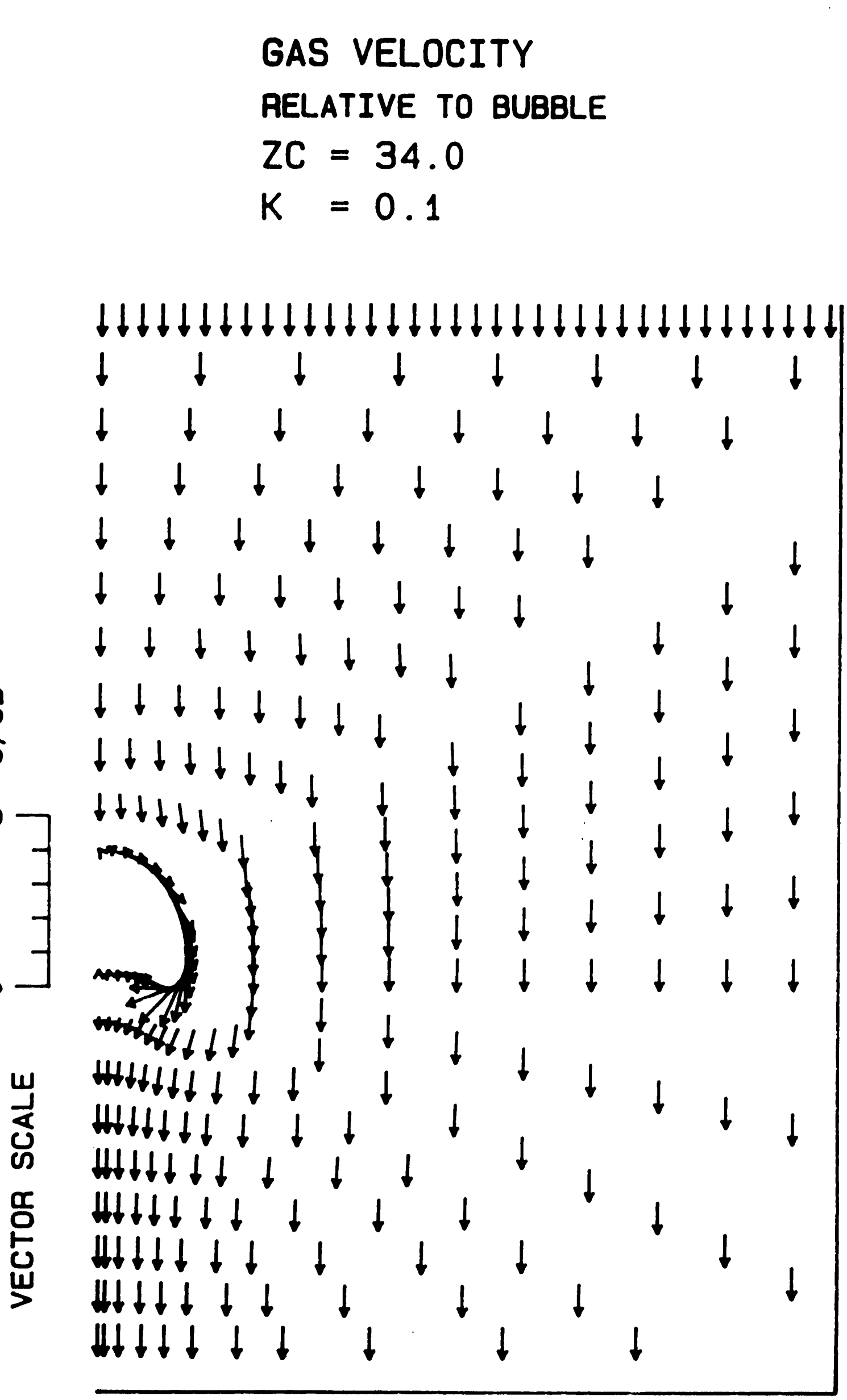

Figure 35. Vector field of interstitial gas velocity relative to bubble for Z_c = 34.0 and K = 0.1.

GAS VELOCITY

RELATIVE TO BUBBLE

ZC = 34.0

K = 0.1

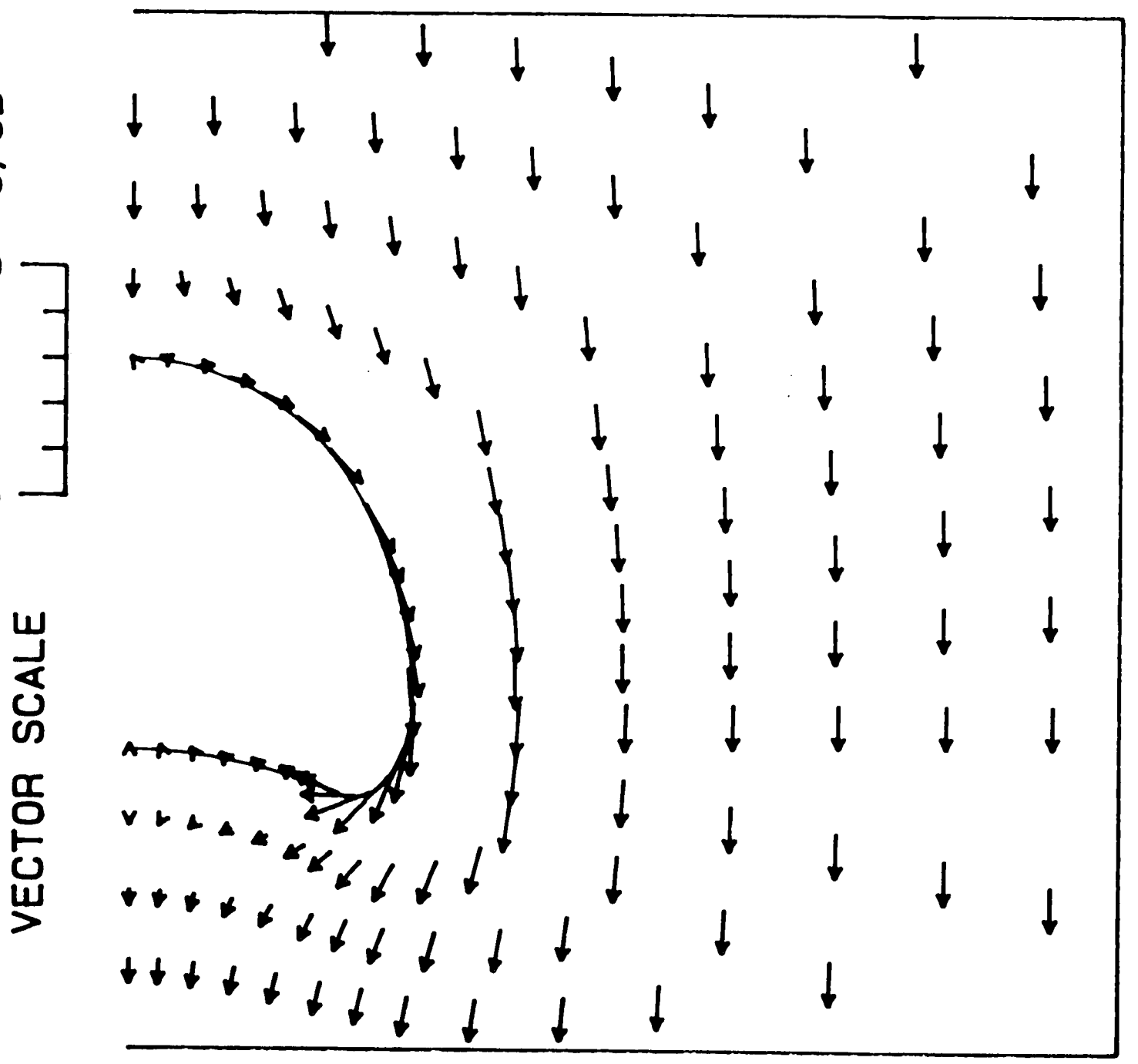

Figure 36. Vector field of interstitial gas velocity relative to bubble highlighting area near bubble for Z_C = 34.0 and K = 0.1.

GAS VELOCITY

RELATIVE TO BUBBLE

ZC = 38.6

K = 0.1

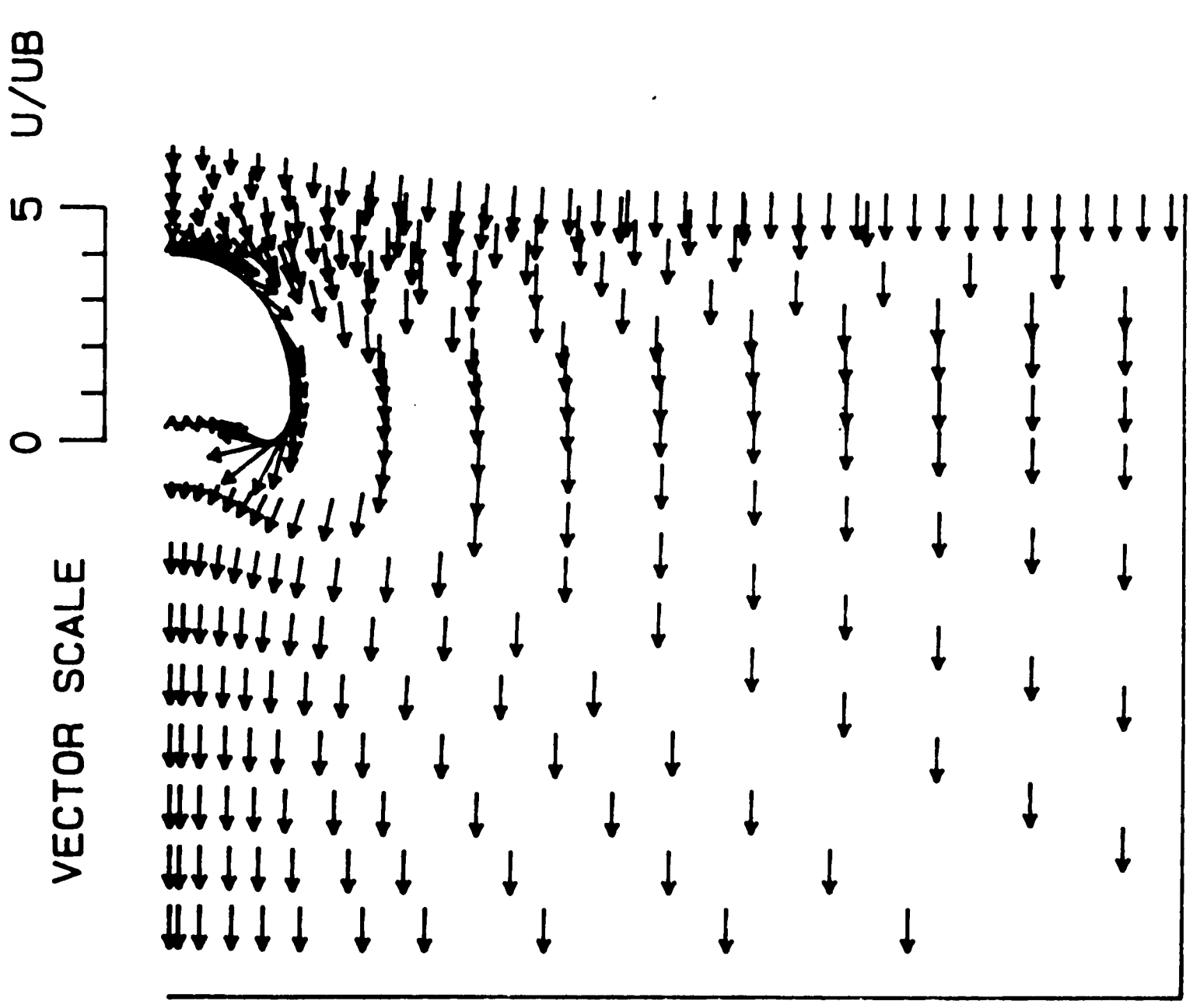

Figure 37. Vector field of interstitial gas velocity relative to bubble for Z_C = 38.6 and K = 0.1.

GAS VELOCITY

RELATIVE TO BUBBLE

ZC = 38.6

K = 0.1

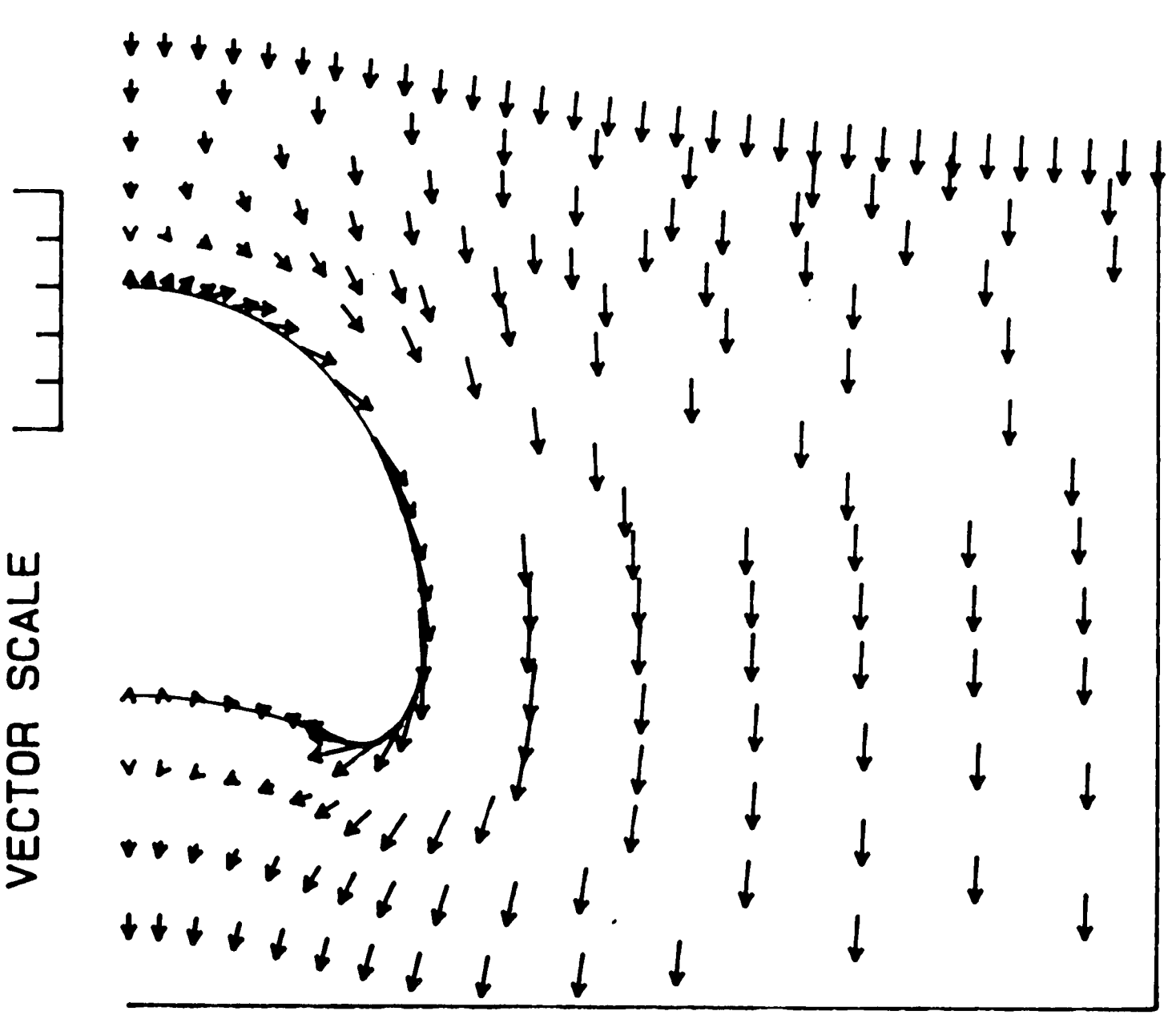

Figure 38. Vector field of interstitial gas velocity relative to bubble highlighting area near bubble for Z_C = 38.6 and K = 0.1.

GAS VELOCITY

RELATIVE TO BUBBLE

ZC = 39.3

K = 0.1

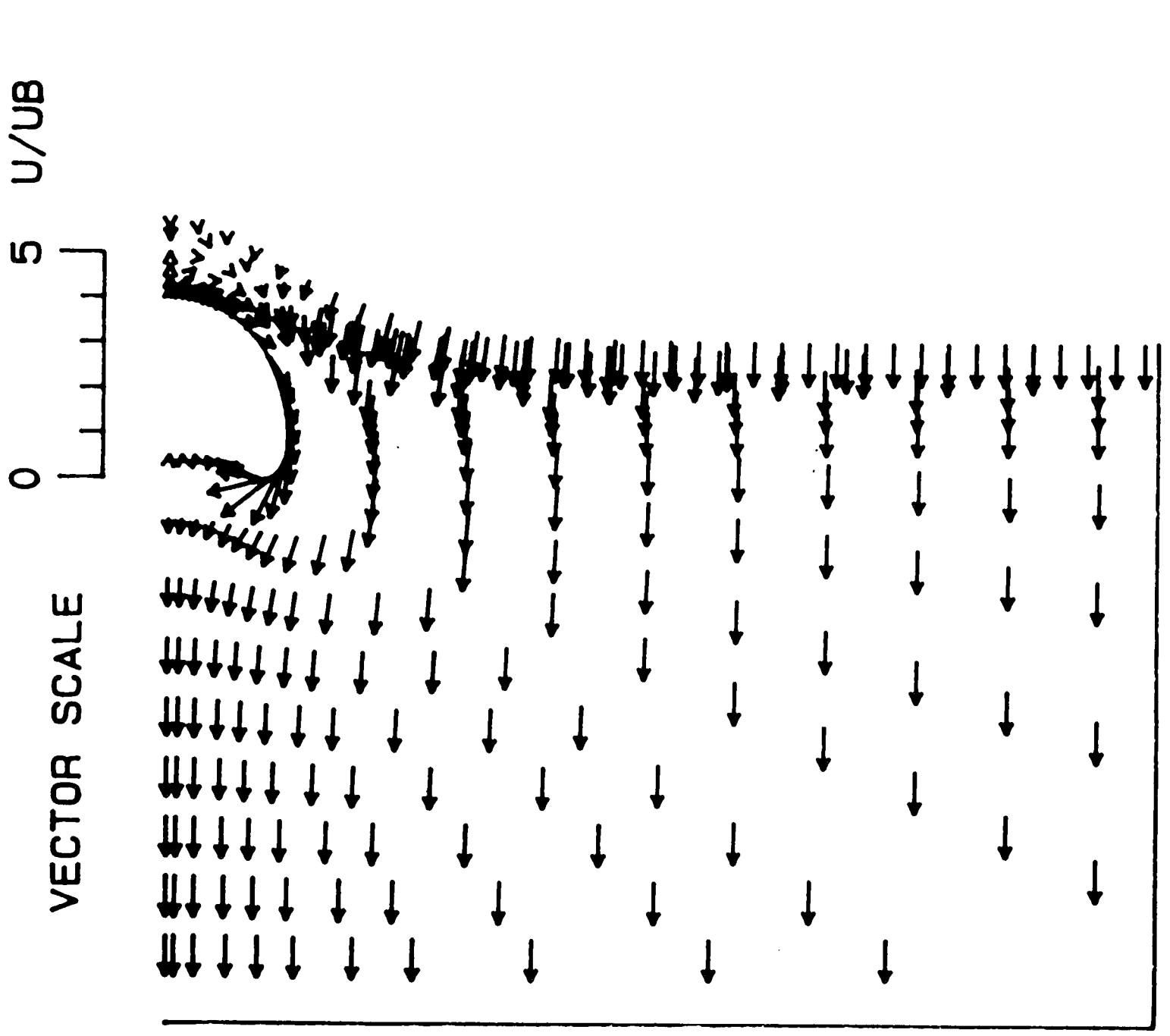

Figure 39. Vector field of interstitial gas velocity relative to bubble for Z_C = 39.3 and K = 0.1.

GAS VELOCITY

RELATIVE TO BUBBLE

ZC = 39.3

K = 0.1

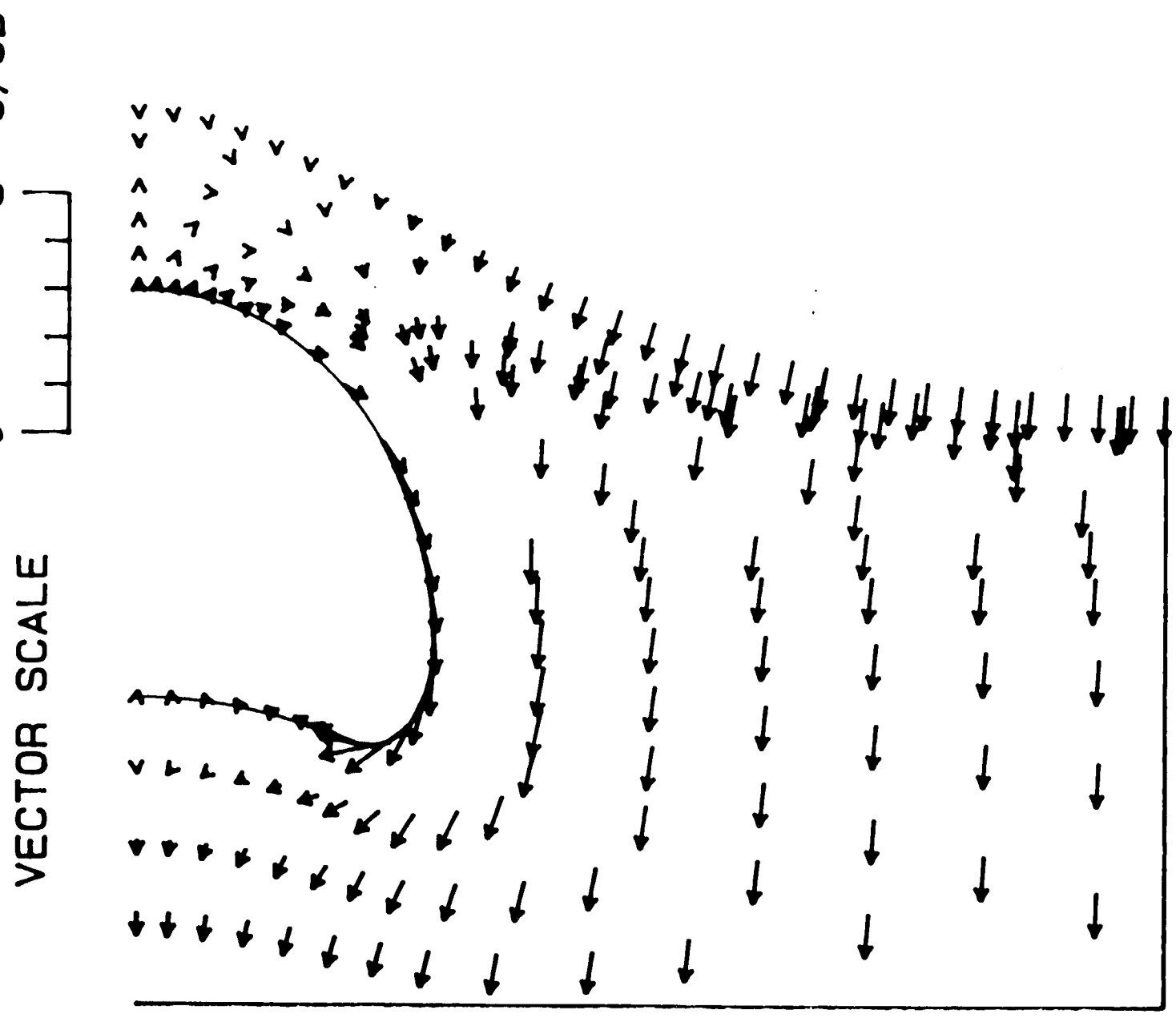

Figure 40. Vector field of interstitial gas velocity relative to bubble highlighting area near bubble for Z_c = 39.3 and K = 0.1.

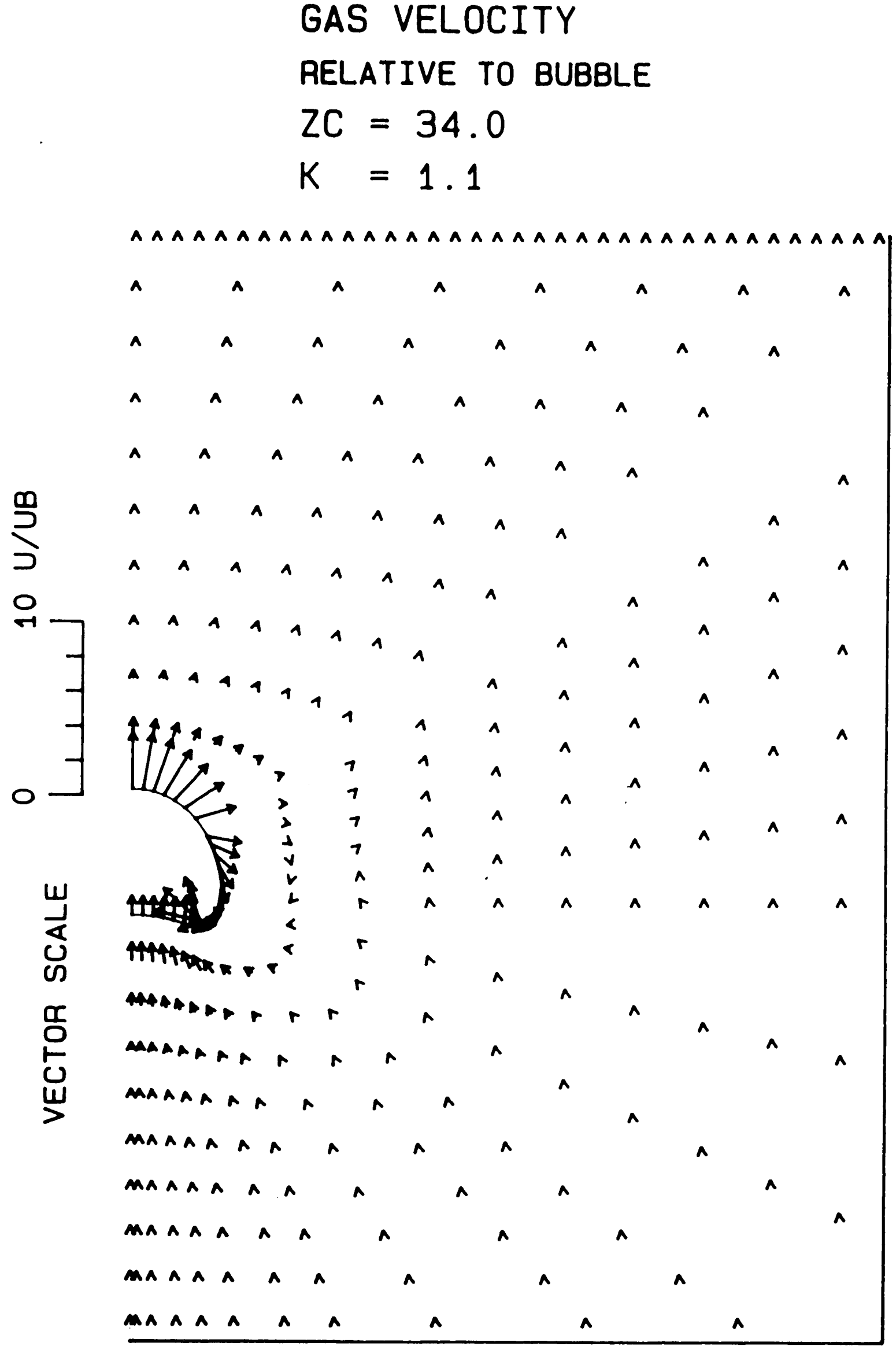

Figure 41. Vector field of interstitial gas velocity relative to bubble for Z_c = 34.0 and K = 1.1.

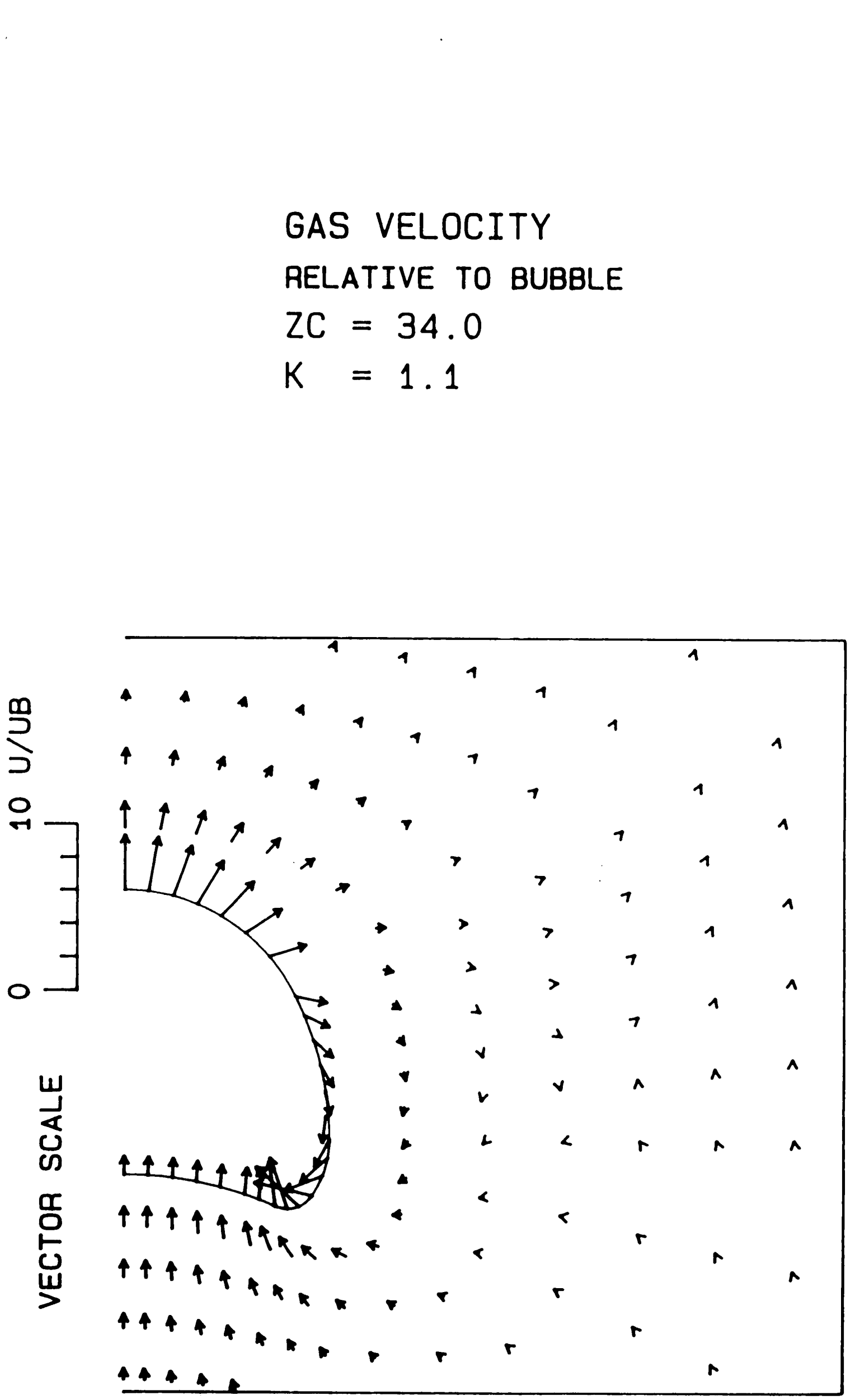

Figure 42. Vector field of interstitial gas velocity relative to bubble highlighting area near bubble for Z_c = 34.0 and K = 1.1.

GAS VELOCITY

RELATIVE TO BUBBLE

ZC = 38.6

K = 1.1

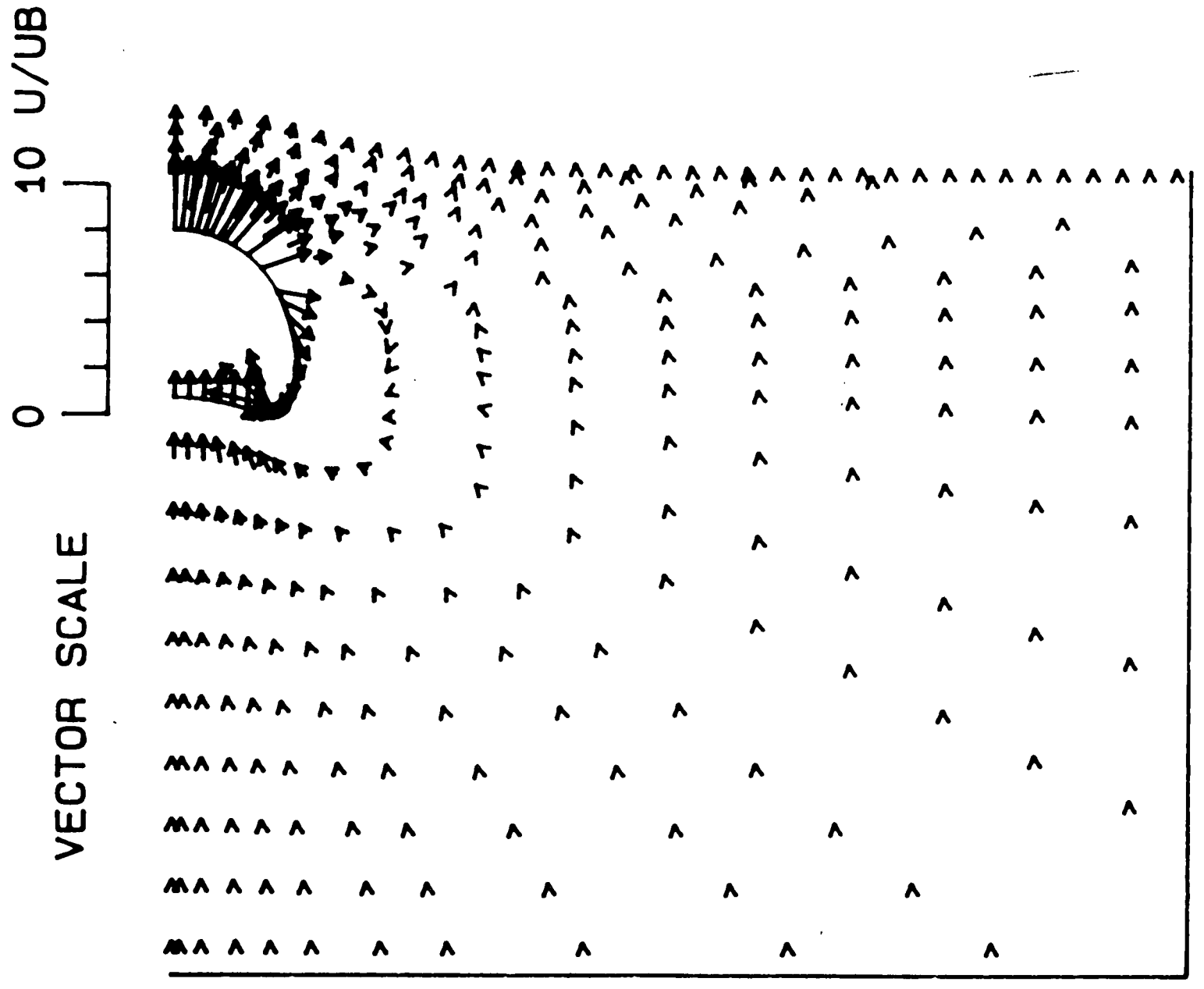

Figure 43. Vector field of interstitial gas velocity relative to bubble for Z_c = 38.6 and K = 1.1.

GAS VELOCITY

RELATIVE TO BUBBLE

ZC = 38.6

K = 1.1

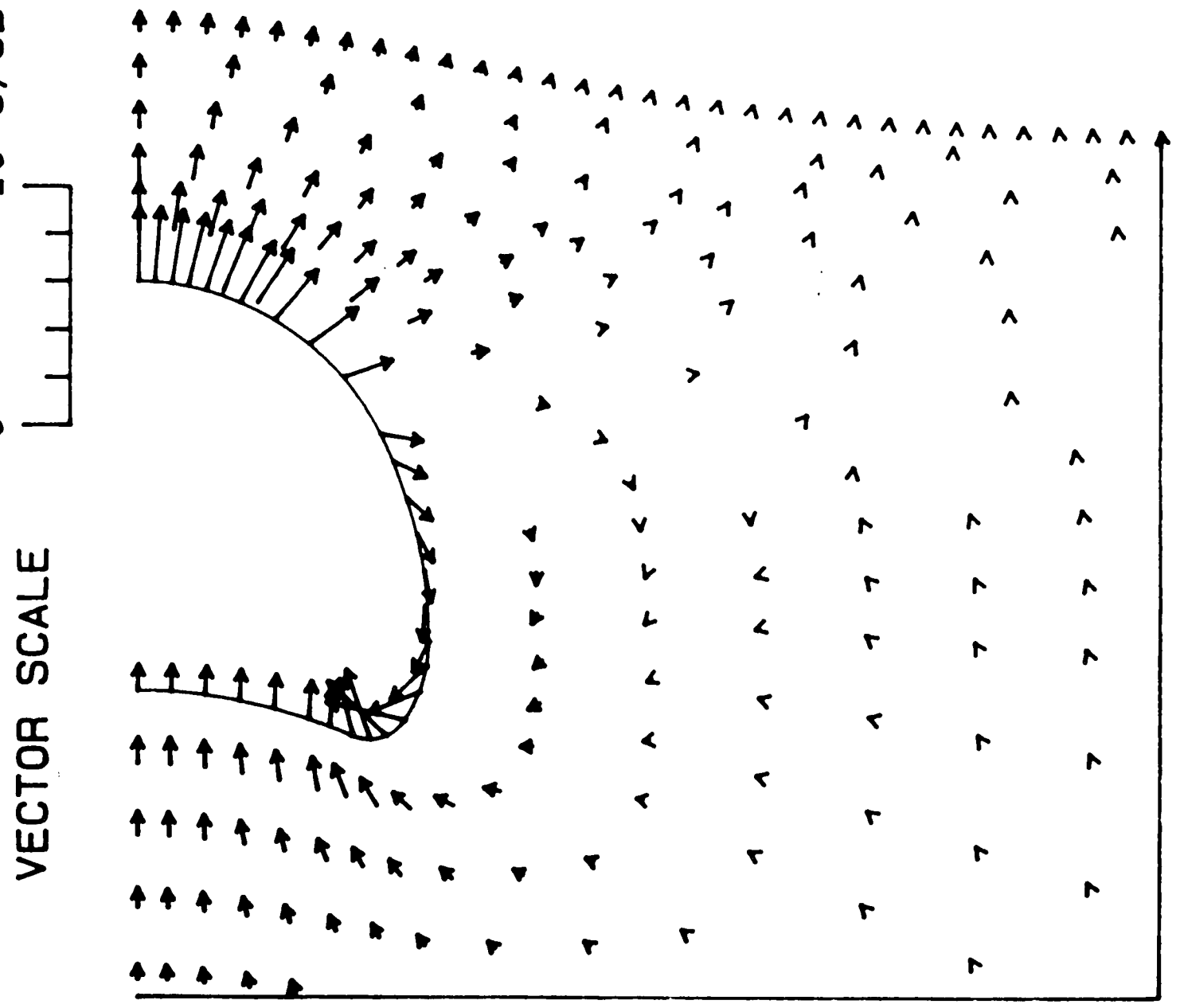

Figure 44. Vector field of interstitial gas velocity relative to bubble highlighting area near bubble for Z_C = 38.6 and K = 1.1.

GAS VELOCITY

RELATIVE TO BUBBLE

ZC = 39.3

K = 1.1

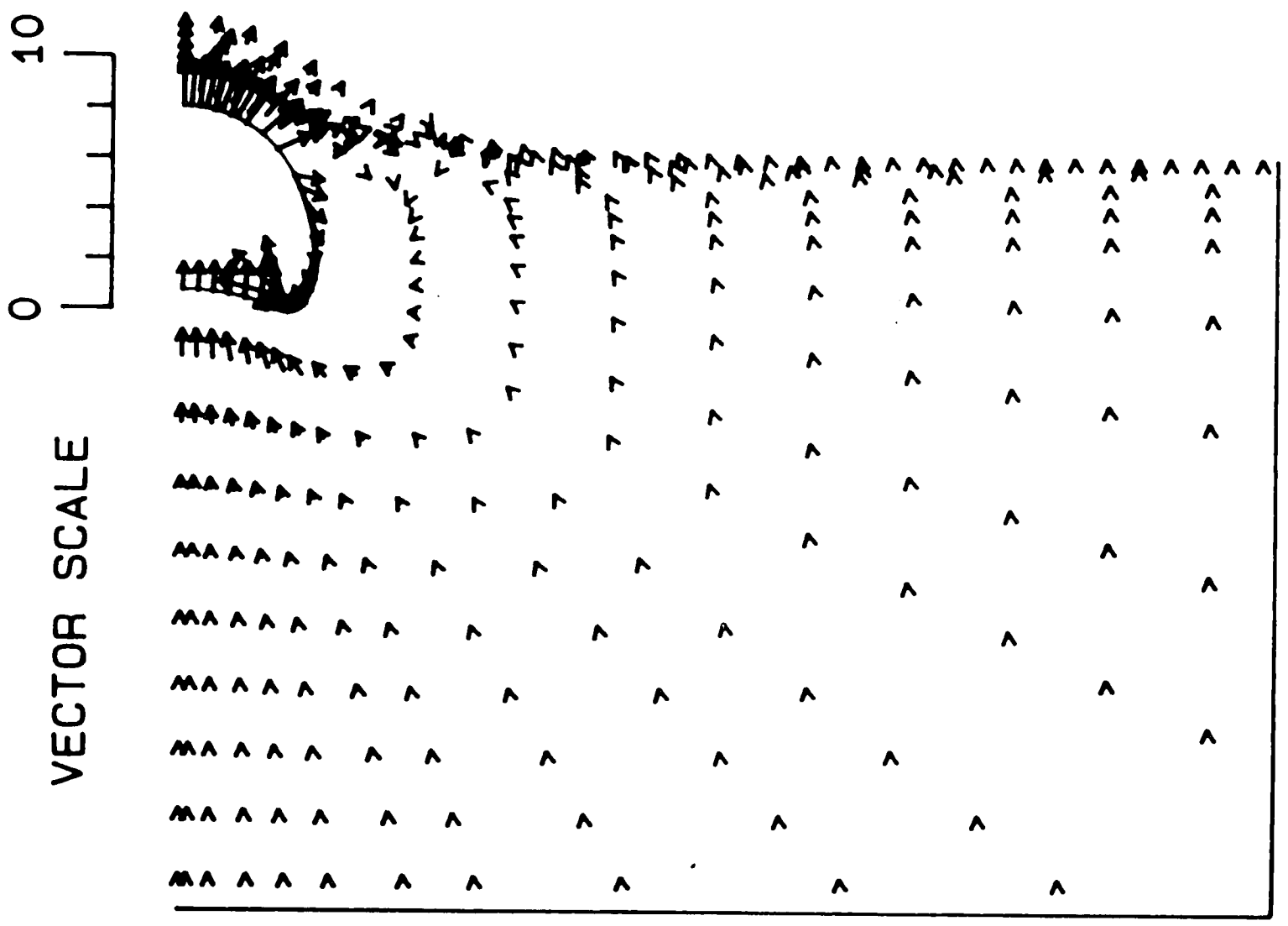

Figure 45. Vector field of interstitial gas velocity relative to bubble for Z_C = 39.3 and K = 1.1.

GAS VELOCITY

RELATIVE TO BUBBLE

ZC = 39.3

K = 1.1

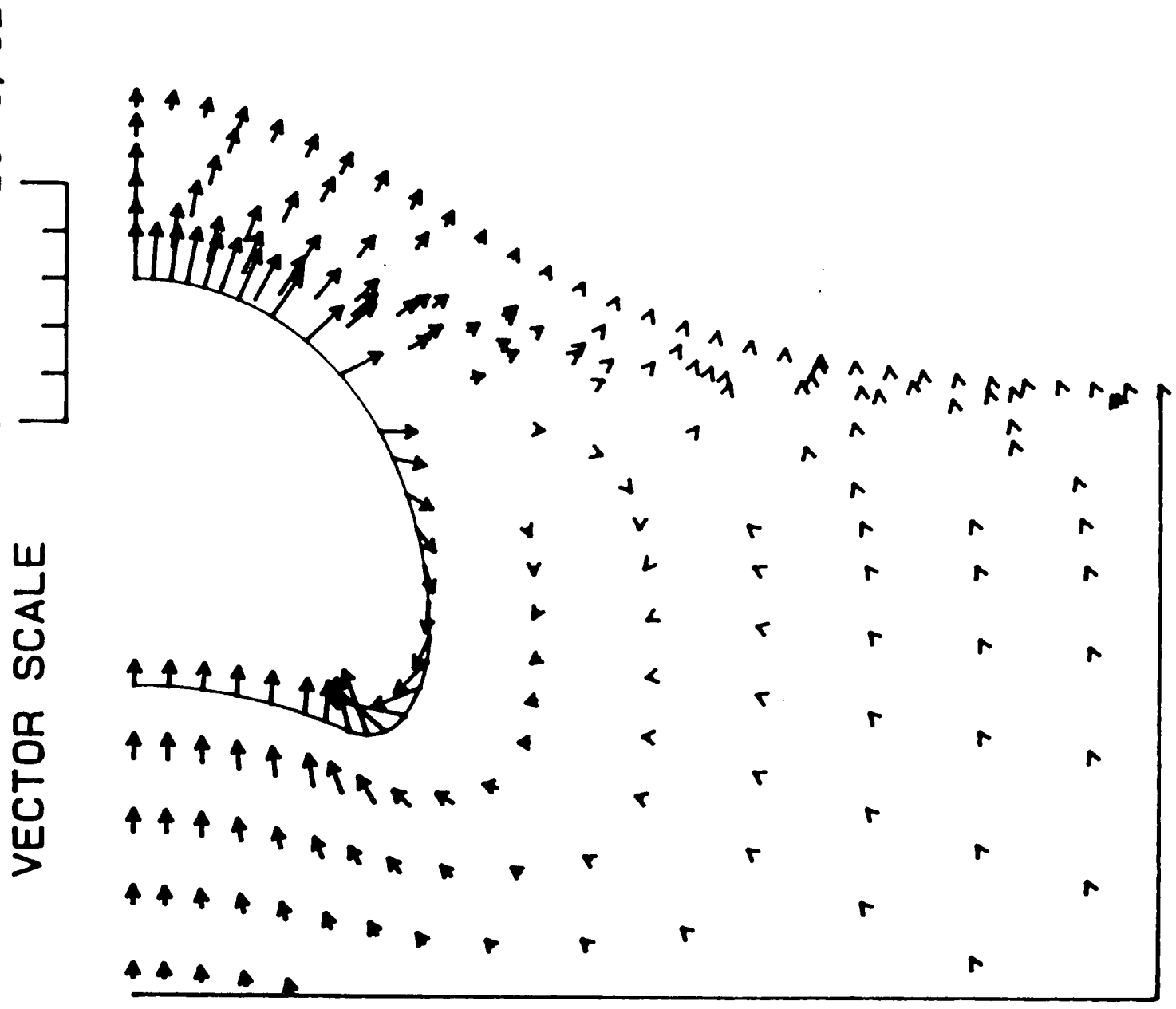

Figure 46. Vector field of interstitial gas velocity relative to bubble highlighting area near bubble for Z_C = 39.3 and K = 1.1.

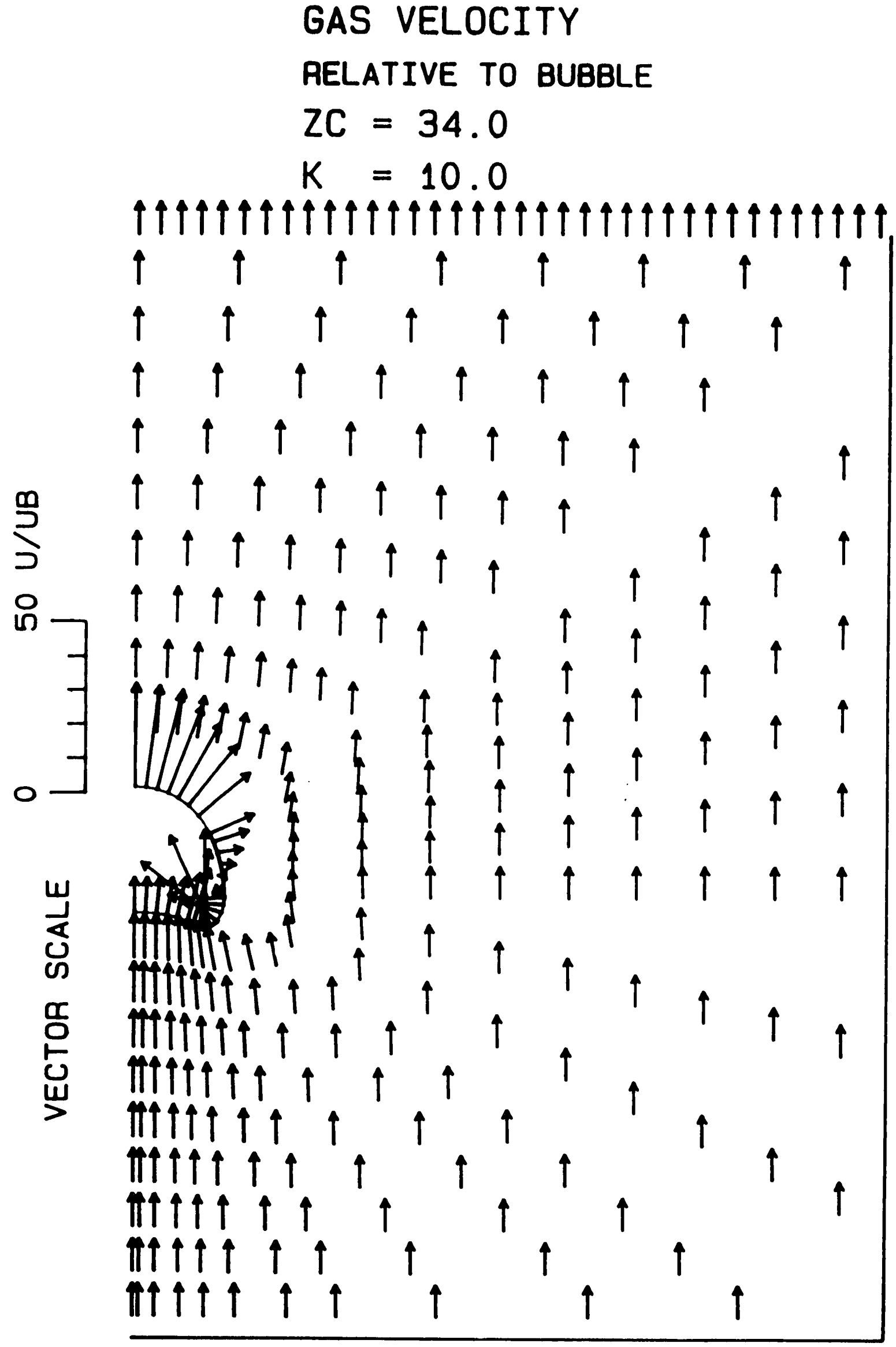

Figure 47. Vector field of interstitial gas velocity relative to bubble for Z_c = 34.0 and K = 10.0.

GAS VELOCITY

RELATIVE TO BUBBLE

ZC = 34.0

K = 10.0

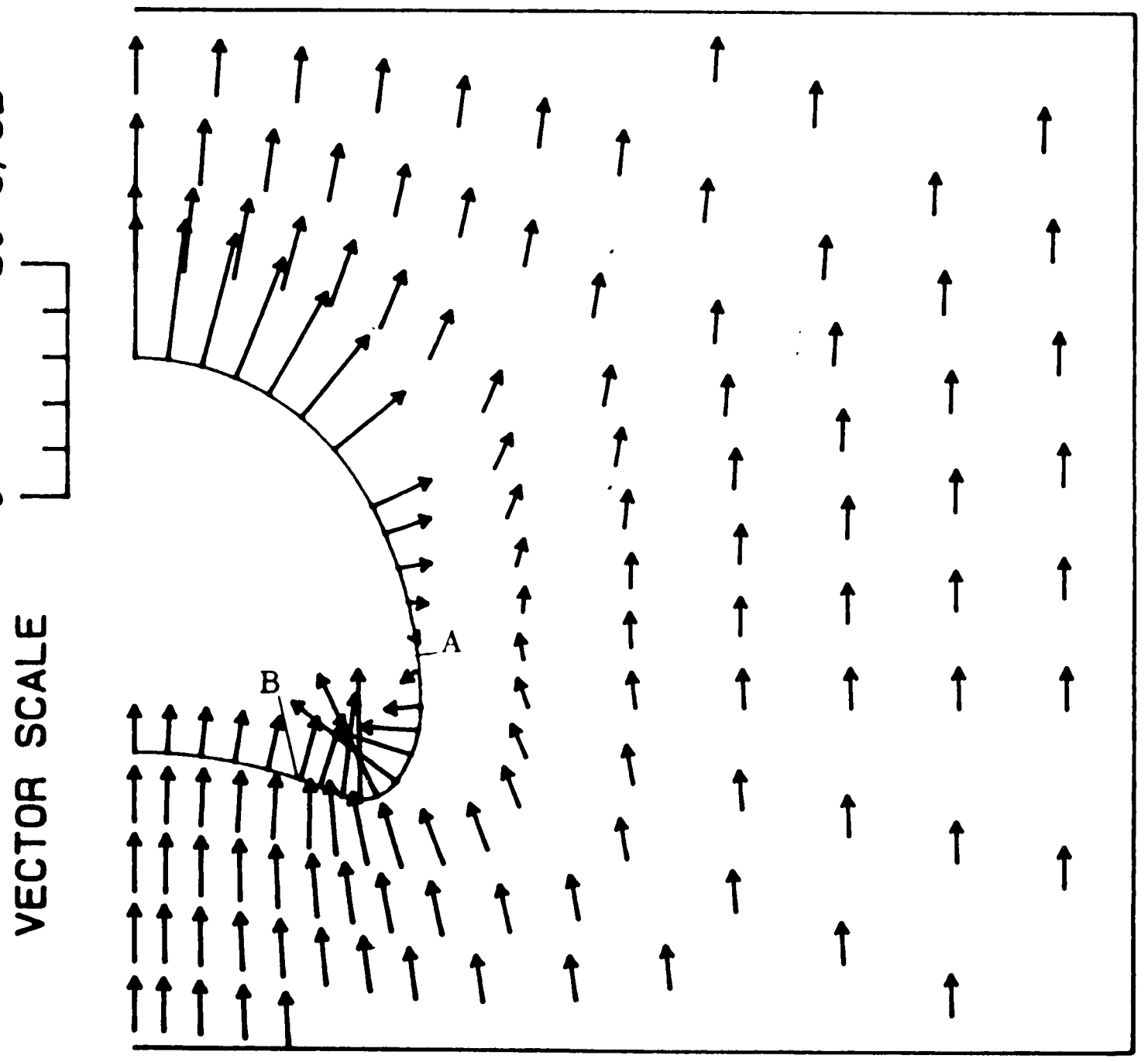

Figure 48. Vector field of interstitial gas velocity relative to bubble highlighting area near bubble for Z_c = 34.0 and K = 10.0.

GAS VELOCITY

RELATIVE TO BUBBLE

ZC = 38.6

K = 10.0

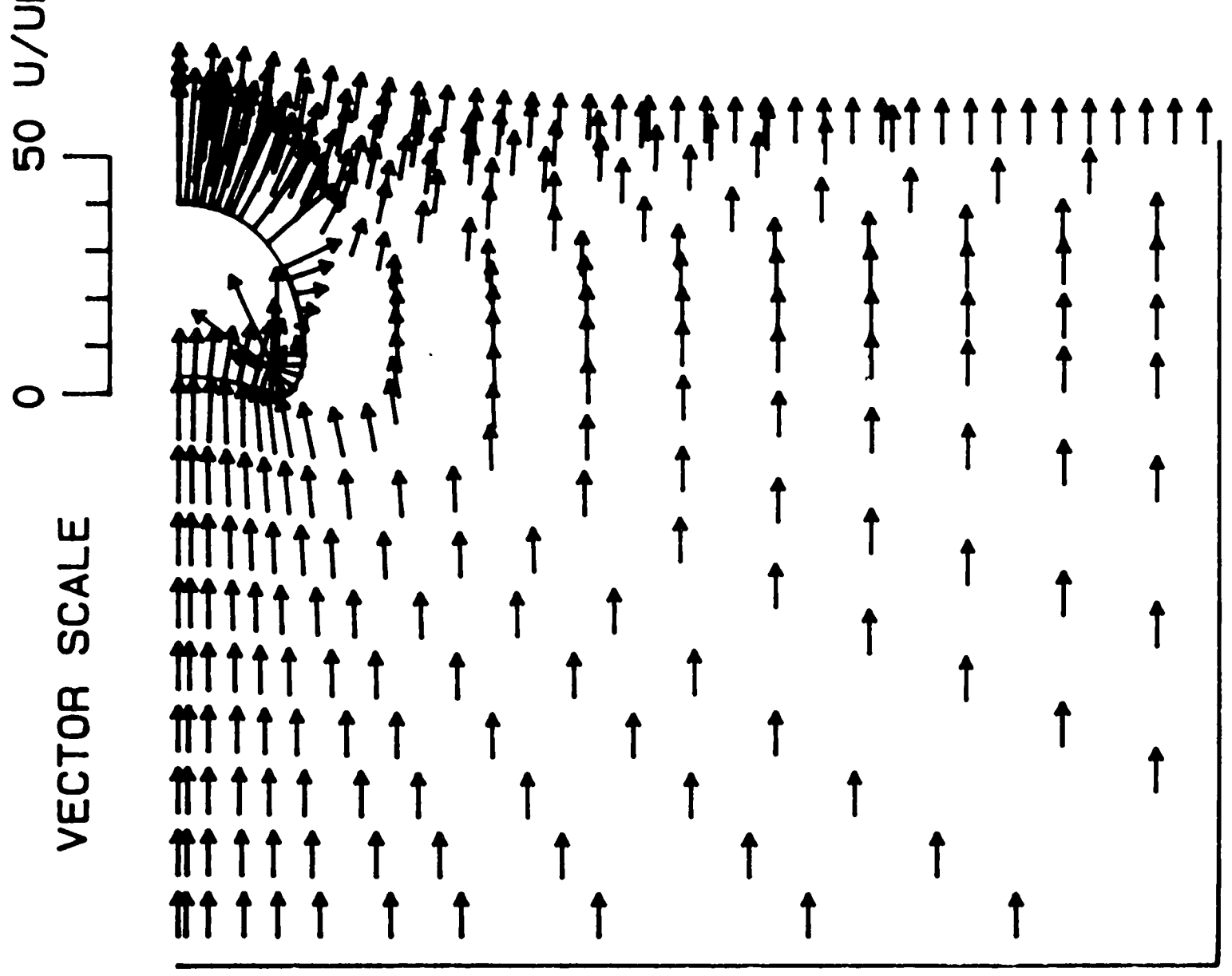

Figure 49. Vector field of interstitial gas velocity relative to bubble for Z_c = 38.6 and K = 10.0.

GAS VELOCITY

RELATIVE TO BUBBLE

ZC = 38.6

K = 10.0

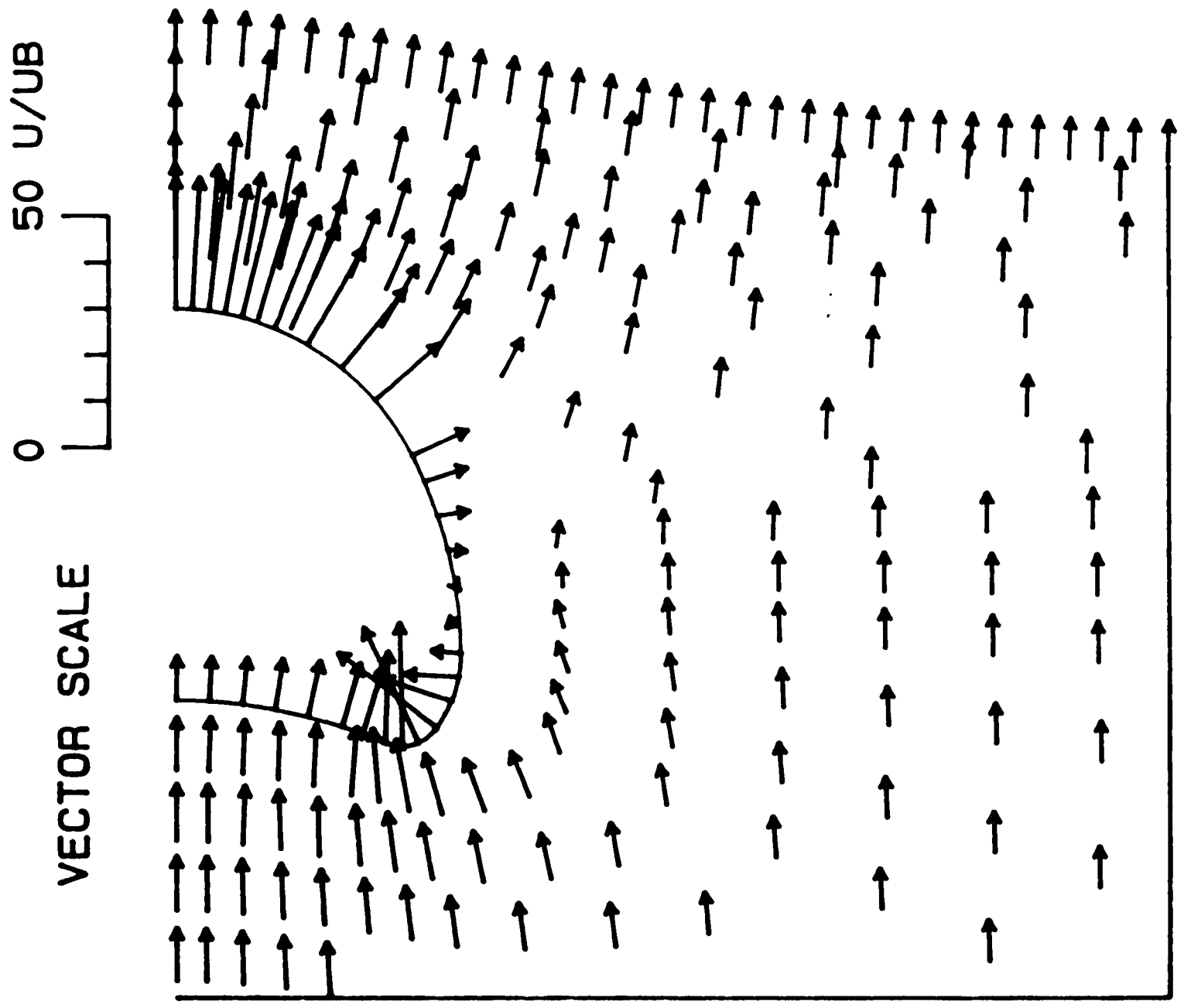

Figure 50. Vector field of interstitial gas velocity relative to bubble highlighting area near bubble for Z_c = 38.6 and K = 10.0.

GAS VELOCITY

RELATIVE TO BUBBLE

ZC = 39.3

K = 10.0

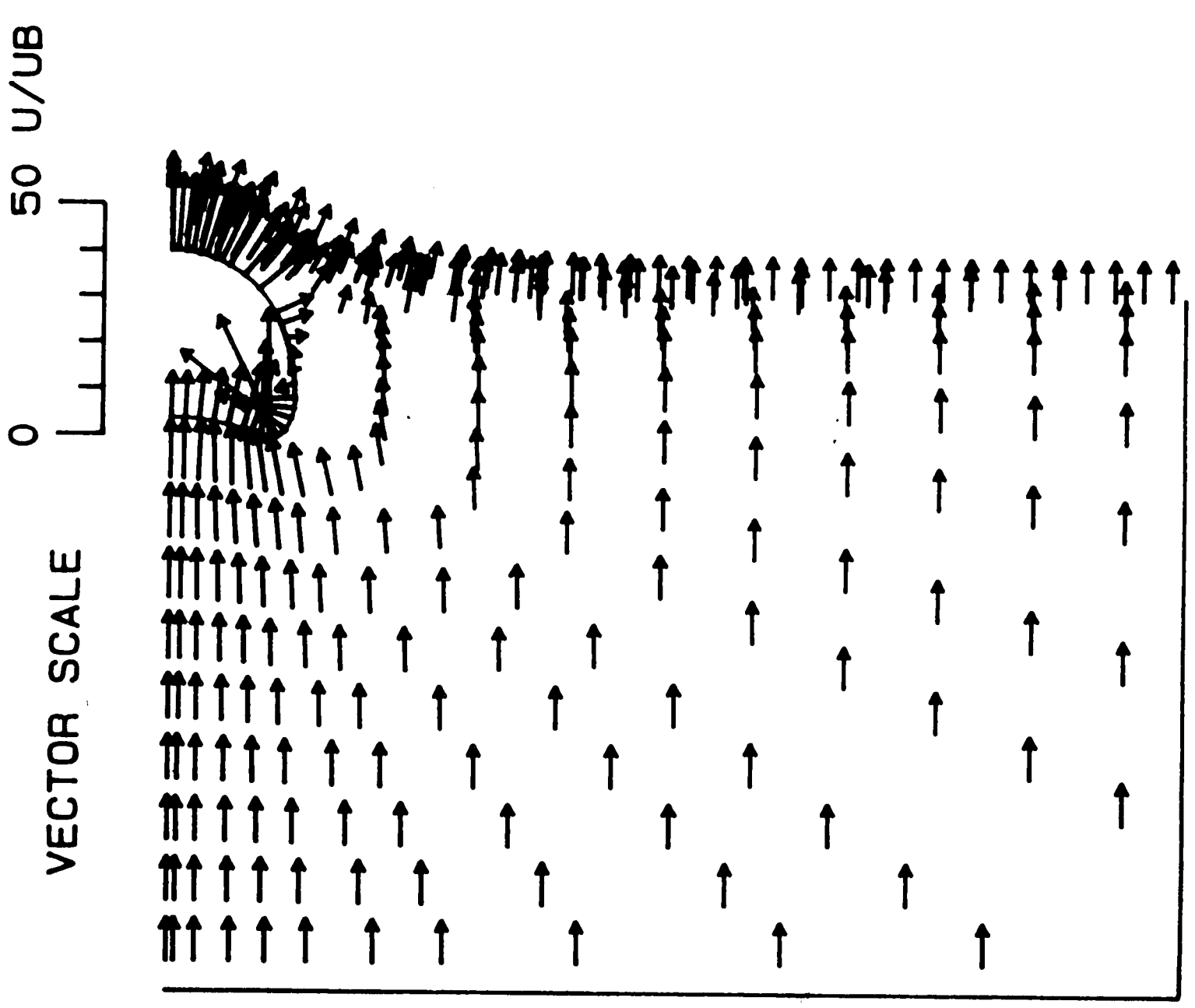

Figure 51. Vector field of interstitial gas velocity relative to bubble for Z_C = 39.3 and K = 10.0.

GAS VELOCITY

RELATIVE TO BUBBLE

ZC = 39.3

K = 10.0

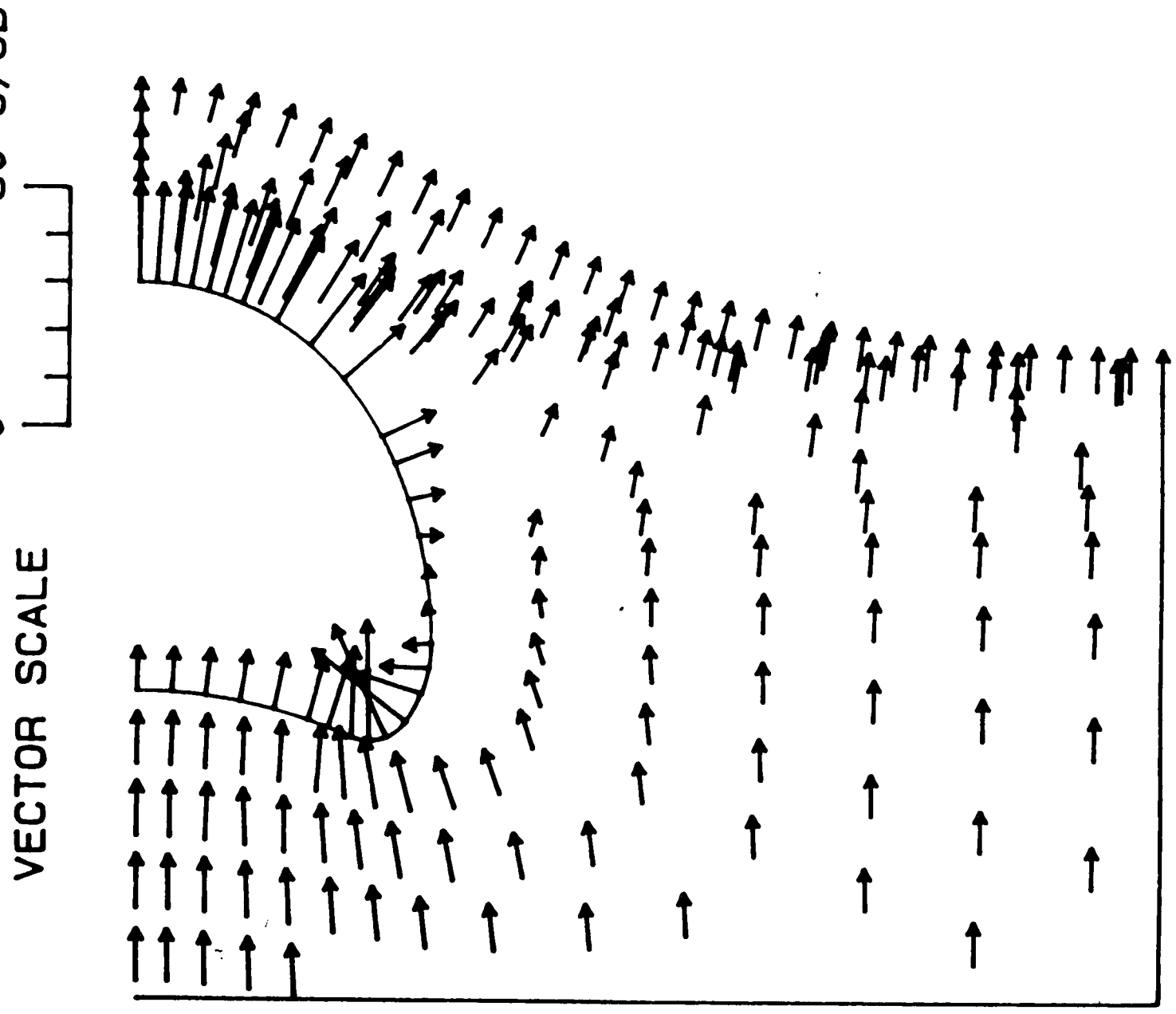

Figure 52. Vector field of interstitial gas velocity relative to bubble highlighting area near bubble for Z_c = 39.3 and K = 10.0.

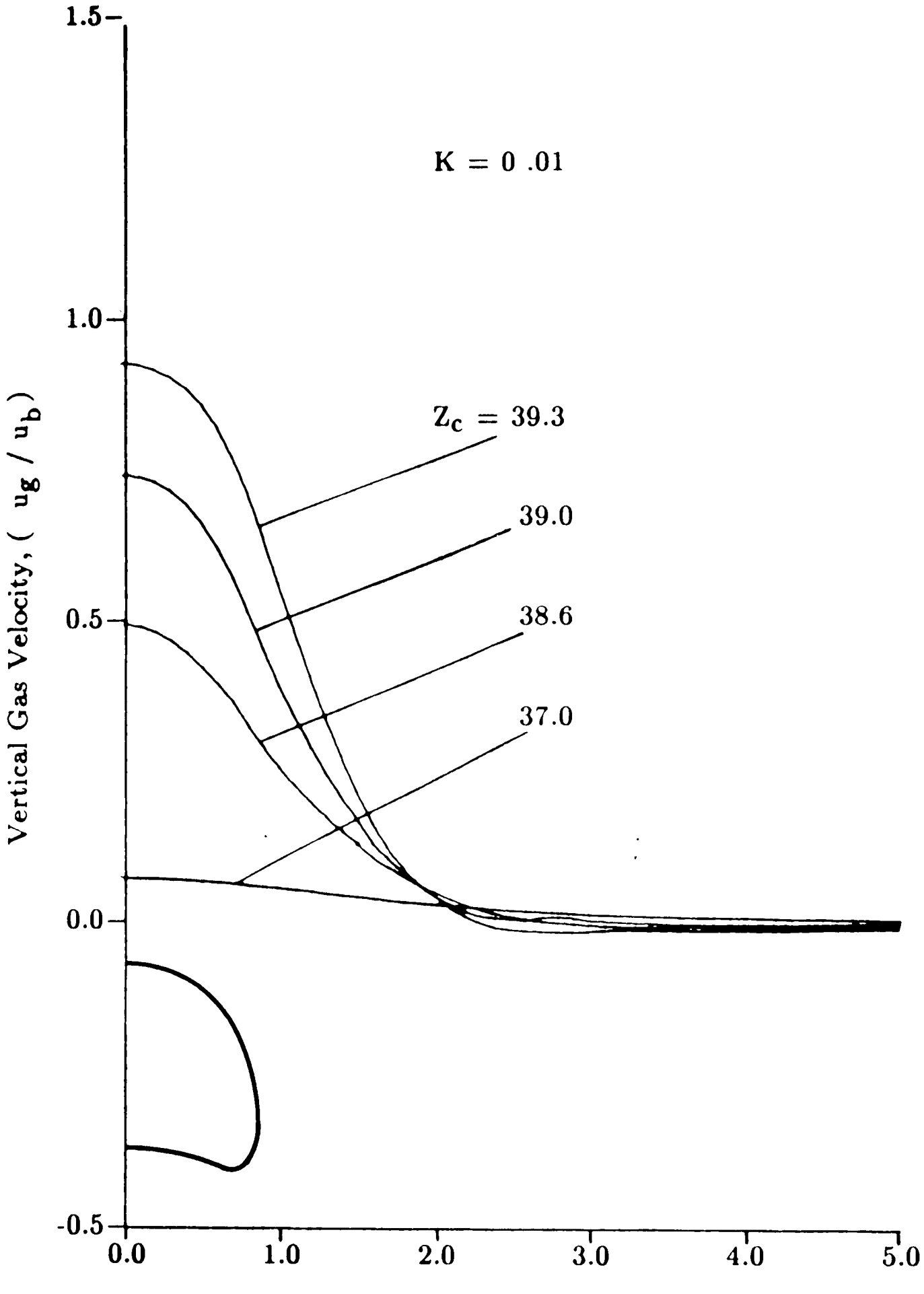

Figure 53. Vertical component of absolute interstitial gas velocity at free surface for K = 0.01

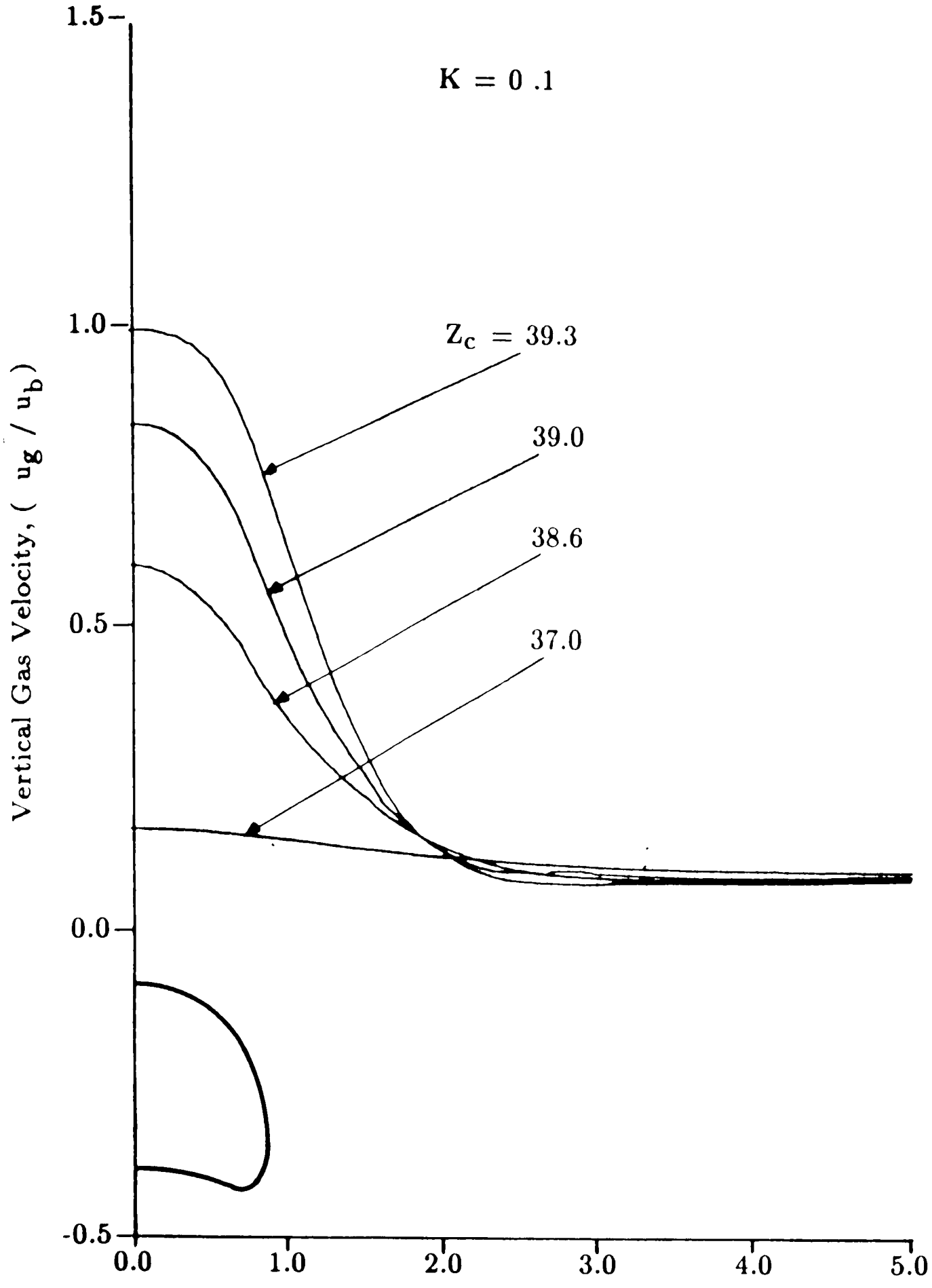

Figure 54. Vertical component of absolute interstitial gas velocity at free surface for K = 0.1

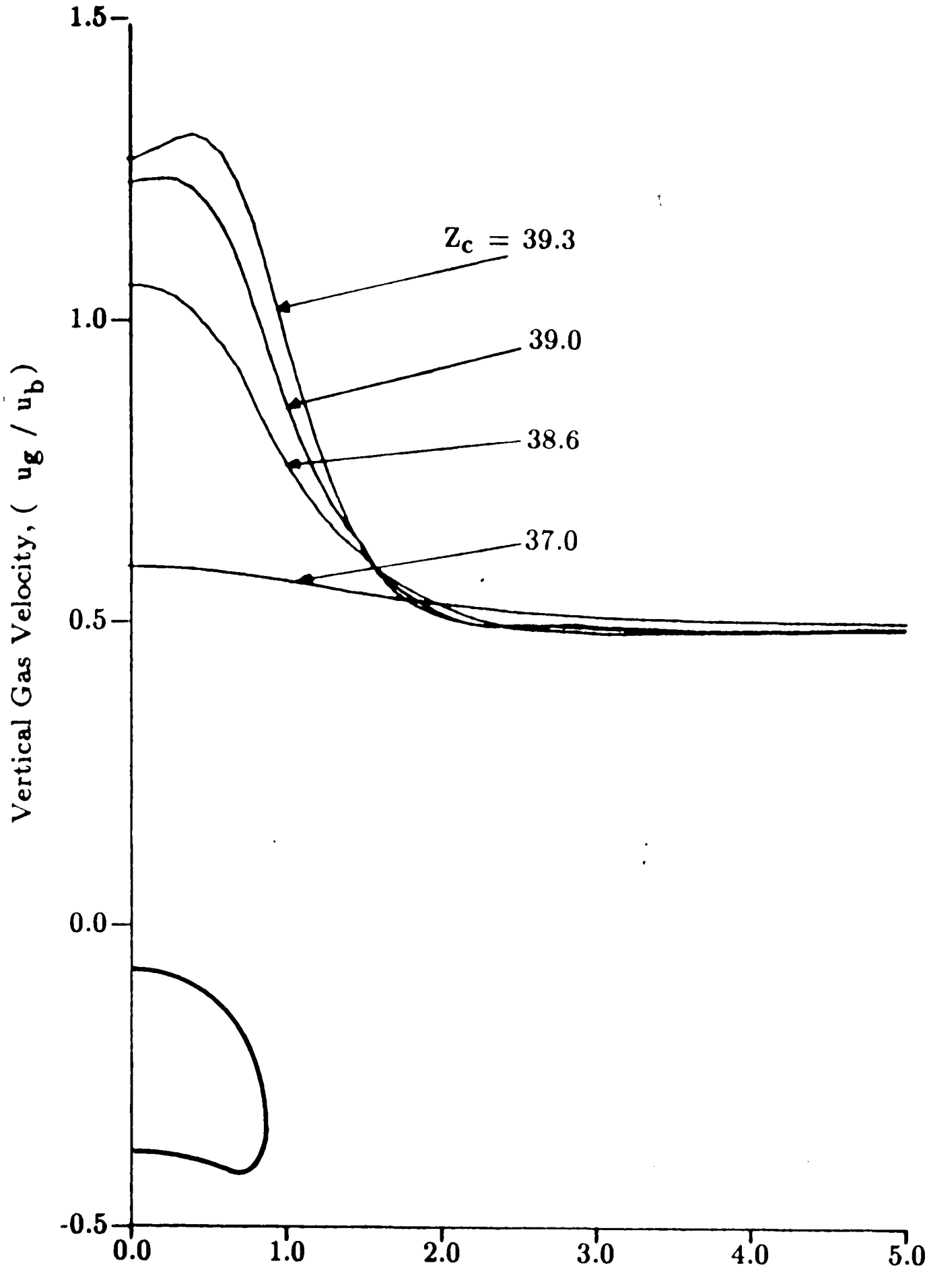

Figure 55. Vertical component of absolute interstitial gas velocity at free surface for K = 0.5

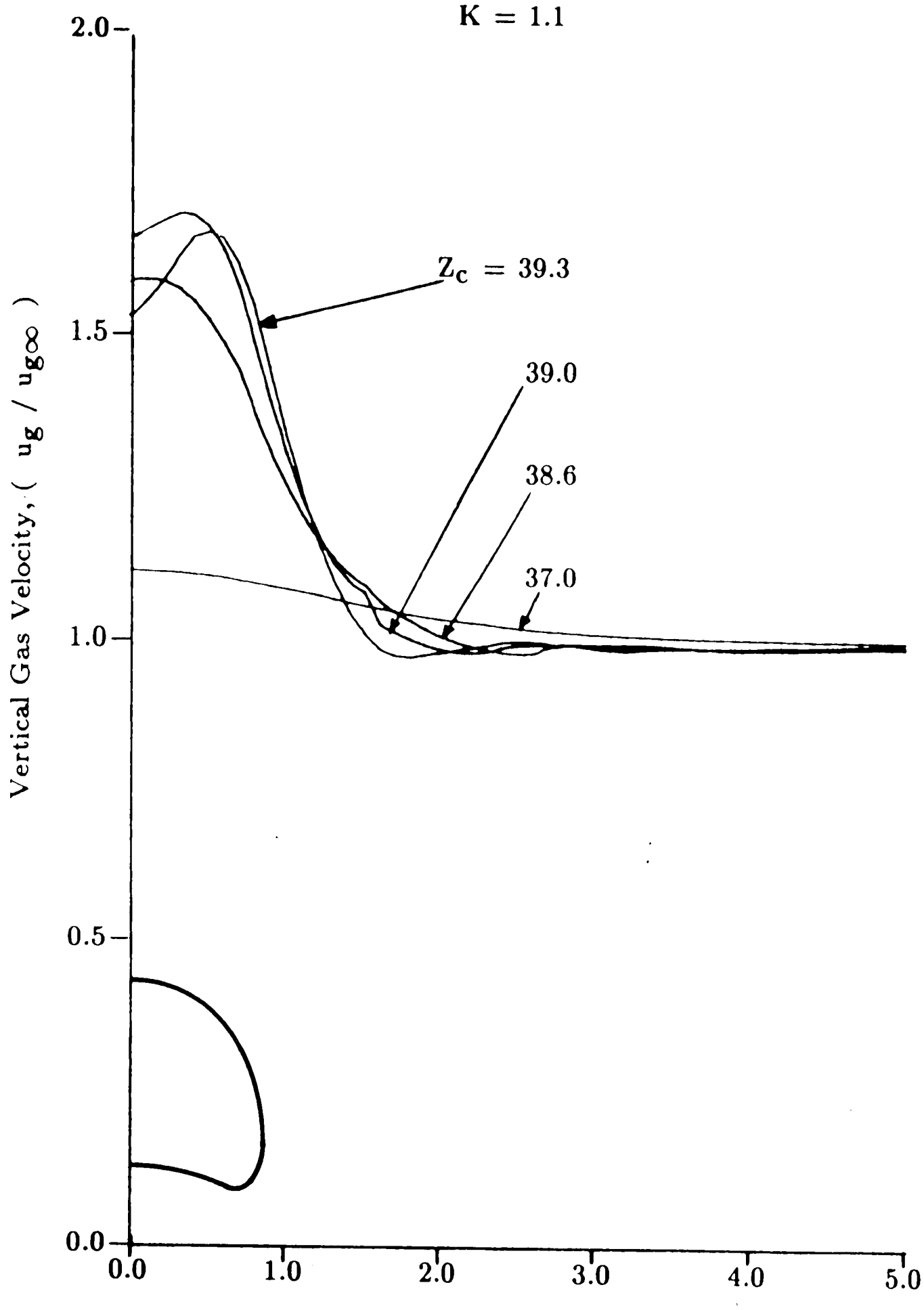

Figure 56. Vertical component of absolute interstitial gas velocity at free surface for K = 1.1

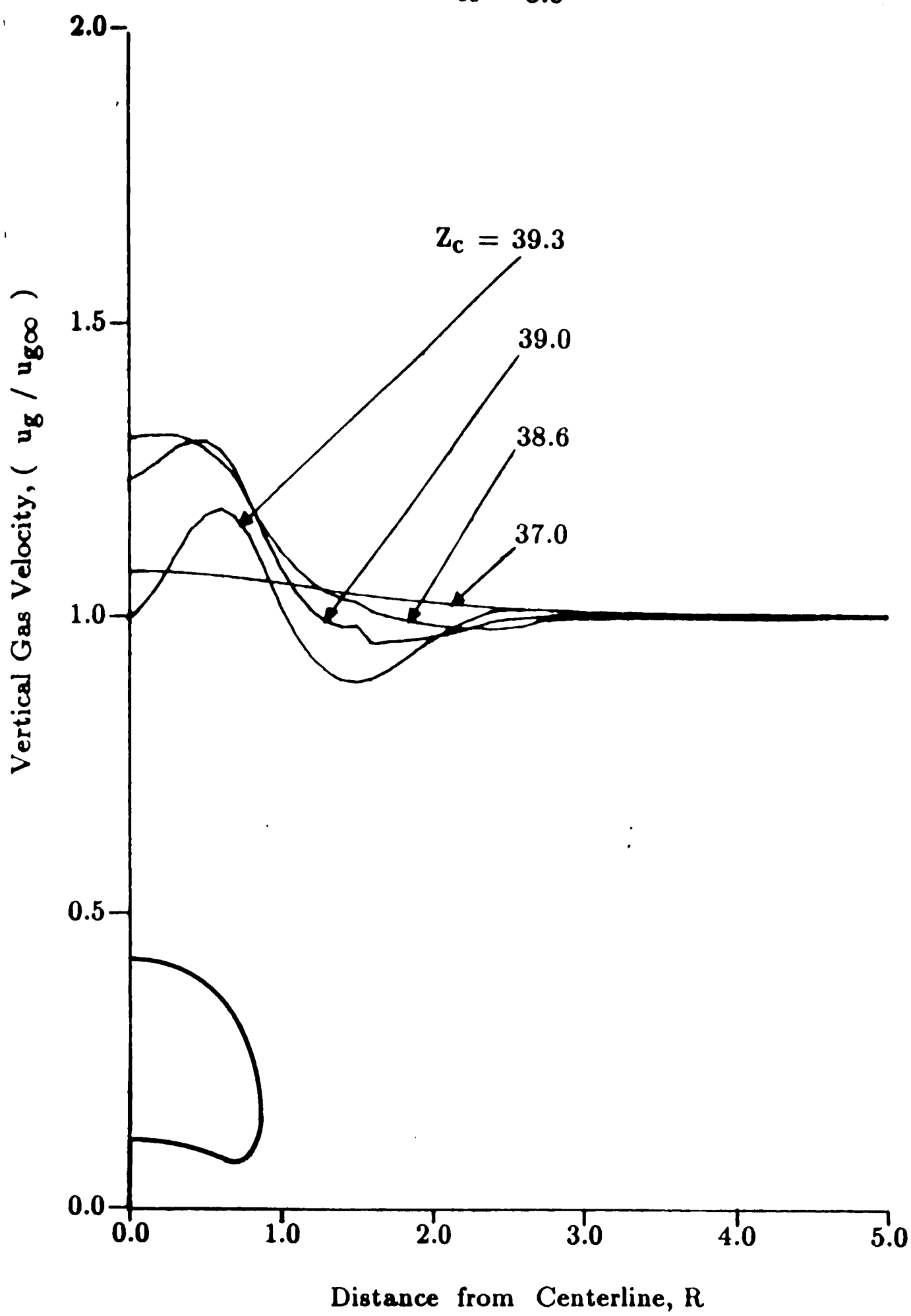

Figure 57. Vertical component of absolute interstitial gas velocity at free surface for K = 3.0

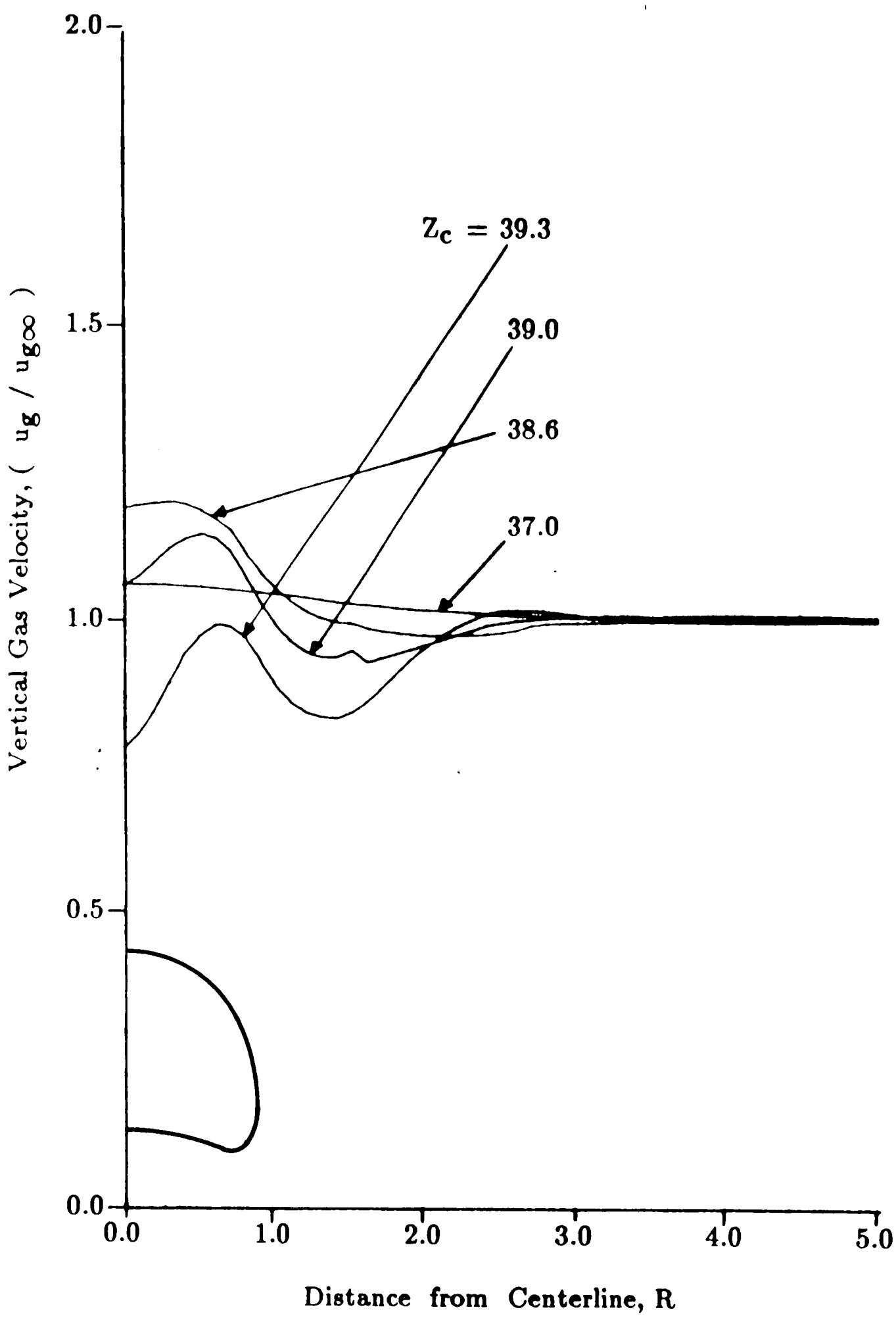

Figure 58. Vertical component of absolute interstitial gas velocity at free surface for K = 10.0

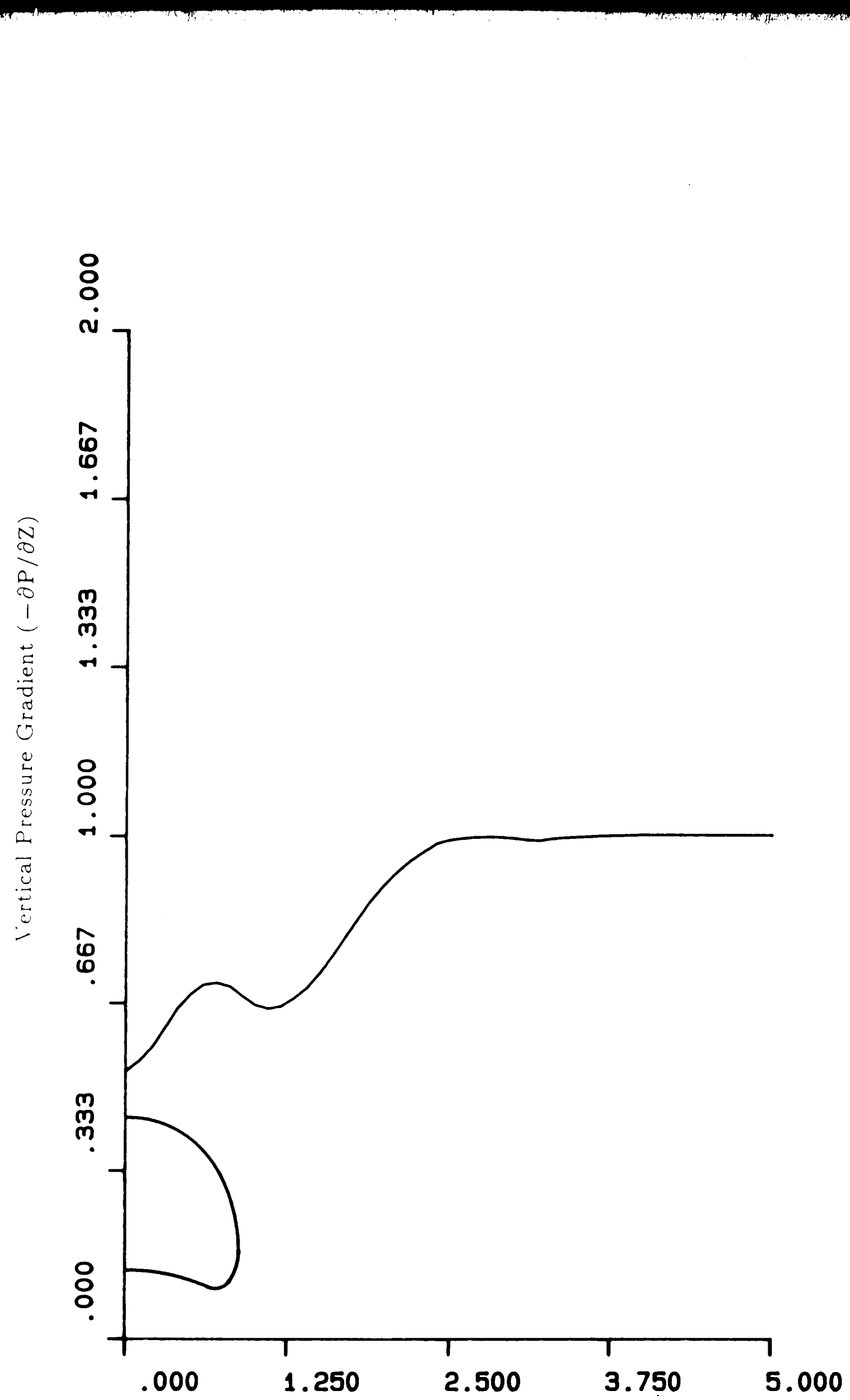

Figure 59. Variation of the vertical pressure gradient at the free surface for Z_c=39.3 and K=0.01

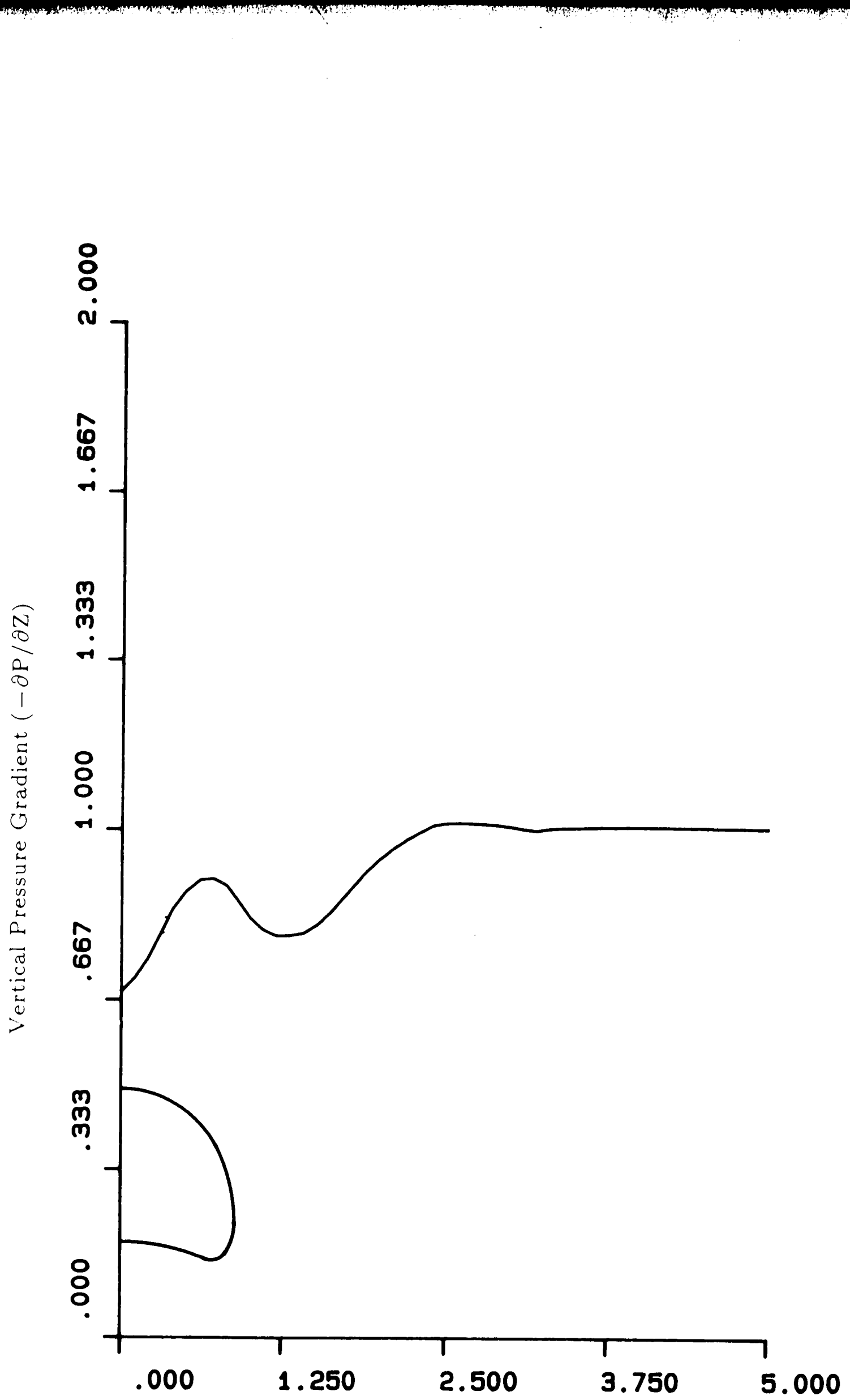

Figure 60. Variation of the vertical pressure gradient at the free surface for Z_c=39.3 and K=0.5

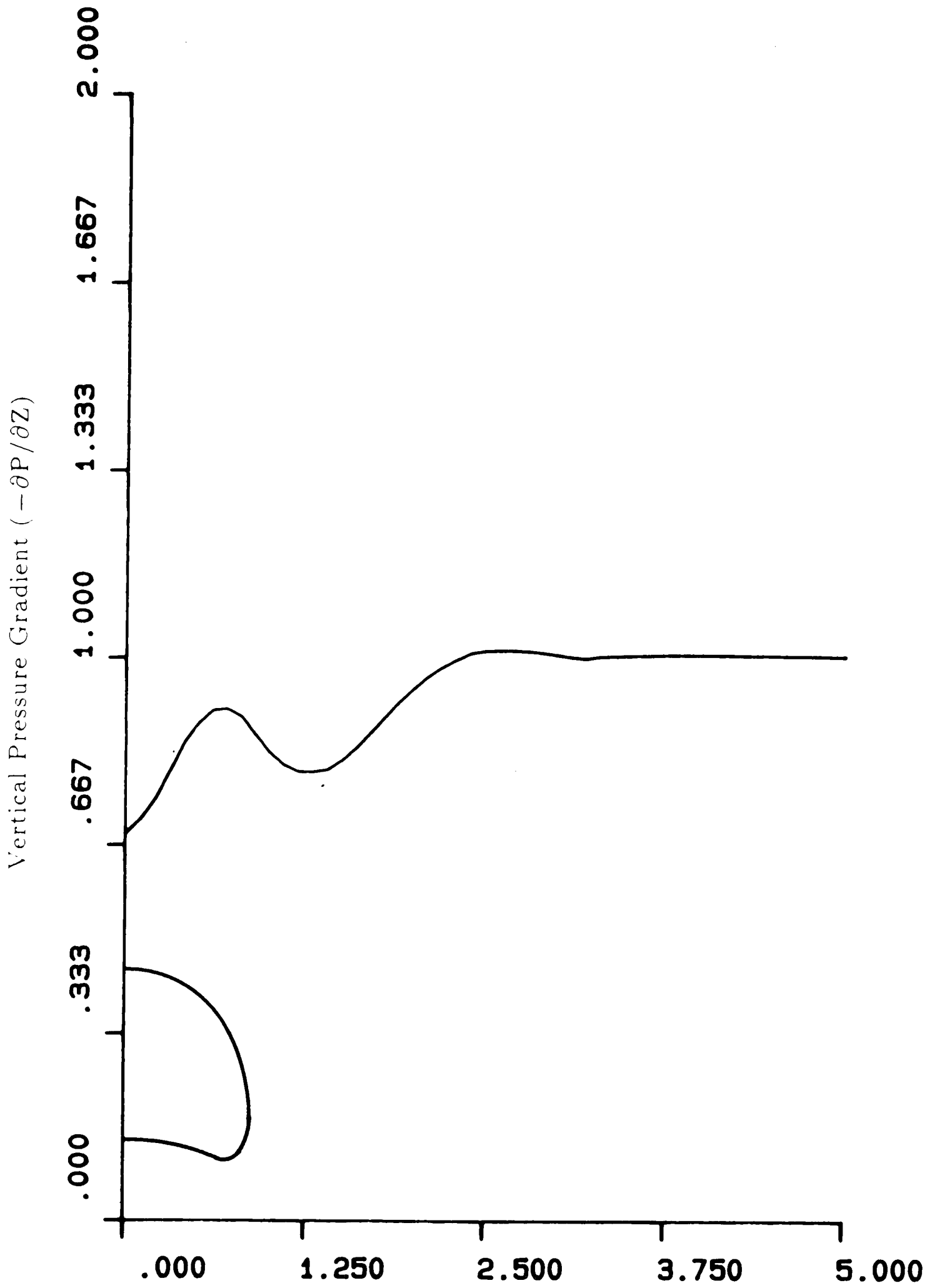

Figure 61. Variation of the vertical pressure gradient at the free surface for Z_c=39.3 and K=10.0

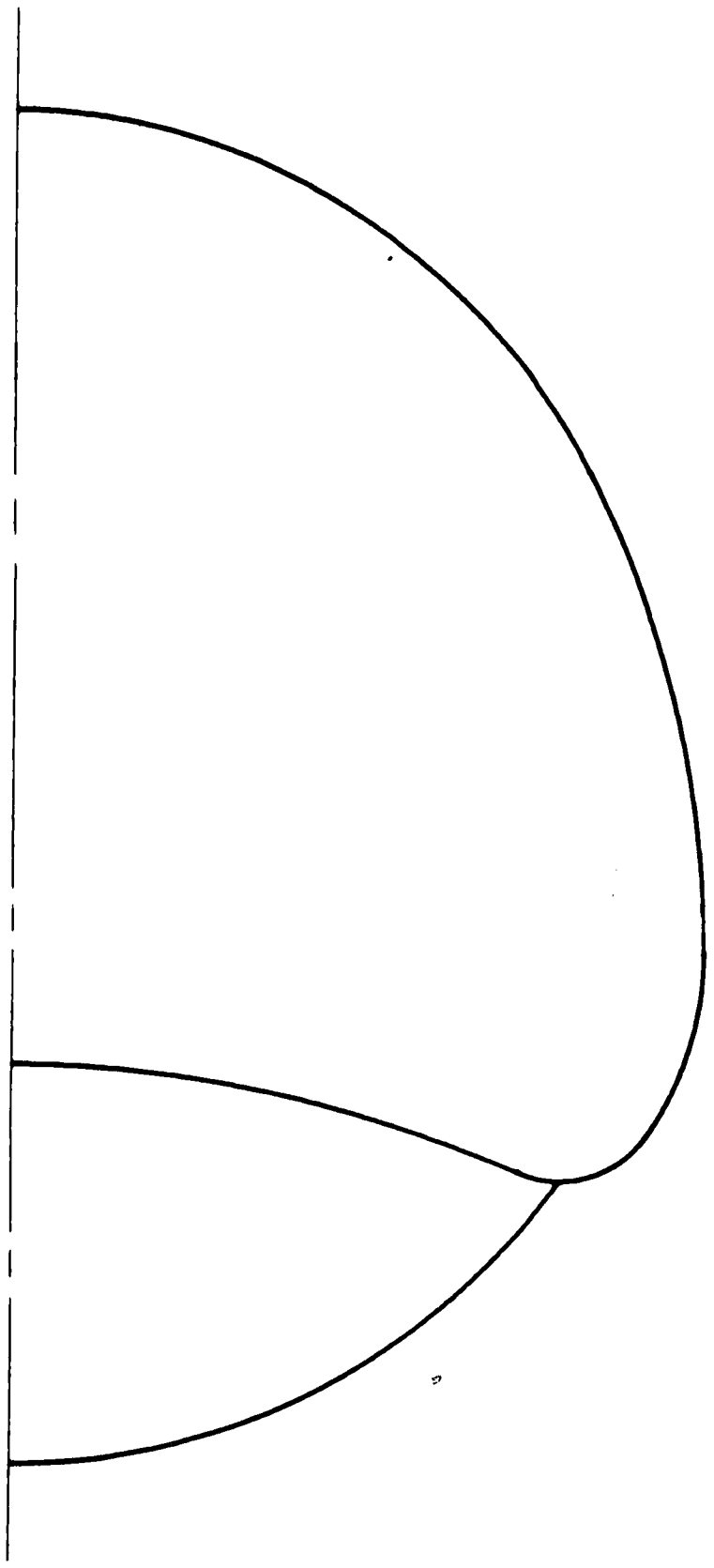

Figure 62. Symmetric portion of the bubble and the wake.

Figure 63. Particle velocity relative to bubble crossing the wake.

REFERENCES

1. Kunii, D., and Levenspiel O. Fluidization Engineering, Robert E. Kreiger Publishing Co., Huntington, NY 1977.

2. Rowe, P. N. and Partridge, B. A. "An X-Ray Study of Bubbles in Fluidised Beds", Trans. Inst. Chem. Eng., Vol. 43 (1965) pp. T157-175.

3. Davies, R. M., and Taylor G. I. "The Mechanics of Large Bubbles Rising Through Extended Liquids and Through Liquids in Tubes", Proc. R. Soc. London A, Vol. 200(1950) pp. 375-390.

4. Clift R. *In* "Gas Fluidization Technology" edited by D. Geldart, John Wiley and Sons, New York, 1986.

5. Rowe, P. N. *In* "Fluidization" edited by J. F. Davidson and D. Harrison, Chapter 4, pp. 121-191. Academic Press, New York, 1971.

6. Davidson J. F. Trans. Inst. Chem. Eng., Vol. 39 (1961) pp. 230-232.

7. Murray, J. D. "On the Mathematics of Fluidization", J. Fluid Mechanics, Vol. 21(1965) p465.

8. Jackson, R. Trans. Inst. Chem. Eng., Vol. 41 (1963) pp. 22-28.

9. Jackson, R. *In* "Fluidization" edited by J. F. Davidson and D. Harrison, Chapter 3, pp. 65-119. Academic Press, New York, 1971.

10. Collins, R. "An extension of Davidson's Theory of Bubbles in Fluidized Beds", Chem. Eng. Sci., Vol. 20 (1965) p747.

11. Littman, H. and Homolka, G. "The Pressure Field around a Two-Dimensional Gas Bubble in a Fluidized Bed", Chem. Eng. Sci., Vol. 28 (1973) pp. 2231-2243.

12. Do, H. T., Grace J. R., and Clift, R. "Particle Ejection and Entrainment from Fluidised Beds", Powder Technology, Vol. 6 (1972) pp. 195-200.

13. Chen, T. P., and Saxena, S. C. *In* "Fluidization" edited by J. F. Davidson and D. L. Keairns, pp. 151-156. Cambridge University Press, London and New York,1978.

14. Levy, E. K., Caram H. S., Dille, J. C., and Edelstein, S. "Mechanisms for Solids Ejection from Gas-Fluidized Beds", AIChE J., Vol. 29 (1983) pp. 383-388.

15. Pemberton, S. T., and Davidson, J. F. "Turbulence in the Freeboard of a Gas-Fluidized Bed", Chem. Eng. Sci., Vol. 39 (1984) pp. 829-840.

16. Radcliff, R. "A Mathematical Model of a Bubble Approaching the Free Surface of a Fluidized Bed", Master's Thesis, Lehigh University, 1984.

17. Chen, H. K. "Gas Flow Through Bubbles in a Fluidized Bed", Master's Thesis, Lehigh University, 1986.

18. Davidson, J. F., and Harrison, D., Fluidised Particles, Cambridge University Press, London, 1963.

19. Milne-Thomson, L. M., Theoretical Hydrodynamics, Macmillan, 1968, 5th ed.

20. Clift, R., and Grace, J. R. *In* "Fluidization" edited by J. F. Davidson, R. Clift, and D. Harrison, Chapter 3, p. 114. Academic Press, New York, 1985.

21. International Mathematical and Statistical Libraries, Inc., TWODEPEP A General Purpose Finite Element Program, User's Manual, Houston, TX, 1980.

22. Huebner, K., Finite Element Method for Engineers, John Wiley and Sons, New York, 1975.

23. Anderson, D. A., Tannehill J. C., and Pletcher R. H. Computational Fluid Mechanics and Heat Transfer, Hemisphere Publishing Co., New York, 1984.

NOMENCLATURE

A_b	Surface area of the bubble over which gas flows out
A_b^*	Dimensionless surface area of the bubble; $A_b^*=A_b/r_n^2$
A_w	Surface area of the wake over which particles flow out
A_w^*	Dimensionless surface area of the wake $A_w^*=A_w/r_n^2$
C	Absolute constant
C(t)	Instantaneous constant
d_{eq}	Equivalent diameter of bubble; $d_{eq}=(6V_b/\pi)^{1/3}$
f_w	Wake fraction of bubble
Fr	Froude number; $Fr=u_b^2/gd_{eq}$
g	Gravitational acceleration
H	Dimensionless free surface displacement; $H=\eta/r_n$
k	Permeability constant
K	Dimensionless interstitial gas velocity far from the bubble; $K=u_{g\infty}/u_b$
n	Normal to surface
n,n+1	Consecutive levels of time
p	pressure
p_f	pressure at free surface of bed

P	Dimensionless pressure; $P=p/[\rho_s(1-\epsilon_{mf})r_n g]$
P_b	Dimensionless pressure inside the bubble
q_b	Gas flow rate through the bubble
q_s	Flow rate of solids through the wake
Q_b	Dimensionless gas flow rate through the bubble; $Q_b=q_b/u_b r_n^2$
Q_s	Dimensionless flow rate of solids through the wake; $Q_w=q_w/u_b r_n^2$
r	Radial coordinate
r_{eq}	Equivalent radius of the bubble; $r_{eq}=(3V_b/4\pi)^{1/3}$
r_n	Nose radius of bubble
R	Dimensionless radial coordinate; $R=r/r_n$
t	time
T	Dimensionless time; $T=tu_b/r_n$
u_b	Bubble rise velocity
u_g	Interstitial gas velocity
u_{gr}	Interstitial gas velocity relative to bubble
$u_{g\infty}$	Interstitial gas velocity far from the bubble
u_o	Superficial velocity of gas
u_{mf}	Minimum fluidization velocity
U_g	Dimensionleass interstitial gas velocity; $U_g=u_g/u_b$
U_{gr}	Dimensionless interstitial gas velocity relative to bubble; $U_{gr}=u_{gr}/u_b$

v_p	Particle velocity
v_{pr}	Particle velocity relative to bubble
v_r	Radial component of particle velocity
v_z	Vertical component of particle velocity
V_b	Dimensionless volume of the bubble
V_w	Dimensionless volume of the wake
V_p	Dimensionless particle velocity; $V_p=v_p/u_b$
V_{pr}	Dimensionless particle velocity relative to bubble; $V_{pr}=v_{pr}/u_b$
z	Vertical coordinate
z_c	Vertical position of the effective bubble center
z_f	Height of free surface
z_o	Level of surface of undisturbed bed
Z	Dimensionless vertical coordinate; $Z=z/r_n$
Z_c	Dimensionless vertical position of the effective bubble center; $Z_c=z_c/r_n$
Δt	Time interval
ϵ_{mf}	Voidage of the bed at minimum fluidization
η	Deformation of the free surface
ϕ	Velocity potential of emulsion phase
Φ	Dimensionless velocity potential; $\Phi=\phi/u_b r_n$
ρ_s	Density of the solids

APPENDIX A

1. Derivation of the Dimensionless Ratio K.

Darcy's law is given by

$$u_g = v_p - k \nabla p \tag{A1}$$

Using the definition of the nondimensional parameters shown in Chapter 3, this equation is expressed as

$$U_g \; u_b = V_p \; u_b - k \; \nabla P \; \frac{\rho_s(1-\epsilon_{mf}) r_n g}{r_n} \tag{A2}$$

or,

$$U_g = V_p - \frac{k}{u_b} \rho_s(1-\epsilon_{mf}) g \; \nabla P \tag{A3}$$

Far from the bubble and from the upper and lower surfaces, the following relation holds between the interstitial gas velocity and the undisturbed pressure gradient,

$$u_{g\infty} = - k \; (\frac{\partial p}{\partial z})_\infty \tag{A4}$$

Assuming the gas density is negligible compared to the density of the solids, the pressure gradient $(\frac{\partial p}{\partial z})_\infty$ must also be constant,

$$- \; (\frac{\partial p}{\partial z})_\infty = \rho_s(1-\epsilon_{mf}) g \tag{A5}$$

Then,

$$u_{g\infty} = k \; \rho_s(1-\epsilon_{mf}) g \tag{A6}$$

Substitution into equation (A3) results in

$$U_g = V_p - \frac{u_{g\infty}}{u_b} \nabla P \qquad (A7)$$

Defining

$$K = \frac{u_{g\infty}}{u_b} \qquad (A8)$$

Equation (A7) becomes

$$U_g = V_p - K \nabla P \qquad (A9)$$

2. Derivation of the Pressure Boundary Conditions on the right and bottom edges.

It follows from equation (A3) that

$$\Delta p = - \Delta z \ \rho_s \ (1-\epsilon_{mf}) \ g \qquad (A10)$$

From the definition of dimensionless pressure

$$p = P \ r_n \ \rho_s \ (1-\epsilon_{mf}) \ g \qquad (A11)$$

Substituting (A11) into (A10) gives

$$\Delta P = - \frac{\Delta z}{r_n} = - \Delta Z \qquad (A12)$$

Referring to Figure 1.,

$$\Delta z = z - z_o - \eta \qquad (A13)$$

When equation (A13) is made nondimensional, and then substituted into equation (A12),

$$\Delta P = - \Delta Z = Z_o + H - Z \qquad (A14)$$

Noting that P = 0 at the surface, the pressure for the points on the right and bottom edges can be written as

$$P = Z_o + H - Z \qquad (A15)$$

APPENDIX B

1. The Shape and the Volume of the Bubble.

The shape of the bubble was obtained from video recordings taken in the experiments with glass beads. A typical shape was determined and copied directly from the screen, then a curve fitting procedure was tried. After a number of trials, a combination of five circular arcs, with different centers and radii(shown in Figure 64, page 126), seemed to be representing the original shape with reasonable accuracy. Care was taken for the smoothness of the joining points and the continuity of the functions and their slopes were satisfied with an accuracy higher than that is required by the finite element software.

The volume of the bubble was calculated by applying the concept of volume of revolution, since the equations of the curves making up the boundary of the bubble were known. Referring to Figure 64, these equations, correct to three decimal points, are:

$$R_1 = \sqrt{(0.811)^2-(Z-0.189)^2} \qquad 1.0 \geq Z \geq 0.574$$

$$R_2 = -0.351 + \sqrt{(1.209)^2-Z^2} \qquad 0.574 \geq Z \geq 0.0$$

$$R_3 = 0.496 + \sqrt{(0.363)^2 - Z^2} \qquad 0.0 \geq Z \geq -0.218$$

$$R_4^+ = 0.680 + \sqrt{(0.133)^2 - Z^2} \qquad -0.218 \geq Z \geq -0.271$$

$$R_4^- = 0.680 - \sqrt{(0.133)^2 - Z^2} \qquad -0.271 \geq Z \geq -0.261$$

$$R_5 = \sqrt{(1.647)^2 - (Z+1.783)^2} \qquad -0.261 \geq Z \geq -0.136$$

The volume that is formed by rotating the the region bounded by the Z axis and these 5 curves around the Z-axis is equal to the volume of the bubble, and can be written as

$$V_b = V_1 + V_2 + V_3 + V_4^+ - V_4^- - V_5 \qquad \text{(B1)}$$

where

$$V_1 = \int_{0.574}^{1.0} \pi \, R_1^2 \, dZ \qquad V_4^+ = \int_{-0.271}^{-0.218} \pi \, R_4^2 \, dZ$$

$$V_2 = \int_{0.0}^{0.574} \pi \, R_2^2 \, dZ \qquad V_4^- = \int_{-0.271}^{-0.261} \pi \, R_4^2 \, dZ \qquad \text{(B2)}$$

$$V_3 = \int_{-0.218}^{0.0} \pi \, R_3^2 \, dZ \qquad V_5 = \int_{-0.261}^{-0.136} \pi \, R_5^2 \, dZ$$

In the above integrals, the integrand has the following general form

$$\left\{ a \pm \sqrt{b^2 - (Z+c)^2} \right\}^2$$

Expanding, this becomes

$$a^2 + \left\{b^2 - (Z+c)^2\right\} \pm 2a\sqrt{b^2-(Z+c)^2}$$

Employing the substitution

$$u = Z+c \ , \qquad du = dZ$$

and subsequently,

$$u = b\ \mathrm{Sin}\theta \ , \qquad du = b\ \mathrm{Cos}\theta\ d\theta$$

it can be shown that

$$\int_{Z_1}^{Z_2} \pi\left\{a \pm \sqrt{b^2 - (Z+c)^2}\right\}^2 dZ = \pi\Big\{(a^2+b^2)(Z_2-Z_1)$$

$$-\frac{1}{3}\left[(Z_2+c)^3-(Z_1+c)^3\right] \pm ab^2\left[(\theta_2-\theta_1) + \frac{1}{2}(\mathrm{Sin}2\theta_2 - \mathrm{Sin}2\theta_1)\right]\Big\} \qquad (B3)$$

where $\theta_2 = \mathrm{Sin}^{-1}\left\{\dfrac{Z_2+c}{b}\right\}$

$$\theta_1 = \mathrm{Sin}^{-1}\left\{\frac{Z_1+c}{b}\right\}$$

Now, applying this result to the equations (B2) the volume of the bubble can be obtained as

$$V_b = 2.076$$

Then, from the definition of the equivalent radius

$$V_b = \frac{4}{3}\pi\ r_{eq}^3$$

it follows that

$$r_{eq} = 0.7914$$

and

$$d_{eq} = 1.5828$$

Since the nose radius is the reference parameter

$$r_n = 1.0$$

so that

$$d_{eq} = 1.5828\ r_n \qquad \text{(B4)}$$

2. The Wake Fraction of the Bubble.

The boundary of the wake, drawn in Figure 62, is represented by the following expression:

$$R_6 = \sqrt{(0.851)^2-(Z-0.241)^2} \qquad -0.610 \leq Z \leq -0.271$$

with the origin of the coordinate system located at the effective bubble center as shown in Figure 64.

Applying the argument of the previous section, the volume of the wake is given by

$$V_W = V_6 + V_4 + V_5 \qquad \text{(B5)}$$

where

$$V_6 = \int_{-0.610}^{-0.271} \pi\ R_6^2\ dZ \qquad \text{(B6)}$$

and V_4 and V_5 are as defined in equation (B2).

The result is

$$V_w = 0.266$$

Now, the wake fraction can be obtained from

$$f_w = \frac{V_w}{V_b + V_w} \tag{B7}$$

as

$$f_w = 0.176$$

A(0.713,0.574)

B(0.858,0.0)

C(0.786,−0.218)

D(0.629,−0.261)

E(0.680,−0.271)

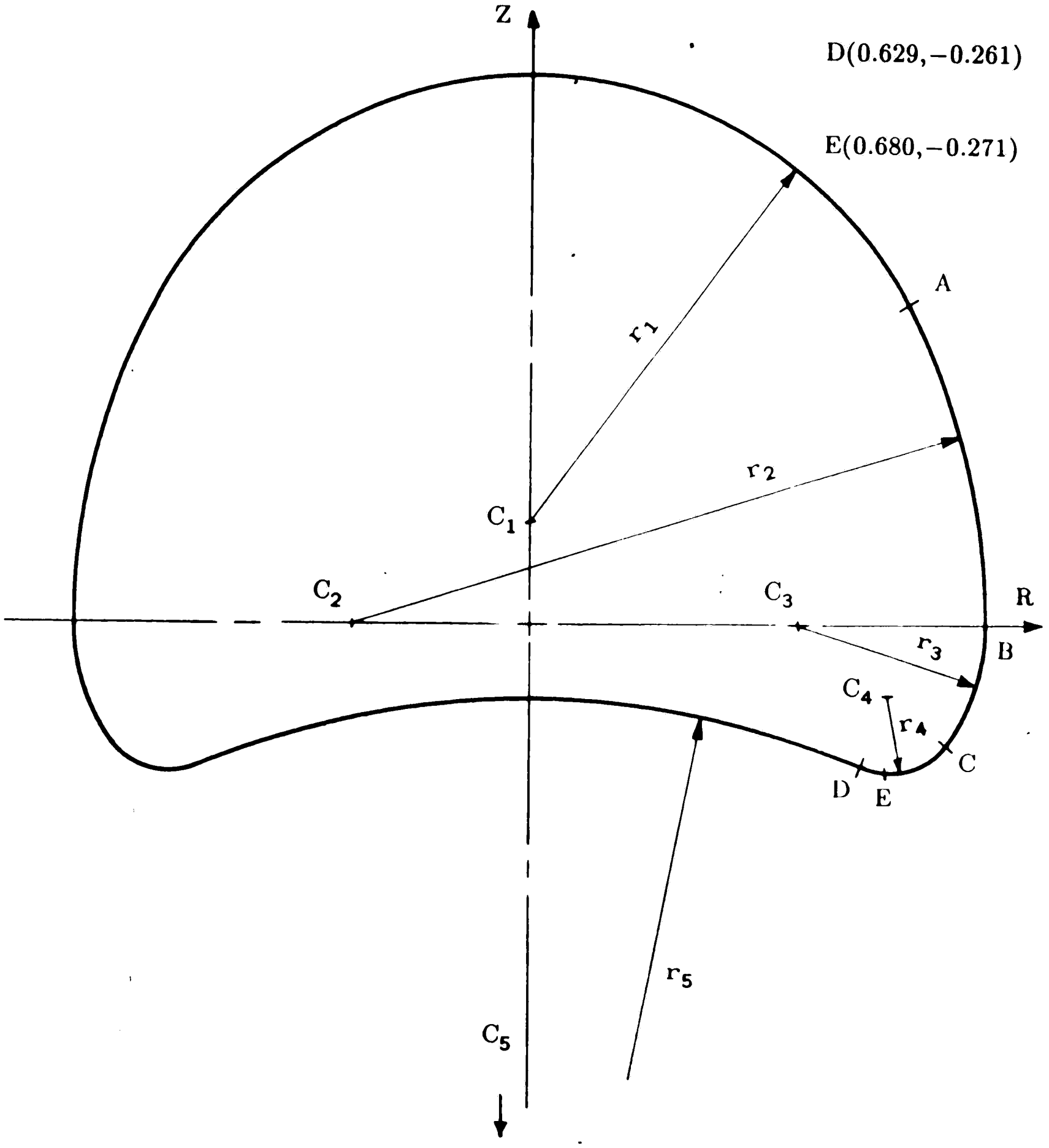

Figure 64. Geometry of the simulated bubble.

VITA

Bulent Kocatulum, son of Serpin and Selahattin Kocatulum, was born on October 20, 1964 in Havran, Turkey.

He attended Aktepe High School in Ankara, Turkey and received his diploma in 1981. He was graduated summa cum laude from Middle East Technical University, Ankara, Turkey with a Bachelor of Science degree in Mechanical Engineering in July 1986.

In September 1986, he entered the Graduate School at Lehigh University and completed his M.S. program in January 1989. During his course of study he worked as a teaching assistant and as a research assistant in the Department of Mechanical Engineering and Mechanics.